

EFFECT OF SOLVENT DEASPHALTING PROCESS ON THE PROPERTIES OF  
DEASPHALTED OIL AND ASPHALTENES FROM BITUMEN

by

Annapurna Sri Sowmya Turuga

A thesis submitted in partial fulfillment of the requirements for the degree of

Master of Science

in

Chemical Engineering

Department of Chemical and Materials Engineering  
University of Alberta

© Annapurna Sri Sowmya Turuga, 2017

## ABSTRACT

Asphaltenes are a solubility class of bitumen known to have undesirable properties. As asphaltenes are insoluble in paraffinic solvents, they can be separated from bitumen by adding a solvent such as *n*-pentane or *n*-heptane to produce better quality deasphalted oil (DAO). This process is called Solvent Deasphalting (SDA). Several methods of SDA are reported in literature. The solvent, solvent to bitumen (S/B) ratio, precipitation time, temperature and pressure affect the yield and properties of asphaltenes.

The objective of this work is to study the effect of solvent, S/B ratio and precipitation time in the SDA process on the properties of asphaltenes and DAO. Characterization of asphaltenes and DAO produced at different conditions of the SDA process could help in predicting how the SDA process affects the thermal cracking process and downstream processes. Experiments were performed using Canadian oil sands bitumen from Athabasca region. *n*-pentane, *n*-hexane and *n*-heptane were used as solvents at S/B ratios 3:1, 4:1, 5:1 and 40:1 (ml/g), and the effect of changing precipitation time from the most commonly used 24h, to longer time (330h), was also studied. All the experiments were performed at room temperature and atmospheric pressure.

The solvent and S/B ratio were found to affect the yield and the following characteristics of asphaltenes and DAO: hydrogen to carbon ratio, heteroatoms (N, S), metal content (Ni, V), distillation curve, micro carbon residue, free radical content, liquefying point and refractive index. The separation selectivity and extractability of components from bitumen into asphaltenes and DAO respectively, change with solvent and S/B ratio in the SDA process. These process variables also impact the thermal cracking behavior of asphaltenes and DAO. The change in precipitation time from 24h to 330h in the SDA process did not significantly affect the boiling point distribution

and micro carbon residue of asphaltenes and DAO. This work could be extended to the temperatures and pressures used in the industrial process of solvent deasphalting, and to a wider range of solvents with different structural aspects.

## ACKNOWLEDGEMENTS

The first person I would like to say thanks to is my supervisor, Dr. Arno De Klerk, for giving me the opportunity to join his research group and for his support and guidance during these two years. He always believed in me and gave me the confidence that I could do research myself. I developed my analytical skills and learned a lot in these two years.

Secondly, I would like to thank my parents, sister and my entire family in India, for their love and encouragement throughout my studies in Canada.

I am also thankful to my entire research group for their support and friendship. Special thanks to Dr. Cibele Melo Halmenschlager, Dr. Glaucia Carvalho Do Prado, Ioan Tudor Apan, Cloribel Santiago Flores, Giselle Uzcategui Barrios and Natalia Montoya for helping me get trained in the lab, and for their valuable suggestions in my research.

Next, I would like to thank my best friend, Sumanth Kumar Arnipally, for always being there for me. He helped me in writing my thesis successfully, by teaching me how to use Microsoft Office, EndNote and OriginPro.

I would like to thank all my friends in Canada, India and USA for their love and support.

I would like to extend my sincere thanks to the University of Alberta, for supporting my graduate studies.

Finally, I would like to acknowledge Nexen for funding this work.

# TABLE OF CONTENTS

CHAPTER 1. INTRODUCTION .....	1
1.1 Background .....	1
1.2 Objective and Scope of Work .....	2
1.3 Contribution to the work .....	3
1.4 References .....	3
CHAPTER 2. LITERATURE REVIEW ON SOLVENT DEASPHALTING PROCESS .....	5
2.1 Introduction .....	5
2.2 Characteristics of Bitumen .....	5
2.2.1 Chemical Composition.....	5
2.2.2 SARA Fractionation.....	6
2.2.3 Distillation Profile of Bitumen.....	7
2.2.4 Density .....	8
2.3 SDA Process.....	9
2.3.1 Industrial SDA Processes.....	9
2.3.2 Analytical Methods for Asphaltenes Precipitation .....	13
2.3.3 Process Variables .....	14
2.3.4 Solubility Parameters .....	15
2.4 Some Important Properties of the Products.....	21
2.4.1 Elemental Composition.....	21
2.4.2 Refractive Index of Liquids .....	21
2.4.3 Free radical content.....	21
2.4.4 Distillation Curve.....	22
2.4.5 Coking Tendency .....	23
2.4.6 Melting point of asphaltenes .....	23

2.5	Conclusions .....	24
2.6	References .....	24
CHAPTER 3. EXPERIMENTAL – PRECIPITATION OF ASPHALTENES FROM BITUMEN AT DIFFERENT SDA PROCESS CONDITIONS .....		
27		
3.1	Introduction .....	27
3.2	Experimental .....	27
3.2.1	Materials .....	27
3.2.2	Equipment and Procedure .....	27
3.2.3	Analyses .....	30
3.2.4	Results .....	36
3.2.5	Discussion .....	38
3.2.6	Conclusions .....	45
3.3	References .....	45
CHAPTER 4. CHARACTERIZATION OF ASPHALTENES AND DAO FRACTIONS OF BITUMEN FROM THE SOLVENT DEASPHALTING PROCESS .....		
47		
4.1	Introduction .....	47
4.2	Materials and Methods .....	47
4.2.1	Materials .....	47
4.2.2	Analyses .....	47
4.3	Results .....	48
4.3.1	Elemental Analysis .....	48
4.3.2	Metal content by X-Ray Fluorescence .....	54
4.3.3	FTIR Spectra .....	55
4.3.4	Free Radical Content .....	59
4.3.5	Refractive Index of DAO .....	63
4.4	Discussion .....	67

4.4.1	Effect of SDA process on the chemical composition of asphaltenes and DAO .....	67
4.4.2	FTIR Spectra of asphaltenes and DAO at different conditions of SDA process ....	81
4.4.3	Effect of SDA process on free radical content of asphaltenes and DAO .....	82
4.4.4	Effect of SDA process on the refractive index of DAO .....	84
4.5	Conclusions .....	85
4.6	References .....	87
CHAPTER 5. EFFECT OF SDA PROCESS ON THE THERMAL PROPERTIES OF ASPHALTENES AND DAO .....		89
5.1	Introduction .....	89
5.2	Materials and Methods .....	89
5.2.1	Materials .....	89
5.2.2	Analyses .....	89
5.3	Results .....	90
5.3.1	Boiling Point Distribution by Simdis.....	90
5.3.2	Thermogravimetric Analysis .....	98
5.3.3	Liquefying Point of Asphaltenes .....	105
5.4	Discussion .....	109
5.4.1	Boiling Point distribution of asphaltenes and DAO .....	109
5.4.2	Selectivity of the SDA process at different process conditions for the extraction of boiling fractions of bitumen.....	110
5.4.3	Cracking behavior of asphaltenes and DAO.....	114
5.4.4	Microcarbon residue (MCR).....	122
5.4.5	Liquefaction of asphaltenes .....	125
5.5	Conclusions .....	125
5.6	References .....	127
CHAPTER 6. CONCLUSIONS .....		129

6.1	Background .....	129
6.2	Experimental Approach.....	129
6.3	Major Conclusions .....	130
6.3.1	Asphaltene yield and material balance in the solvent deasphalting process.....	130
6.3.2	Chemical characterization of asphaltenes and DAO .....	130
6.3.3	Thermal properties of asphaltenes and DAO.....	131
6.4	Recommendations for future work.....	132
BIBLIOGRAPHY.....		133

## LIST OF TABLES

<b>Table 2-1.</b> Properties of Conventional Crude Oil vs Bitumen. <sup>2</sup> .....	6
<b>Table 2-2.</b> Mass loss upon distillation (volume %) vs. Boiling point (°C) of Athabasca Bitumen. <sup>2</sup> .....	7
<b>Table 2-3.</b> Standard Methods for Asphaltenes Precipitation. <sup>6,7</sup> .....	13
<b>Table 2-4.</b> Distillation Fractions commonly used in Upgrading and Refining of Crude Oils and Bitumen. <sup>2</sup> .....	23
<b>Table 3-1.</b> Boiling Ranges of Distillation Fractions used in this study.....	32
<b>Table 3-2.</b> Characterization of Athabasca Bitumen Feed <sup>a</sup> .....	34
<b>Table 3-3.</b> Yields of Fractions and Losses from SDA of bitumen with contact time of 24h <sup>a</sup> .....	37
<b>Table 3-4.</b> Yields of fractions and Losses from SDA of bitumen with contact time of 330h <sup>a</sup> ...	38
<b>Table 3-5.</b> Comparison of bitumen characterization in this study with values reported in literature .....	39
<b>Table 4-1.</b> Carbon content (wt%) of asphaltenes obtained with different solvents and S/B ratios by solvent deasphalting when the precipitation time was 24h <sup>a</sup> .....	49
<b>Table 4-2.</b> Hydrogen content (wt%) of asphaltenes obtained with different solvents and S/B ratios by solvent deasphalting when the precipitation time was 24h <sup>a</sup> .....	49
<b>Table 4-3.</b> Nitrogen content (wt%) of asphaltenes obtained with different solvents and S/B ratios by solvent deasphalting when the precipitation time was 24h <sup>a</sup> .....	50
<b>Table 4-4.</b> Sulfur content (wt%) of asphaltenes obtained with different solvents and S/B ratios by solvent deasphalting when the precipitation time was 24h <sup>a</sup> .....	50
<b>Table 4-5.</b> Oxygen content (wt%) of asphaltenes obtained with different solvents and S/B ratios by solvent deasphalting when the precipitation time was 24h <sup>a</sup> .....	51
<b>Table 4-6.</b> Carbon content (wt%) of DAO obtained with different solvents and S/B ratios by solvent deasphalting when the precipitation time was 24h <sup>a</sup> .....	51
<b>Table 4-7.</b> Hydrogen content (wt%) of DAO obtained with different solvents and S/B ratios by solvent deasphalting when the precipitation time was 24h <sup>a</sup> .....	52
<b>Table 4-8.</b> Nitrogen content (wt%) of DAO obtained with different solvents and S/B ratios by solvent deasphalting when the precipitation time was 24h <sup>a</sup> .....	52
<b>Table 4-9.</b> Sulfur content (wt%) of DAO obtained with different solvents and S/B ratios by solvent deasphalting when the precipitation time was 24h <sup>a</sup> .....	53

<b>Table 4-10.</b> Oxygen content (wt%) of DAO obtained with different solvents and S/B ratios by solvent deasphalting when the precipitation time was 24h <sup>a</sup> .....	53
<b>Table 4-11.</b> g-factors of organic free radical signal in the ESR spectra of asphaltenes precipitated using different solvents and at different S/B ratios in the SDA process, with precipitation time = 24h.....	62
<b>Table 4-12.</b> g-factors of vanadyl peak in the ESR spectra of asphaltenes precipitated using different solvents and at different S/B ratios in the SDA process, with precipitation time = 24h	63
<b>Table 4-13.</b> Calculated elemental (C, H, N, S) losses during precipitation of asphaltenes using different solvents and S/B ratios .....	67
<b>Table 4-14.</b> H/C ratio of C <sub>5</sub> and C <sub>7</sub> asphaltenes precipitated at different S/B ratios in the SDA process with precipitation time=24h.....	69
<b>Table 4-15.</b> H/C ratio of C <sub>5</sub> and C <sub>7</sub> maltenes precipitated at different S/B ratios in the SDA process with precipitation time=24h.....	70
<b>Table 4-16.</b> Separation selectivities of C <sub>5</sub> and C <sub>7</sub> asphaltenes for nitrogen in bitumen at different conditions of SDA process. Precipitation Time = 24h .....	73
<b>Table 4-17.</b> Separation selectivities of C <sub>5</sub> and C <sub>7</sub> asphaltenes for sulfur in bitumen at different conditions of SDA process. Precipitation Time = 24h .....	74
<b>Table 4-18.</b> Separation selectivities of C <sub>5</sub> and C <sub>7</sub> asphaltenes for oxygen in bitumen at different conditions of SDA process. Precipitation Time = 24h .....	76
<b>Table 4-19.</b> Hansen solubility parameters of <i>n</i> -pentane, <i>n</i> -hexane, <i>n</i> -heptane and bitumen. <sup>7</sup> .....	77
<b>Table 4-20.</b> Separation selectivities of C <sub>5</sub> and C <sub>7</sub> asphaltenes for nickel in bitumen at different conditions of SDA process. Precipitation Time = 24h .....	80
<b>Table 4-21.</b> Separation selectivities of C <sub>5</sub> and C <sub>7</sub> asphaltenes for vanadium in bitumen at different conditions of SDA process. Precipitation Time = 24h .....	80
<b>Table 5-1.</b> Middle distillate fraction (wt%) of C <sub>5</sub> , C <sub>6</sub> and C <sub>7</sub> asphaltenes precipitated at different S/B ratios in the SDA process, Precipitation time = 24h.....	93
<b>Table 5-2.</b> Gas Oil fraction (wt%) of C <sub>5</sub> , C <sub>6</sub> and C <sub>7</sub> asphaltenes precipitated at different S/B ratios in the SDA process, Precipitation time = 24h.....	93
<b>Table 5-3.</b> Residue fraction (wt%) of C <sub>5</sub> , C <sub>6</sub> and C <sub>7</sub> asphaltenes precipitated at different S/B ratios in the SDA process, Precipitation time = 24h.....	94

<b>Table 5-4.</b> Middle distillate fraction (wt%) of C <sub>5</sub> , C <sub>6</sub> and C <sub>7</sub> maltenes precipitated at different S/B ratios in the SDA process, Precipitation time = 24h.....	94
<b>Table 5-5.</b> Gas Oil fraction (wt%) of C <sub>5</sub> , C <sub>6</sub> and C <sub>7</sub> maltenes precipitated at different S/B ratios in the SDA process, Precipitation time = 24h.....	95
<b>Table 5-6.</b> Residue fraction (wt%) of C <sub>5</sub> , C <sub>6</sub> and C <sub>7</sub> maltenes precipitated at different S/B ratios in the SDA process, Precipitation time = 24h.....	95
<b>Table 5-7.</b> Effect of precipitation time in SDA process on the Middle distillate fraction of asphaltenes .....	96
<b>Table 5-8.</b> Effect of precipitation time in SDA process on the Gas Oil fraction of asphaltenes .	96
<b>Table 5-9.</b> Effect of precipitation time in SDA process on the Residue fraction of asphaltenes .	97
<b>Table 5-10.</b> Effect of precipitation time in SDA process on the Middle distillate fraction of DAO .....	97
<b>Table 5-11.</b> Effect of precipitation time in SDA process on the Gas Oil fraction of DAO .....	98
<b>Table 5-12.</b> Effect of precipitation time in SDA process on the Residue fraction of DAO.....	98
<b>Table 5-13.</b> Comparison of mass loss of bitumen, C <sub>5</sub> asphaltenes and maltenes in TGA and SimDis analyses in different ranges of temperature .....	100
<b>Table 5-14.</b> MCR of Asphaltenes (wt%), Precipitation Time = 24h <sup>a</sup> .....	103
<b>Table 5-15.</b> MCR of Asphaltenes (wt%), Precipitation Time = 330h .....	103
<b>Table 5-16.</b> MCR of maltenes (wt%), Precipitation Time = 24h <sup>a</sup> .....	104
<b>Table 5-17.</b> MCR of maltenes (wt%), Precipitation Time = 330h.....	104
<b>Table 5-18.</b> Liquefying Point of C <sub>5</sub> and C <sub>7</sub> asphaltenes at different S/B ratios by Visual Observation.....	106
<b>Table 5-19.</b> Separation selectivities of C <sub>5</sub> , C <sub>6</sub> and C <sub>7</sub> asphaltenes for middle distillate, gas oil and residue fractions in bitumen at different conditions of SDA process. Precipitation Time = 24h	114
<b>Table 5-20.</b> Comparison of ‘effective’ mass loss and mass of residue from asphaltenes and DAO on bitumen basis with the mass loss and mass of residue from bitumen.....	116

## LIST OF FIGURES

<b>Figure 2-1.</b> Process Diagram of SARA Fractionation. <sup>3</sup> .....	7
<b>Figure 2-2.</b> Relation between solubility parameter and amount of asphaltenes precipitated from bitumen. <sup>1</sup> .....	17
<b>Figure 2-3.</b> 3D solubility parameters of liquids at 25°C. <sup>1</sup> .....	18
<b>Figure 2-4.</b> ESR spectrum of Athabasca asphaltenes. <sup>1</sup> .....	22
<b>Figure 3-1.</b> Process Diagram of Asphaltene Precipitation in this study .....	29
<b>Figure 3-2.</b> Simulated Distillation Curve of Athabasca Bitumen .....	32
<b>Figure 3-3.</b> ESR spectrum of bitumen .....	34
<b>Figure 3-4.</b> Yields of C <sub>5</sub> , C <sub>6</sub> and C <sub>7</sub> asphaltenes precipitated at different S/B ratios. Precipitation Time = 24h.....	41
<b>Figure 3-5.</b> Appearance of C <sub>5</sub> asphaltenes precipitated at S/B ratios 5:1 and 40:1 .....	42
<b>Figure 3-6.</b> Effect of precipitation time on the yield of (a) C <sub>5</sub> asphaltenes and (b) C <sub>7</sub> asphaltenes at different S/B ratios .....	43
<b>Figure 4-1.</b> Metal content in asphaltenes (a) Ni and (b) V expressed in ppm .....	55
<b>Figure 4-2.</b> FTIR spectra of asphaltenes precipitated at different solvents and S/B ratios in the SDA process when the precipitation time = 24h .....	56
<b>Figure 4-3.</b> FTIR spectra of asphaltenes precipitated at different solvents and S/B ratios in the SDA process when the precipitation time = 330h .....	57
<b>Figure 4-4.</b> FTIR spectra of bitumen, and DAO for different solvents and S/B ratios in the SDA process when the precipitation time = 24h .....	58
<b>Figure 4-5.</b> FTIR spectra of DAO for different solvents and S/B ratios in the SDA process when the precipitation time = 330h .....	58
<b>Figure 4-6.</b> Graph showing first Derivative of Absorption Spectrum of asphaltenes vs. g-factor in the ESR spectroscopy of asphaltenes.....	59
<b>Figure 4-7.</b> Absorption spectra of asphaltenes as a function of g-factor obtained in ESR spectroscopic analysis .....	60
<b>Figure 4-8.</b> Double integral values of organic free radical peak in the ESR spectroscopy of C <sub>5</sub> , C <sub>6</sub> and C <sub>7</sub> asphaltenes at different S/B ratios. Precipitation Time = 24h.....	61
<b>Figure 4-9.</b> Double integral values of vanadyl radical peak in the ESR spectroscopy of C <sub>5</sub> , C <sub>6</sub> and C <sub>7</sub> asphaltenes at different S/B ratios. Precipitation Time = 24h .....	61

<b>Figure 4-10.</b> Refractive Indexes of DAO with temperature at different S/B ratios and precipitation time = 24h for (a) C <sub>5</sub> maltenes, (b) C <sub>6</sub> maltenes and (c) C <sub>7</sub> maltenes.....	65
<b>Figure 4-11.</b> Effect of precipitation time in SDA process on the refractive Indexes of DAO.....	66
<b>Figure 4-12.</b> Nitrogen content of C <sub>5</sub> and C <sub>7</sub> asphaltenes, expressed as wt% of bitumen, at different S/B ratios of SDA process. Precipitation time = 24h .....	72
<b>Figure 4-13.</b> Sulfur content of C <sub>5</sub> and C <sub>7</sub> asphaltenes, expressed as wt% of bitumen, at different S/B ratios of SDA process. Precipitation time = 24h .....	74
<b>Figure 4-14.</b> Oxygen content of C <sub>5</sub> and C <sub>7</sub> asphaltenes, expressed as wt% of bitumen, at different S/B ratios of SDA process. Precipitation time = 24h .....	76
<b>Figure 4-15.</b> (a) Nickel (Ni) and (b) Vanadium (V) content of C <sub>5</sub> and C <sub>7</sub> asphaltenes, expressed as wt% of bitumen, at different S/B ratios of SDA process. Precipitation time = 24h .....	79
<b>Figure 4-16.</b> Correlation between double integral values of vanadyl free radical peak of asphaltenes from ESR spectroscopy and their vanadium content from XRF spectrometry. ....	84
<b>Figure 5-1.</b> SimDis curves of C <sub>5</sub> and C <sub>7</sub> asphaltenes precipitated at S/B ratio 4:1 and with precipitation time = 24h.....	91
<b>Figure 5-2.</b> SimDis curves of C <sub>5</sub> asphaltenes precipitated at different S/B ratios and with precipitation time = 24h.....	92
<b>Figure 5-3.</b> TGA curves of Bitumen, C <sub>5</sub> asphaltenes and C <sub>5</sub> maltenes, precipitated at S/B ratio 40:1 and with precipitation time = 24h.....	99
<b>Figure 5-4.</b> TGA curves of C <sub>5</sub> asphaltenes precipitated at different S/B ratios and with precipitation time = 24h.....	101
<b>Figure 5-5.</b> TGA curves of C <sub>5</sub> maltenes precipitated at different S/B ratios and with precipitation time = 24h.....	102
<b>Figure 5-6.</b> Microscopic Images of (a) C <sub>5</sub> asphaltenes and (b) C <sub>7</sub> asphaltenes precipitated at S/B ratio 5:1 .....	105
<b>Figure 5-7.</b> Reflected light intensity against temperature for (a) C <sub>5</sub> -asphaltenes and (b) C <sub>7</sub> -asphaltenes at different S/B ratios.....	108
<b>Figure 5-8.</b> DSC curves of C <sub>7</sub> asphaltenes precipitated at S/B ratio 5:1.....	109
<b>Figure 5-9.</b> (a) Middle Distillate (b) Gas Oil (c) Residue fractions of asphaltenes on bitumen weight basis, Precipitation time = 24h.....	113

<b>Figure 5-10.</b> Subtraction of TGA curve from Simdis Curve of (a) C <sub>5</sub> asphaltenes (b) C <sub>7</sub> asphaltenes precipitated at different S/B ratios with precipitation time = 24h .....	118
<b>Figure 5-11.</b> Relationship between GC Oven temperature and Distillation Temperature in SimDis .....	119
<b>Figure 5-12.</b> Subtraction of TGA curve from Simdis Curve of (a) C <sub>5</sub> maltenes (b) C <sub>7</sub> maltenes precipitated at different S/B ratios with precipitation time = 24h .....	121
<b>Figure 5-13.</b> (a) Correlation between MCR of asphaltenes and their yields.....	124

## CHAPTER 1. INTRODUCTION

### 1.1 Background

Canadian oil sands are the third largest oil reserves in the world. Oil sands are a mixture of sand, water, clay and bitumen. Bitumen is the heaviest form of petroleum, having a viscosity greater than  $10^5$  mPa.s and an API gravity lesser than  $10^\circ$ API at the standard temperature of  $15^\circ\text{C}$ .<sup>1</sup> Compared to conventional crude oil, bitumen has a lower H/C ratio, higher content of hetero atoms such as sulphur, nitrogen and oxygen, and higher content of metals such as nickel and vanadium.<sup>2</sup> The poor fluidity and associated chemical characteristics of bitumen make it unsuitable for pipeline transport. Dilution and upgrading are the two main strategies to improve the properties of bitumen and facilitate pipeline transport.<sup>1</sup>

Upgrading of bitumen is achieved by

- a. removal of undesirable components by chemical separations and/or
- b. transformation of the structure of the molecules by chemical reactions

During upgrading of bitumen using thermal cracking reactions, coke formation is a major issue, thus lowering the conversion to valuable liquid oil product. According to literature, a fraction called 'asphaltenes' is mainly responsible for coke formation during thermal cracking of petroleum residua and bitumen.<sup>3,4</sup> Asphaltenes are a solubility class of bitumen that are soluble in aromatic solvents such as toluene and insoluble in paraffinic solvents such as *n*-heptane.<sup>1</sup> Though they do not represent a unique compound class, they are characterized by high aromaticity and molecular weight.<sup>3</sup> Hence, it is desired to remove asphaltenes from bitumen through separation.

Solvent deasphalting (SDA) is a separation process in which asphaltenes are precipitated from bitumen by addition of paraffinic solvent. The remaining fraction of bitumen after separation of asphaltenes is called deasphalted oil (DAO). DAO is a partially upgraded product. The SDA process conditions that affect the yield and quality of DAO and asphaltenes are : type of solvent, solvent to bitumen (S/B) ratio, precipitation time, temperature and pressure.<sup>5,6</sup> The solvent is recovered from the product streams and recycled.

Asphaltenes from SDA process can be

- used as a road packing material (asphalt binder).<sup>7</sup>
- gasified to produce hydrogen for hydrocracking and hydrotreating processes.<sup>6</sup>
- treated by cracking and converted to feedstocks for other conversion processes.<sup>6</sup>

However, asphaltenes have a lower value compared to the DAO. Bitumen contains 14-20wt% of asphaltenes.<sup>2</sup> Removing all the asphaltenes from bitumen represents a significant loss of material. While SDA process is performed to remove compounds that are deleterious, it is possible that not all the molecules separated in the asphaltene phase are deleterious. According to literature, by varying the conditions of the asphaltene precipitation process the yield, molecular weight and chemical composition of the precipitate can be varied.<sup>2,8,9</sup>

On the other hand, DAO is

- sold as partially upgraded bitumen, i.e. intermediate between fully upgraded synthetic crude oil and diluted bitumen (DilBit) via pipeline
- further upgraded using processes such as delayed coking, catalytic cracking etc. to synthetic crude oil.<sup>6,10</sup>

The nature of DAO could have an impact on factors such as process conversion, catalyst deactivation and quality of the products and by-products of downstream conversion processes.

For the above mentioned reasons, it is important to study the effect of SDA conditions on the yield and properties of DAO and asphaltenes.

## **1.2 Objective and Scope of Work**

The objective of this work is to study the effect of solvent, S/B ratio and precipitation time on the yield and properties of DAO and asphaltenes in the SDA process.

The approach taken to accomplish this objective can be divided into three parts:

1. Literature review of SDA process and some important properties of bitumen fractions (Chapter 2)

2. Separation of bitumen into DAO and asphaltenes using different solvents, S/B ratios and precipitation times in the lab, along with feed characterization, yield measurements of the fractions and mass balance calculations (Chapter 3)
3. Characterization of the DAO and asphaltene samples using various techniques, followed by data analysis and interpretation (Chapter 4 and Chapter 5).

The conclusions from this work are summarized in Chapter 6.

### 1.3 Contribution to the work

The solvent deasphalting experiments and the characterization of the feed and products, except simulated distillation and elemental analysis were performed by me. Elemental analysis of the samples was performed by Analytical Chemistry department in University of Alberta. Simulated distillation analysis along with calibration and data generation were performed by my colleague, Cloribel Santiago Flores.

### 1.4 References

1. Gray, M. R., *Upgrading Oilsands Bitumen and Heavy Oil*. University of Alberta Press: Edmonton, Alberta, 2015.
2. Strausz, O. P. and Lown, E. M., *The Chemistry of Alberta Oil Sands, Bitumens and Heavy Oils*. Alberta Energy Research Institute: Calgary, 2003.
3. Wiehe, I. A., *Process Chemistry of Petroleum Macromolecules*. CRC Press: Boca Raton, 2008.
4. Rahimi, P., Gentzis, T., Dawson, W. H., Fairbridge, C., Khulbe, C., Chung, K., Nowlan, V. and DelBianco, A., Investigation of Coking Propensity of Narrow Cut Fractions from Athabasca Bitumen Using Hot-Stage Microscopy. *Energy & Fuels* **1998**, *12* (5), 1020-1030.
5. Speight, J. G., Long, R. B. and Trowbridge, T. D., Factors Influencing the Separation of Asphaltenes from Heavy Petroleum Feedstocks. *Fuel* **1984**, *63* (5), 616-620.
6. Speight, J. G., *Fouling in Refineries*. Elsevier: Amsterdam, 2015.
7. Lee, J. M., Shin, S., Ahn, S., Chun, J. H., Lee, K. B., Mun, S., Jeon, S. G., Na, J. G. and Nho, N. S., Separation of Solvent and Deasphalted Oil for Solvent Deasphalting Process. *Fuel Processing Technology* **2014**, *119*, 204-210.
8. Ancheyta Juárez, J., *Asphaltenes Chemical Transformation During Hydroprocessing of Heavy Oils*. Taylor & Francis: Boca Raton, 2009; p 461 p.

9. Luo, P., Wang, X. and Gu, Y., Characterization of Asphaltenes Precipitated with Three Light Alkanes under Different Experimental Conditions. *Fluid Phase Equilibria* **2010**, 291 (2), 103-110.
10. Hamidi Zirasefi, M., Khorasheh, F., Ivakpour, J. and Mohammadzadeh, A., Improvement of the Thermal Cracking Product Quality of Heavy Vacuum Residue Using Solvent Deasphalting Pretreatment. *Energy & Fuels* **2016**, 30 (12), 10322-10329.

## **CHAPTER 2. LITERATURE REVIEW ON SOLVENT DEASPHALTING PROCESS**

### **2.1 Introduction**

The purpose of this literature review is to gain an understanding of the key elements of the solvent deasphalting (SDA) process. As indicated in chapter 1, the end goal of the project is to study the effect of SDA process of bitumen on the properties of DAO and asphaltenes. The literature review focuses on three subtopics: 1. Characteristics of the feed (bitumen), 2. SDA process variables and methods and 3. Characteristics of the products (DAO and asphaltenes). This knowledge of existing scientific literature was applied in experimental planning, product analysis and data interpretation in this study.

### **2.2 Characteristics of Bitumen**

#### **2.2.1 Chemical Composition**

The elemental compositions of most bitumens are in the range: Carbon  $83.1 \pm 0.5\%$ , Hydrogen  $10.3 \pm 0.3\%$ , Nitrogen  $0.4 \pm 0.1\%$ , Oxygen  $1.1 \pm 0.3\%$ , Sulfur  $4.6 \pm 0.5\%$ .<sup>1</sup>

It is comprised of hydrocarbons principally of three types: paraffinic, naphthenic and aromatic.<sup>1</sup> The hydrogen to carbon (H/C) ratio, which is an important property of crude oils, is  $\sim 1.5$  for bitumen, whereas 2-2.3 for conventional crude oils.<sup>1</sup> This indicates the low paraffinic nature of bitumen.

Bitumen has a higher heteroatom (O,N,S) and metal content compared to conventional crude oils.<sup>1</sup> Table 2-1 shows the S, V, Ni contents of conventional crude oil and bitumen, along with the physical properties, viscosity and API gravity. The microbiological degradation of light crude oil during the cretaceous period led to the depletion of hydrogen rich (paraffinic) components and enrichment of sulfur and metals, making bitumen a heavy crude oil rich in naphthenic and aromatic type of hydrocarbons.<sup>1,2</sup>

**Table 2-1.** Properties of Conventional Crude Oil vs Bitumen.<sup>2</sup>

Crude Oil	Gravity (°API)	Viscosity (m <sup>2</sup> /s × 10 <sup>6</sup> ), at 40°C	Sulfur (wt%)	Nitrogen (wt%)	Metals (ppm by weight)
West Texas Intermediate	40.8	4	0.3	0.08	3.2
Athabasca Bitumen	9.0	7000	4.9	0.5	280

Physical properties such as viscosity, density, boiling point distribution (distillation curve) etc. can be correlated with the chemical composition of bitumen.<sup>1,2</sup>

### 2.2.2 SARA Fractionation

Based on solubility or adsorption characteristics, bitumen can be fractionated into four classes: saturates, aromatics, resins and asphaltenes.<sup>1,3</sup> This process is called SARA fractionation and the process is shown in Figure 2-1. Asphaltenes are precipitated from bitumen using *n*-pentane or *n*-heptane. The remaining portion of bitumen is called maltenes or deasphalted oil (DAO).

ASTM D2007, based on clay-gel chromatographic analysis, is used for separation of saturates, aromatics and resins.<sup>4</sup> Two percolation columns, the upper column containing clay and the lower column containing clay at the top section and silica gel at the bottom section, are connected in series. The heavy oil or bitumen sample, diluted with *n*-pentane is added from the top of the upper column. The polar compounds adsorb on clay, and the aromatics adsorb on silica gel. Saturates have poor affinity for both silica gel and clay, hence *n*-pentane is added in sufficient amounts to elute saturates from silica gel and clay. The upper and lower columns are then separated. The polar compounds are desorbed from clay by adding toluene-acetone mixture in 1:1 (v/v) ratio. Aromatics adsorbed on silica gel are desorbed using hot toluene. The solvents are evaporated from the separated fractions.

The composition of the SARA fractions in bitumen is in the following range: saturates 15-21%, aromatics 18-19%, resins 44-48% and asphaltenes 14-20%.<sup>1</sup>

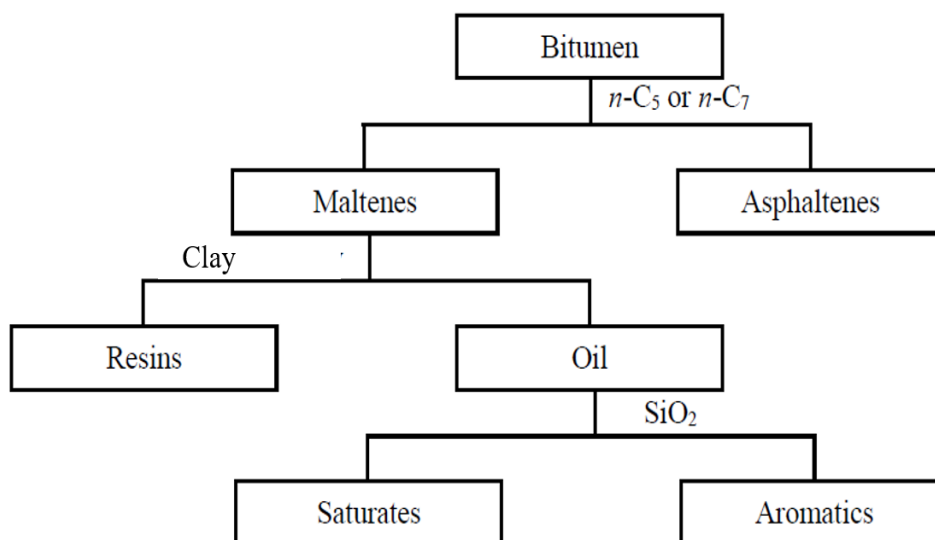


**Figure 2-1.** Process Diagram of SARA Fractionation.<sup>3</sup>

### 2.2.3 Distillation Profile of Bitumen

The boiling point distribution of Athabasca bitumen is shown in **Table 2-2**, obtained by using ASTM D1160.

**Table 2-2.** Mass loss upon distillation (volume %) vs. Boiling point (°C) of Athabasca Bitumen.<sup>2</sup>

Volume %	T <sub>b</sub> , °C
Initial	257
10	326
20	383
30	434
40	483
50	530
50.9	536

The boiling point of a fraction can be correlated with the average molar mass of the fraction.<sup>2</sup> The higher the molar mass, higher is the boiling point of the fraction. According to Speight,<sup>5</sup> generally speaking, the proportion of aliphatic compounds in crude oils decreases with increase in boiling point or molecular weight. As the boiling point increases, the proportion of naphthenes, aromatics

and naphtheno-aromatic compounds increases. Heteroatomic compounds are mainly present in the non-volatile (residue) fraction of the oil.<sup>5</sup>

#### 2.2.4 Density

American Petroleum Institute (API) gravity, a measure of density, is widely used in petroleum industry. The relationship between API gravity and density is given in Eq. 2-1.

$$^{\circ}API = \frac{141.5}{SG \text{ at } 15.6^{\circ}C} - 131.5 \quad \text{Eq. 2-1}$$

where SG is the specific gravity of crude oil or bitumen. API gravity greater than or equal to 19°API (940 kg/m<sup>3</sup>) at 15 °C is the specification for pipeline transport. The API gravity of bitumen is lesser than 10°API.

Density of heavy oils can be correlated with the elemental composition using Eq. 2-2,<sup>2</sup> at 15.6°C.

$$\rho = 1033 - 13.69H + 13.85S + 115.7N \quad \text{Eq. 2-2}$$

where  $\rho$  is the density of heavy oil in  $\frac{kg}{m^3}$ , and H, S, N are hydrogen, sulfur and nitrogen respectively, all in wt%. Thus, the density increases with increase in hydrogen content, and decreases in the presence of sulfur and nitrogen. The density further increases in the presence of trace metals.

Viscosity of a fluid is defined as its resistance to undergo deformation under shear stress. It is represented in two forms: dynamic viscosity and kinematic viscosity.

The SI units for dynamic viscosity are Pa.s, N.s/m<sup>2</sup> or Kg/(s.m), and the engineering units are centipoise (cP), where 1cP=1mPa.s. It is represented by the symbol  $\eta$  and given by Eq. 2-3.

$$\eta = \frac{\sigma}{\gamma} \quad \text{Eq. 2-3}$$

where  $\sigma$  is the shear stress in Pa and  $\gamma$  is the shear rate in s<sup>-1</sup>

Kinematic viscosity is the ratio between dynamic viscosity and density of the fluid. The SI units for kinematic viscosity are  $\text{m}^2/\text{s}$ , and the engineering units are centistokes (cSt), where  $1\text{cSt}=1\text{mm}^2/\text{s}$ . It is represented by the symbol  $\mu$ .

Viscosity lesser than or equal to 350 cSt at pipeline temperature, is the pipeline specification. The pipeline temperature depends on the ground along the pipeline. These temperatures usually range between 5 and  $38^\circ\text{C}$ .

The density and viscosity of bitumen are given in Table 2-1. Dilution or upgrading of bitumen is required in order to meet the pipeline specifications of density and viscosity.

Density and viscosity are dependent on temperature. They decrease with an increase in temperature. Eq. 2-4 and Eq. 2-5 can be used to calculate the density and viscosity respectively, at different temperatures.

$$\rho = \rho_0 - 0.62T \quad \text{Eq. 2-4}$$

$$\ln[\ln(\mu)] = a_1 + a_2\ln(T) \quad \text{Eq. 2-5}$$

where  $\rho$  is the density in  $\text{kg}/\text{m}^3$  at temperature  $T$  in units K,  $\rho_0$  is the density in  $\text{kg}/\text{m}^3$  at  $0^\circ\text{C}$  (273K),  $\mu$  is the viscosity in  $\text{mPa}\cdot\text{s}$ ,  $T$  is the temperature in K and  $a_1, a_2$  are adjustable parameters.

## 2.3 SDA Process

### 2.3.1 Industrial SDA Processes

SDA process separates asphaltenes from oil using a solvent-based extraction. The SDA process was described in detail by Speight, et al.<sup>6</sup> Heavy feedstock (such as vacuum residuum) is diluted with a little amount of solvent to reduce its viscosity and sent into an extraction tower at a point about one-third from the top of the tower. An alkane solvent is pumped from the solvent accumulator and enters the extraction tower from the bottom. The extraction tower normally contains multistage baffle trays, allowing the contact of solvent flowing in upward direction with the heavy feedstock flowing in the downward direction. The separation of asphaltenes (also called deasphalter bottoms or pitch) takes place and they move towards the bottom of the tower, while the DAO and solvent rise in the tower. The temperature at the top of the tower is controlled by

the temperature of the feed inlet and flow of steam to the heating coils located at the top of the tower. The bottom temperature of the tower is controlled by the temperature of the solvent stream.

The DAO-solvent mixture exits from the top of the tower and flows into a DAO separator. The solvent is evaporated from DAO using the heat supplied by low pressure steam. The solvent vapor is condensed and collected in a solvent accumulator, from where it is recycled to the extraction tower. The DAO goes into a flash tower equipped with a fired heater, where the residual solvent vaporizes and joins the solvent stream from the evaporator. The minor quantity of solvent present in the DAO is stripped out in a steam stripper at atmospheric pressure using super-heated steam.

The pitch-solvent mixture flows from the bottom of the extraction tower into a flash drum where the solvent is vaporized and sent into solvent accumulator. The remaining solvent is stripped out from the pitch in a steam stripper at atmospheric pressure using super-heated steam. The asphaltenes are pumped from the bottom of the steam stripper into storage.

The solvent type, solvent to oil ratio, temperature, pressure and contact time are the major process variables of the SDA process.<sup>1,6,7</sup> The yield and quality of the DAO and asphaltenes depend on these variables. The existing literature on the effect of process variables will be discussed in detail in section 2.3.3 of this chapter.

Different methods of SDA are used in industry. Low energy deasphalting (LEDA) process, Demex process, MDS process, Residuum Oil Supercritical Extraction (ROSE) process, Solvahl process and Lube deasphalting are the different types of SDA processes.<sup>6</sup> These processes differ in their process conditions, design and the desired qualities of DAO. These methods are described in the subsections 2.3.1.1 to 2.3.1.6 using the process description given by Speight.<sup>6</sup>

### **2.3.1.1 Low Energy Deasphalting (LEDA) process**

In the LEDA process, heavy feedstock such as vacuum residue is diluted with a low-boiling solvent such as propane to reduce its viscosity. The temperature of the mixture is lowered to the extraction temperature and fed to a rotating disk contactor (RDC). RDC has more extraction stages than a baffle-type column or a mixer-settler. This allows production of higher yield of DAO at the same quality or higher DAO quality at the same yield. The solvent is recovered from DAO and recycled into the bottom portion of the RDC, after adjusting its temperature. In the RDC, the vacuum residue

flows downwards and the solvent flows upwards, extracting more paraffinic components from the feed, while rejecting aromatic components.

The DAO-solvent mixture leaves the extraction tower from the top and sequentially flows through an evaporator, high pressure flash tower, pressure vapor heat exchanger, low pressure flash tower, reboiler and superheated steam stripper, where the solvent is recovered from DAO. Similarly, solvent is removed from the deasphalter bottoms, by flashing the volatiles, followed by superheated steam stripping. The recovered solvent vapors from DAO and deasphalter bottoms are condensed and recycled.

### **2.3.1.2 DEMEX process**

Demetallization of vacuum residue with a high metal content is achieved by solvent extraction in the DEMEX process. The products of this process are demetallized oil, that has a low metal content and asphaltenes, that has a high metal content. The feedstock is mixed with the DEMEX solvent before it is sent into the first stage extractor, where constituents of asphaltenes are separated. The overhead from first stage extractor is extracted with hot solvent in the second-stage extractor to remove constituents of resins and aromatics of high molecular weight. The bottoms of the second stage extractor are recycled back to the first stage extractor. The second stage overhead is heated with hot solvent. The temperature of the mixture is raised above the critical temperature of the solvent using a fired heater, resulting in the separation of demetallized oil from the mixture.

The solvent circulation required in this process is low, reducing the size of the process unit and the utility costs. The solvent vapors from the demetallized oil and bottoms are flashed, steam stripped, condensed and then sent into a supercritical separator. The solvent stream, which is hot, is used for heat exchange in the process.

### **2.3.1.3 MDS process**

In the MDS process, the feed-solvent mixture is fed to a deasphalting tower. The extraction takes place in the upper half portion of the tower. The deasphalter bottoms comes into contact with solvent flowing in countercurrent direction, which extracts oil from the bottoms fraction. After separation of the bottoms, the DAO-solvent mixture flows from the top of the tower into a heating furnace and flash tower, to remove most of the solvent under pressure. The remaining smaller amount of solvent is removed by heating, followed by stripping operation. Similarly, the

deasphalter bottoms, which accumulate at the bottom of the deasphalting tower, are sent into a heating furnace, flash tower and asphalt stripper to remove the solvent. The solvent recovered from deasphalter bottoms and DAO is condensed and recycled.

#### **2.3.1.4 ROSE process**

Supercritical solvents are used in the ROSE process. Low boiling solvents such as pentane, butane and propane are used as solvents depending on the nature of feedstock and desired characteristics of DAO. The feed is blended with several fold-volume of the liquefied solvent in a mixer at high temperature and pressure. The mixture is sent into a separator, where asphaltenes are precipitated from the feed by the solvent flowing in countercurrent direction. The overhead solution is fed to a second stage separator, where it is subjected to a higher temperature. In this stage the resins are separated. The overhead solution from the second stage is fed to a third stage separator, where it is subjected to supercritical temperature. In this stage, the insoluble oil constituents are separated.

The extracted oil-solvent mixture from the top of the third separator flows into an oil separator, followed by a steam stripper, where solvent is separated and recycled. The solvent from the asphaltenes is removed by heating and steam stripping, and then recycled. The advantages of this process are flexibility and precise blending of constituents to desired compositions. Typically, the process efficiency when propane is used is ~75-83%.

#### **2.3.1.5 Solvahl Process**

High yields of higher quality DAO is obtained in the Solvahl process by using solvents in the range C<sub>4</sub>-C<sub>5</sub> at low solvent to oil ratios. Asphaltenes separated in this process have a high softening point, and hence appear as pellets. The metal content of the feed is reduced to a level that is compatible with the downstream operations.

#### **2.3.1.6 Lube Deasphalting**

The Lube deasphalting process is used to remove heavy asphaltic materials from lubricating oil. Propane is mixed with the feed in a baffle tower or RDC. Solvent is recovered using evaporators or supercritical solvent recovery processes. In the Duo-Sol process, batch extractions in series are used to deasphalt lubricating oil with propane and using a mixture of phenols and cresylic acids such as cresols and hydroxyl toluenes as extraction solvent. Solvent recovery takes place in multistage flash distillation units and stripping towers.

### 2.3.1.7 Nexen's SDA Process

In Nexen's partial upgrading process, asphaltenes separation from bitumen takes place in two stages. The first separator is maintained at 160°C and the second separator is maintained at 140°C. Paraffinic solvents such as 100% *n*-pentane, a blend of 60wt% *i*-pentane, 25wt% *n*-pentane, 15wt% *n*-hexane are used in this process at a solvent to feed ratio of  $1.7 \pm 0.3$  wt/wt. The aim of this process is to separate 80wt%± 20wt% of the *n*-pentane insolubles originally present in bitumen.

### 2.3.2 Analytical Methods for Asphaltenes Precipitation

Standard analytical methods for asphaltenes precipitation from petroleum feedstocks are listed in Table 2-3. *n*-pentane and *n*-heptane are used as precipitants.<sup>6,7</sup> These methods recommend a solvent to oil ratio of 10-50ml/g when *n*-pentane is used, and >30ml/g when *n*-heptane is used.<sup>7,8</sup> The recommended contact times for *n*-pentane are 0.5-15h and for *n*-heptane 1-24h.<sup>7</sup> Some methods also use heat to warm up the solvent-oil mixture, and during filtration.<sup>7</sup>

**Table 2-3.** Standard Methods for Asphaltenes Precipitation.<sup>6,7</sup>

<b>Method</b>	<b>Precipitant</b>	<b>Precipitant to sample ratio (ml/g)</b>
ASTM D893	<i>n</i> -pentane	10
ASTM D2007	<i>n</i> -pentane	10
ASTM D2006	<i>n</i> -pentane	50
ASTM D6560	<i>n</i> -heptane	30
ASTM D3279	<i>n</i> -heptane	100
ASTM D4124	<i>n</i> -heptane	100
IP 143	<i>n</i> -heptane	100

### **2.3.3 Process Variables**

#### **2.3.3.1 Solvent**

The choice of solvent plays an important role in determining not just the yield and quality of DAO, but the operating flexibility of the unit. The operating limits of temperature would depend on the type of solvent used. The temperature has to be maintained below the critical temperature of the solvent but not too low to increase the viscosity of the feedstock.<sup>6</sup> Liquid propane is the most widely used solvent for deasphalting lighter hydrocarbons.<sup>6</sup> The operating temperature is maintained below 82°C when propane is used, as its critical temperature is 97°C.<sup>6</sup> This makes propane unsuitable as solvent for deasphalting heavy or high viscosity feedstocks. For heavy feedstocks a higher temperature is needed to reduce their viscosity and allow good mixing with the solvent. *n*-butane and iso-butane are suitable as their critical temperatures are higher than propane (152°C and 134°C respectively).<sup>6</sup> It is reported in literature that with increase in the carbon number of *n*-alkane solvent, the yield of asphaltene fraction decreases, and the molecular weight and aromaticity of the precipitated asphaltene increase.<sup>1,9</sup> A blend of solvents is used in the SDA process when it is required to handle feedstocks varying from light to heavy oils and/or to produce variable yields of DAO.<sup>6</sup>

#### **2.3.3.2 Solvent to Oil Ratio**

The solvent to oil ratio is determined by the properties of feedstock (such as viscosity) and the desired characteristics of the DAO.<sup>6</sup> Industries use S/B ratios of 3:1 to 10:1 due to high costs of solvent recovery.<sup>2,6</sup> According to literature, the amount of asphaltene precipitated increases with increase in solvent to bitumen (S/B) ratio, and reaches a saturation.<sup>1</sup> For *n*-pentane-bitumen mixture, the asphaltene yield reaches saturation at a S/B ratio of 30ml/g.<sup>1</sup> In a study on solvent deasphalting of heavy vacuum residue by Hamidi Zirasefi, et al.<sup>10</sup> it was observed that the coke yield of thermal cracking of DAO decreased with an increase in solvent to feed ratio when *n*-pentane was used as precipitant in the deasphalting process.

#### **2.3.3.3 Temperature**

As mentioned earlier, the lower limit of operating temperature is determined by the viscosity of the feedstock and the upper limit by the critical temperature of the solvent. The temperature gradient in the extraction tower also influences the separation.<sup>6</sup> It was reported in literature, that when *n*-alkane (C<sub>5</sub>-C<sub>8</sub>) solvents are used, the amount of asphaltene precipitated decreases with

increase in temperature, indicating that the solubility of asphaltenes in n-alkane solvents increases with a rising temperature.<sup>1</sup> Temperature was also found to affect the molecular weight of the precipitate.<sup>1</sup> At higher temperatures, the lower molecular weight material tends to remain soluble in solution leading to precipitation of higher molecular weight fraction.<sup>1</sup> So, as temperature increases, the molecular weight of the precipitate increases.

#### **2.3.3.4 Pressure**

The operating pressure is always maintained higher than the vapor pressure of the solvent to ensure that it remains in liquid phase.<sup>6</sup> According to literature, the solubility of asphaltenes in crude oil increases with increase in pressure when C<sub>3</sub>, C<sub>5</sub>, C<sub>6</sub> and C<sub>7</sub> solvents are used.<sup>1</sup> In case of Venezuelan crude oil, the solubility of asphaltenes is affected by pressure above bubble point.<sup>1</sup> Above the bubble point, solubility increases with increase in pressure (changes in pressure are of the order of MPa) and below the bubble point the effect of pressure is overruled by changes in composition.<sup>1</sup>

#### **2.3.3.5 Contact Time**

In most of the previous studies, the effect of contact time on precipitation of asphaltenes was neglected. In general, a precipitation time of few hours to two days is used for experimental studies.<sup>7,11</sup> The yield of asphaltenes is assumed to reach a constant value in that duration. However, Maqbool, et al.<sup>11</sup> studied the kinetics of asphaltenes precipitation for crude oils over extended periods of time varying from 0 to 2000h at different solvent to oil ratios. It was observed that the onset of precipitation and the time at which the asphaltenes precipitation reaches equilibrium depend on the solvent to oil ratio. In their study, at lower solvent to oil ratios, the onset time was several months. Hence, from their study it was concluded that contact time could play an important role in experimental studies involving asphaltenes precipitation and should not be neglected. These results indicate that solvent deasphalting is a kinetic process.

#### **2.3.4 Solubility Parameters**

Solubility parameter, denoted by the symbol  $\delta$ , is a measure used to predict the solubility behavior of substances. According to Hildebrand, solubility parameter of non-polar liquids is related to internal pressure or cohesive energy density.<sup>1</sup> It is expressed in two forms  $\delta_1$  and  $\delta_2$ , given in Eq. 2-6 and Eq. 2-7.

$$\delta_1 = \gamma V^{-1/3} \quad \text{Eq. 2-6}$$

where  $\delta_1$  is the solubility parameter ( $\text{J}\cdot\text{mol}^{1/3}\cdot\text{m}^{-3}$ ),  $\gamma$  is the surface tension ( $\text{J}\cdot\text{m}^{-2}$ ) and  $V$  is the molar volume ( $\text{m}^3\cdot\text{mol}^{-1}$ ),<sup>1</sup> and

$$\delta_2 = \sqrt{c} = \sqrt{\frac{\Delta E_v}{V}} = \sqrt{\frac{\Delta H_v - RT}{V}} \quad \text{Eq. 2-7}$$

where  $c$  is the cohesive energy density defined as the energy of vaporization per unit molar volume,  $\Delta E_v$  is the energy of vaporization,  $\Delta H_v$  is the heat (enthalpy) of vaporization,  $R$  is the universal gas constant and  $T$  is the temperature.<sup>1</sup> The solubility parameter  $\delta_2$  is expressed in units  $\text{MPa}^{1/2}$ . Between  $\delta_1$  and  $\delta_2$ ,  $\delta_2$  is the most widely used form of Hildebrand solubility parameters.<sup>1</sup>

Eq. 2-7 indicates that there exists a correlation between vaporization and solubility behavior of the liquid. The intermolecular attractive forces holding the molecules of the liquid together must be overcome to vaporize it. And the same forces must be overcome to dissolve it or mix the liquid with another. Hence, solubility parameter is a reflection of the strength of intermolecular forces of the substance. The linear chain length, degree of branching, shape of the molecule, number of bonds (single/double/triple) etc. affect the intermolecular forces in organic compounds. Hence the solubility parameter of a substance would also depend on these factors.

Solubility parameters of mixtures can be calculated using Eq. 2-8.

$$\delta = \sum \phi_i \delta_i = \frac{\sum x_i V_i \delta_i}{\sum x_i V_i} \quad \text{Eq. 2-8}$$

where  $\phi_i$ ,  $\delta_i$ ,  $x_i$ ,  $V_i$  are the volume fraction, solubility parameter, mole fraction and molar volume respectively of component 'i'.

The solubility behavior and precipitation of asphaltenes in solvents and solutions can be predicted using the concept of solubility parameters. Figure 2-2 shows the precipitation of asphaltenes from Athabasca bitumen in non-polar solvents, both pure and solvent blends, as a function of Hildebrand solubility parameters  $\delta_1$  and  $\delta_2$ . With increase in solubility parameter the solubility of asphaltenes increases, thus leading to lesser precipitation.<sup>1</sup>

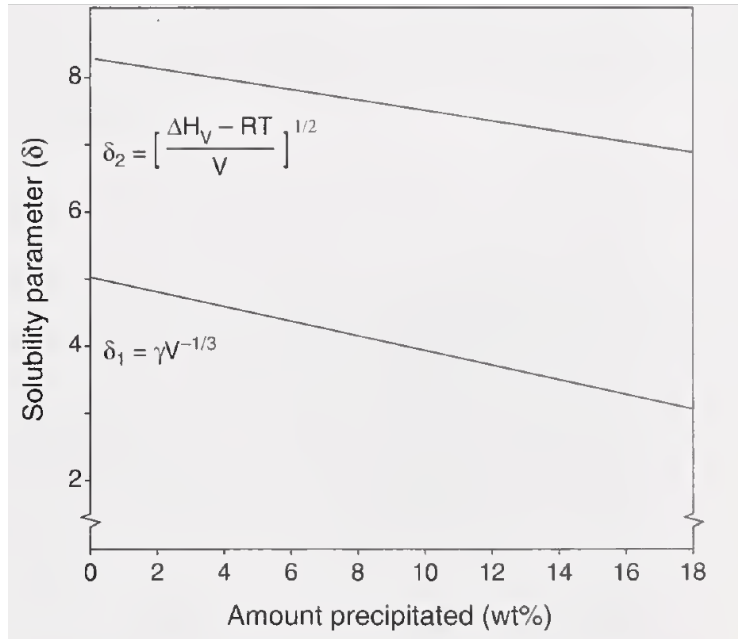


**Figure 2-2.** Relation between solubility parameter and amount of asphaltenes precipitated from bitumen.<sup>1</sup>

As the intermolecular forces in non-polar liquids are predominantly London dispersion forces, Hildebrand solubility parameters do not take into account the polar and hydrogen bonding interactions in the substances. Hence the concept of three dimensional (3D) solubility parameters was later developed to take into consideration the polar and hydrogen bonding forces.<sup>1</sup> The 3D solubility parameter ( $\delta$ ) can be expressed as the sum of three components called Hansen solubility parameters as given in Eq. 2-9.

$$\delta = \sqrt{\delta_D^2 + \delta_P^2 + \delta_H^2} \quad \text{Eq. 2-9}$$

where  $\delta_D$  corresponds to the dispersion forces between molecules and is nearly equal to the  $\delta_2$  values,  $\delta_P$  corresponds to the polar forces and  $\delta_H$  corresponds to the hydrogen bonding interactions between the molecules.<sup>1</sup> Figure 2-3 provides a list of 3D solubility parameters of various solvents.

Solvent	Molar volume $V$	Parameters (MPa <sup>1/2</sup> )			
		$\delta_D$	$\delta_P$	$\delta_H$	$\delta(\text{total})$
benzene	89.4	18.4	0	2.0	18.5
methyl chloride	55.4	15.3	6.1	3.9	16.9
methylene chloride	63.9	13.4	11.7	9.6	20.2
chloroform	80.7	17.8	3.1	5.7	19.0
carbon tetrachloride	97.1	17.8	0	0.6	17.8
tetrahydrofuran	81.7	16.8	5.7	8.0	19.5
diethyl ether	104.8	14.5	2.9	5.1	15.6
acetone	74.0	15.5	10.4	6.9	19.9
acetophenone	117.4	19.6	8.6	3.7	21.7
methyl <i>isobutyl</i> ketone	125.8	15.3	6.1	4.1	17.0
methyl <i>isobutyl</i> ketone	142.8	15.9	5.7	4.1	17.4
nitrobenzene	102.7	17.6	14.0	0.0	22.5
pyridine	80.9	19.0	8.8	5.9	21.8
aniline	91.5	19.4	5.1	10.2	22.5
quinoline	118.0	19.4	6.9	8.9	22.4
carbon disulfide	60.0	20.4	0	0.6	20.4
dimethyl sulfoxide	71.3	18.4	16.3	10.2	26.6
dimethyl sulfone	75.0	19.0	19.4	12.2	29.8
benzyl alcohol	103.6	18.4	6.3	13.7	23.8
cyclohexanol	106.0	17.4	4.1	13.5	22.4
<i>o</i> -dichlorobenzene	112.8	18.0	9.8	0.0	20.5
water <sup>b</sup>	18.0	15.5	15.9	42.2	47.7
asphaltene <sup>c</sup>		20.2	2.0	4.0	20.7
asphaltene					20.3
naphthalene		19.2	2.0	3.9	19.7
$\alpha$ -methylnaphthalene		20.6	0.8	4.7	21.2
phenanthrene					20.0
anthracene					20.3
pentene-1		13.9	4.1	-	14.5
hexene-1		14.4	3.9	-	15.0
heptene-1		14.6	3.6	2.7	15.3
octene-1		15.0	3.5	2.3	15.5
none-1		15.4	3.4	-	15.8
decene-1		15.7	3.3	1.3	16.0
cyclopentene		15.3	5.8	4.1	16.9
methylcyclopentane		15.7	3.5	0.0	16.0
ethylcyclopentane		15.9	3.3	0.0	16.2
ethylcyclohexane		16.1	2.6	0.0	16.3
undecane		16.0	0.0	0.0	16.0
dodecane		16.2	0.0	0.0	16.2

**Figure 2-3.** 3D solubility parameters of liquids at 25°C.<sup>1</sup>

Though the major intermolecular forces in asphaltenes are dispersion forces, they still contain some polar and hydrogen bonding interactions due to the presence of heteroatoms and polar functional groups. Hence, Hansen solubility parameters provide an accurate prediction of solubility behavior of asphaltenes in polar media over the Hildebrand solubility parameters.

According to Wiehe,<sup>12</sup> earlier investigators had concluded that dipole interactions in liquids are not significant. Thus, the polar component of solubility parameter can be neglected. Two

dimensional (2D) solubility parameters were later developed, to determine the solvent power of liquids. The 2D solubility parameter ( $\delta$ ) of a liquid is a combination of two components,  $\delta_f$  and  $\delta_c$ , as indicated in Eq. 2-10.  $\delta_f$  is called the field force solubility parameter component and it represents the dispersive interactions. The electron donor- electron acceptor interactions between molecules that have random spatial orientations (however, the interactions depend on the separation distance between them) are also represented by  $\delta_f$ .  $\delta_c$  is called complexing solubility parameter component and represents hydrogen bonding interactions and electron donor- electron acceptor interactions caused by dipole moment between molecules that have a specific spatial orientation. This reduces the number of components in the solubility parameter from three to two, and makes it more convenient to use solubility parameters.

$$\delta = \delta_f^2 + \delta_c^2 \quad \text{Eq. 2-10}$$

where  $\delta_f \geq 0$  and  $\delta_c \geq 0$ .

For a mixture (M) of N liquids, the 2D solubility parameters are given by Eq. 2-11 and Eq. 2-12.

$$\delta_f^M = \sum_1^N \varphi_i \delta_{fi} \quad \text{Eq. 2-11}$$

$$\delta_c^M = \sum_1^N \varphi_i \delta_{ci} \quad \text{Eq. 2-12}$$

where  $\varphi_i$  is the volume fraction of the liquid 'i' in the mixture, and  $\delta_{fi}$  and  $\delta_{ci}$  are the field force solubility parameter component and complexing solubility parameter component respectively of liquid 'i'.

It has been reported in literature that the volume of n-paraffin required for 'onset' of asphaltene precipitation increases upto C<sub>9</sub> and then decreases, suggesting that n-paraffinic solvents with higher carbon number can be poor solvents for asphaltene.<sup>13</sup> However, the amount of asphaltene precipitated decreases with increase in carbon number of n-paraffinic solvents, indicating that higher carbon numbered n-paraffins are better solvents, which is also in agreement with solubility parameters.<sup>1,13</sup> These two observations are contradictory.

According to Wiehe, et al.<sup>13</sup> this paradox can be explained by Gibbs free energy of mixing ( $\Delta G_m$ ). Eq. 2-13 shows the thermodynamic equation for Gibbs free energy:<sup>1</sup>

$$\Delta G_m = \Delta H_m - T\Delta S_m \quad \text{Eq. 2-13}$$

While solubility parameter represents the heat (enthalpy) of mixing ( $\Delta H_m$ ), Gibbs free energy combines it with the entropy of mixing ( $\Delta S_m$ ) of molecules of dissimilar sizes.<sup>13</sup> At higher carbon numbers of the n-paraffin precipitant, Gibbs free energy of mixing increases with increase in carbon number resulting in decrease in the volume of the solvent required at flocculation point.<sup>13</sup> In the study by Wiehe, et al.<sup>13</sup> the need to improve the accuracy of solubility parameters was indicated. Approximations were made to Flory-Huggins thermodynamic equation (RF-HM Model) of Gibbs free energy,<sup>13,14</sup> to calculate the ‘effective’ solubility parameters that can be used to predict the onset of asphaltene precipitation.

In the work by Nikooyeh and Shaw,<sup>15</sup> it was shown that enthalpy of solution and partial specific volume are independent of Hildebrand and Hansen solubility parameters of asphaltene-diluent mixtures, and these values were inconsistent with the concepts of regular solution theory in thermodynamics. It was concluded that solubility parameter and simple thermodynamic theories of solutions cannot accurately describe the behavior of asphaltene-diluent mixtures. In their study, mixtures of asphaltenes from Athabasca bitumen and Maya crude oil and various solvents, at infinite dilution, were used. The need to develop a detailed understanding of the physiochemical phenomena occurring in asphaltene-diluent mixtures was indicated in their study.

Mannistu, et al.<sup>16</sup> measured the solubility of asphaltenes in various organic solvents and compared with the predicted solubility from the models they had developed based on Scatchard-Hildebrand solubility parameters theory. Solvents used in this study were normal alkanes, branched alkanes, cycloalkanes, aromatics etc. The single component solubility parameter models successfully predicted the solubility behavior of asphaltenes in non-polar and slightly polar organic solvents. The accuracy of prediction improved when three component solubility parameter models were used. However, both the single and three component models failed to adequately predict the solubility of asphaltenes in highly polar solvents. It was also found that these models failed to predict the solubility of asphaltenes in mixtures of cycloalkanes and normal alkanes.

## **2.4 Some Important Properties of the Products**

### **2.4.1 Elemental Composition**

H/C ratio is an important indicator of the product quality. The value of the product is more if the H/C ratio is more. Lower H/C ratios imply high aromatic or low paraffinic nature of the product. The density, boiling point and microcarbon residue (MCR) can be correlated with H/C ratio.<sup>1,17</sup>

Compounds that contain nitrogen can lead to inhibition of acid catalysts during cracking reactions.<sup>18</sup> Some nitrogen-containing compounds are also responsible for gum formation in fuel oil products.<sup>18</sup> Liquid density or API gravity can be correlated with the Nitrogen and sulfur content.<sup>2</sup> As shown in Eq. 2-2, the density increases with increase in nitrogen and sulfur content. Oxygen is mainly present in the carboxyl group of naphthenic acids, which can lead to corrosion in refining processes.<sup>2</sup> V, Ni and Fe are the metals present in highest concentration in bitumen, and thus also in its fractions.<sup>2,18</sup> These metals lead to catalyst deactivation in upgrading processes.<sup>18</sup>

Generally, the heteroatom and metal content is higher in high boiling fractions of bitumen.<sup>1,2</sup> SDA process concentrates these compounds in the asphaltenes fraction which has a low H/C ratio compared to the DAO.

### **2.4.2 Refractive Index of Liquids**

Refractive index is defined as the ratio of speed of light in vacuum to the speed of light in a medium.<sup>3</sup> According to literature, there exists a relation between refractive index, molecular weight, density and chemical structures of hydrocarbons.<sup>19</sup> The refractive index of paraffins < naphthenes < aromatics within a specific boiling range and the refractive index for any compound class increases with increase in molecular weight.<sup>19</sup> “Refractive index may be used as an indicator of the degree of upgrading for similar boiling range fractions”.<sup>3</sup>

### **2.4.3 Free radical content**

Free radicals are species that contain an unpaired electron, which potentially makes them very reactive. Free radicals participate in hydrogen transfer, oxidation and polymerization reactions in petroleum upgrading and refining processes. According to literature, free radicals in asphaltenes also play a role in aggregation and de-aggregation of asphaltenes when dissolved in solvents, and vanadium free radicals could lead to catalyst deactivation in upgrading and refining processes.<sup>20</sup>

For these reasons, it is important to measure the free radical concentration, in order to develop methods to modify or reduce the free radicals present in asphaltenes.

It is reported that asphaltenes and resins contain a very high free radical concentration of  $8.9 \times 10^{18}$  /g and  $1.2\text{-}2.5 \times 10^{17}$  /g respectively.<sup>21</sup> The free radical content is measured using the Electron Spin Resonance (ESR) spectrometry. According to literature, the central organic radical peak, having a g-factor of  $\sim 2.003$  is exhibited by the polycyclic aromatic carbocations present in asphaltenes.<sup>22</sup> The presence of paramagnetic  $\text{VO}^{+2}$  ions (valency of vanadium = 4) in asphaltenes displays a signal in ESR spectrum of asphaltenes.<sup>22</sup> The g-factor of vanadyl ion is  $\sim 1.96$ .<sup>23</sup> In the previous studies, it was observed that the vanadyl or  $\text{VO}^{+2}$  ions generate multiple peaks due to hyperfine splitting.<sup>1,22,20</sup> The ESR spectrum of Athabasca asphaltenes is shown in Figure 2-4.

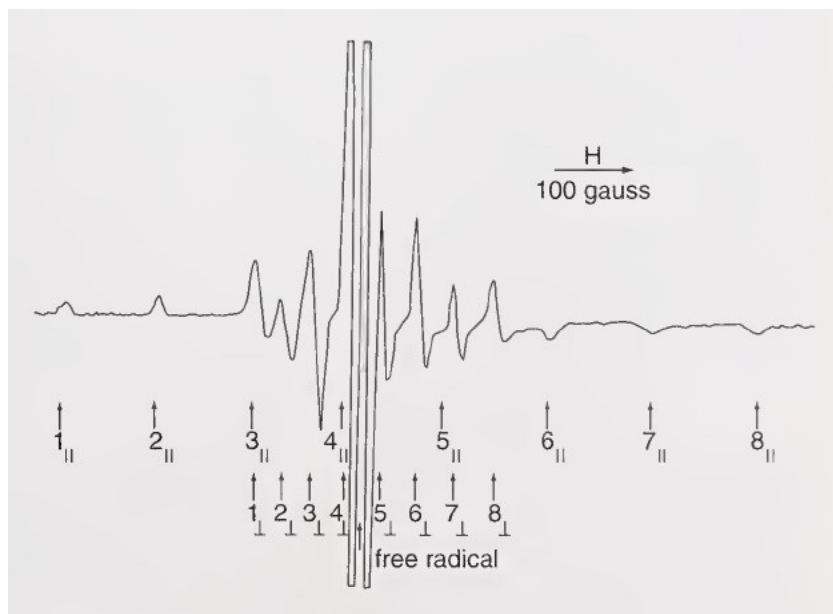


**Figure 2-4.** ESR spectrum of Athabasca asphaltenes.<sup>1</sup>

#### 2.4.4 Distillation Curve

The separation of chemical substances by virtue of differences in their vapor pressures is called distillation. Fractions of the material are separated based on their boiling ranges as shown in Table 2-4. The fractions not just differ in their boiling ranges but their chemical composition and other physical properties. For complex mixtures, the boiling ranges of the fractions overlap at cut points.

5-10% of the material boils below the minimum cut point and 5-10% of the material boils above the maximum cut point.<sup>2</sup>

**Table 2-4.** Distillation Fractions commonly used in Upgrading and Refining of Crude Oils and Bitumen.<sup>2</sup>

Name	Boiling Range, °C	Uses
Naptha	26-193	Reformed for gasoline or bitumen diluent
Kerosene	165-271	Jet fuel or gasoline blend
Light gas oil (LGO)	215-321	Diesel fuel or jet fuel
Heavy gas oil (HGO)	321-426	Feedstock for catalytic cracker or hydrocracker
Vacuum gas oil (VGO)	426-565	Feedstock for catalytic cracker or hydrocracker
Vacuum residue (resid or residuum)	>524-565	Asphalt or feedstock for coker or hydroconversion unit

#### 2.4.5 Coking Tendency

Coke is the byproduct of thermal cracking reactions of petroleum feeds. Asphaltenes are mainly responsible for coke formation. Thermal cracking of DAO or maltenes also produces some coke. A series of condensation and polymerization reactions take place during thermal cracking of petroleum feeds, leading to increase in aromaticity and molar mass.<sup>2,12,24</sup> During this process, oils form asphaltenes which self-associate and phase separate to form a second ordered liquid phase, called mesophase, which ultimately leads to coke formation.<sup>24</sup>

Microcarbon residue (MCR) is a measure of coking tendency. MCR is defined as the solid residue left after the oil sample is heated to 500°C.<sup>2</sup> ASTM D4530 is the standard method for testing MCR.<sup>2</sup> The coke formed in a delayed coker is 1.7 times the MCR content of the feed.<sup>2</sup>

#### 2.4.6 Melting point of asphaltenes

In the SDA process, it is important to maintain the temperature of the asphaltenes stream in order to keep them in a fluid state.<sup>6</sup> Solid phase separation of asphaltenes at low temperatures can cause fouling and plugging of the process equipment.<sup>6</sup> When the asphaltenes are present as solids, a

liquid phase is still necessary for slurry transport. The SDA process variables not only affect the yield and chemical composition of products, but may also affect their thermal behavior.

Asphaltenes are a complex mixture that do not have a defined melting point.<sup>25</sup> Previous differential scanning calorimetry (DSC) studies on asphaltenes from crude oil vacuum residuum reported that softening and liquefying occurs in the temperature range between 100 and 230°C.<sup>26</sup> In the study by Kopsch on pyrolysis of asphaltenes in inert atmosphere using DSC, the glass transition temperatures of asphaltenes at different heating rates were determined, and used to calculate a hypothetical melting point temperature using approximations. The calculated melting point temperature fell in the temperature range of pyrolysis of asphaltenes.<sup>25</sup>

## 2.5 Conclusions

- The solvent deasphalting is considered to be promising and is widely used in petroleum industry. However, the effect of the process conditions on the properties and performance of the products has not been studied extensively. Hence, there is a scope for comprehensive investigation on this topic.
- In order to study the effect of solvent deasphalting process conditions on the behavior of asphaltenes and DAO in thermal cracking and downstream processes, it would be important to measure some of the crucial properties of bitumen and its fractions such as elemental composition, density, boiling point profile, free radical content, microcarbon residue, refractive index and melting point.
- As the physical properties of bitumen and its fractions depend on their chemical composition, it is important to perform chemical characterization of bitumen and its fractions to support the observations on physical properties and to determine the governing compositional origin for those observations.

## 2.6 References

1. Strausz, O. P. and Lown, E. M., *The Chemistry of Alberta Oil Sands, Bitumens and Heavy Oils*. Alberta Energy Research Institute: Calgary, 2003.
2. Gray, M. R., *Upgrading Oilsands Bitumen and Heavy Oil*. University of Alberta Press: Edmonton, Alberta, 2015.
3. Yanez Jaramillo, L. M. Visbreaking of Oilsands Bitumen between 150° and 300°C. MSc Thesis, University of Alberta, Edmonton, AB, Canada, 2016.

4. Barman, B. N., Hydrocarbon-Type Analysis of Base Oils and Other Heavy Distillates by Thin-Layer Chromatography with Flame-Ionization Detection and by the Clay—Gel Method. *Journal of Chromatographic Science* **1996**, 34 (5), 219-225.
5. Speight, J. G., *Handbook of Petroleum Analysis*. Wiley-Interscience: New York, 2001.
6. Speight, J. G., *Fouling in Refineries*. Elsevier: Amsterdam, 2015.
7. Speight, J. G., Long, R. B. and Trowbridge, T. D., Factors Influencing the Separation of Asphaltenes from Heavy Petroleum Feedstocks. *Fuel* **1984**, 63 (5), 616-620.
8. Ancheyta Juárez, J., *Asphaltenes Chemical Transformation During Hydroprocessing of Heavy Oils*. Taylor & Francis: Boca Raton, 2009; p 461 p.
9. Luo, P., Wang, X. and Gu, Y., Characterization of Asphaltenes Precipitated with Three Light Alkanes under Different Experimental Conditions. *Fluid Phase Equilibria* **2010**, 291 (2), 103-110.
10. Hamidi Zirasefi, M., Khorasheh, F., Ivakpour, J. and Mohammadzadeh, A., Improvement of the Thermal Cracking Product Quality of Heavy Vacuum Residue Using Solvent Deasphalting Pretreatment. *Energy & Fuels* **2016**, 30 (12), 10322-10329.
11. Maqbool, T., Balgoa, A. T. and Fogler, H. S., Revisiting Asphaltene Precipitation from Crude Oils: A Case of Neglected Kinetic Effects. *Energy & Fuels* **2009**, 23 (7), 3681-3686.
12. Wiehe, I. A., *Process Chemistry of Petroleum Macromolecules*. CRC Press: Boca Raton, 2008.
13. Wiehe, I. A., Yarranton, H. W., Akbarzadeh, K., Rahimi, P. M. and Teclemariam, A., The Paradox of Asphaltene Precipitation with Normal Paraffins. *Energy & Fuels* **2005**, 19 (4), 1261-1267.
14. Wang, J. X. and Buckley, J. S., A Two-Component Solubility Model of the Onset of Asphaltene Flocculation in Crude Oils. *Energy & Fuels* **2001**, 15 (5), 1004-1012.
15. Nikooyeh, K. and Shaw, J. M., On the Applicability of the Regular Solution Theory to Asphaltene + Diluent Mixtures. *Energy & Fuels* **2012**, 26 (1), 576-585.
16. Mannistu, K. D., Yarranton, H. W. and Masliyah, J. H., Solubility Modeling of Asphaltenes in Organic Solvents. *Energy & Fuels* **1997**, 11 (3), 615-622.
17. Speight, J. G., *The Chemistry and Technology of Petroleum, Fifth Edition*. CRC Press: Hoboken, 2014.
18. Speight, J. G., *Petroleum Refining Processes*. Marcel Dekker ;: New York :, 2001.
19. Wauquier, J.-P., *Petroleum Refining, Volume 1 - Crude Oil, Petroleum Products, Process Flowsheets*. Editions Technip: 1995.

20. Khulbe, K. C., Mann, R. S., Lu, B. C. Y., Lamarche, G. and Lamarche, A. M., Effects of Solvents on Free Radicals of Bitumen and Asphaltenes. *Fuel Processing Technology* **1992**, 32 (3), 133-141.
21. *Asphaltenes and Asphalts, 2*. Edited by Yen, T.F. and Chilingar, G.V., Elsevier Science: Amsterdam, 2000.
22. Niizuma, S., Steele, C. T., Gunning, H. E. and Strausz, O. P., Electron Spin Resonance Study of Free Radicals in Athabasca Asphaltene. *Fuel* **1977**, 56 (3), 249-256.
23. Eaton, G. R., Eaton, S. S., Barr, D. P. and Weber, R. T., *Quantitative EPR*. Springer Science & Business Media: 2010.
24. Rahimi, P., Gentzis, T., Dawson, W. H., Fairbridge, C., Khulbe, C., Chung, K., Nowlan, V. and DelBianco, A., Investigation of Coking Propensity of Narrow Cut Fractions from Athabasca Bitumen Using Hot-Stage Microscopy. *Energy & Fuels* **1998**, 12 (5), 1020-1030.
25. Kopsch, H., On the Thermal Behavior of Petroleum Asphaltenes. *Thermochimica Acta* **1994**, 235 (2), 271-275.
26. Zhang, Y., Takanohashi, T., Sato, S., Saito, I. and Tanaka, R., Observation of Glass Transition in Asphaltenes. *Energy & Fuels* **2004**, 18 (1), 283-284.

## **CHAPTER 3. EXPERIMENTAL – PRECIPITATION OF ASPHALTENES FROM BITUMEN AT DIFFERENT SDA PROCESS CONDITIONS**

### **3.1 Introduction**

In this chapter the experimental lab procedure of asphaltene precipitation from bitumen is described. As mentioned in chapter 2, the yield of asphaltene is different when different SDA process conditions are used. The bitumen feed characterization, asphaltene and DAO yields and calculated material losses are presented in this chapter.

### **3.2 Experimental**

#### **3.2.1 Materials**

This study was performed using Canadian oil sands bitumen obtained from the Nexen Energy ULC Long Lake steam-assisted gravity drainage bitumen production facility, which is located in the Athabasca region of Alberta.

The solvents used for asphaltene precipitation were *n*-pentane (99.6%), *n*-hexane (95%) and *n*-heptane (99.6%, HPLC grade) supplied by Fisher Scientific.

#### **3.2.2 Equipment and Procedure**

The procedure that was followed for the precipitation of asphaltene from bitumen is shown in Figure 3-1.

An empty PYREX Erlenmeyer flask made of standard borosilicate glass (volume of 125ml for S/B ratios 3:1, 4:1 and 5:1, and 1000ml for S/B ratio 40:1) was placed in a weighing balance. Mettler XS105 Dual Range analytical balance was used to weigh bitumen, asphaltene, DAO and the paraffinic solvents in this study. The readability of the balance is 0.01mg and 0.1mg at a maximum capacity of 41g and 120g respectively. A certain amount of *n*-paraffinic solvent was taken into the flask and the balance was tared. The solvent prevents the bitumen from sticking to the bottom of the container and makes the mixing of solution easier. ~10g of bitumen was added into the flask. The total amount of solvent required to obtain a certain S/B ratio was calculated. After subtracting the initial amount of solvent taken, the remaining amount of solvent was added into the flask, and the mixture was mixed thoroughly with a spatula. A rubber stopper was inserted into the mouth of

the flask to prevent the evaporation of the solvent. The solvent-bitumen mixture was mixed on Heidolph MR Hei-Standard bar magnetic stirrer (at 125rpm for S/B ratios 3:1 to 5:1 and 400rpm for 40:1) for 1h, after which it was left in an amber bottle for the target precipitation time, either 24h or 330h, in a dark place. The precipitation time in these experiments is the contact time measured after stirring, which doesn't include the 1h stirring period. Except for the 3:1 pentane-bitumen mixture, rest of the products were separated by vacuum filtration with a pre-weighed filter paper. MF-Millipore membrane filter paper composed of mixed cellulose membrane, and having a diameter of 47mm and pore size of 0.22  $\mu\text{m}$  was used for filtration. Due to extreme semi-solid character of the insolubles in the 3:1 pentane-bitumen mixture, this asphaltenes product could be separated only by decantation of the pentane-rich phase.

Filter papers containing unwashed asphaltenes precipitated from *n*-pentane, *n*-hexane and *n*-heptane were placed in pre-weighed aluminium weighing dishes. The weighing dishes were dried at 65°C, 75°C and 100°C respectively in hot air oven (Cole-Parmer, StableTemp vacuum oven, Model 6259) at atmospheric pressure for 1h. The dishes were left overnight in a vacuum-sealed oven (Fisher Scientific™ Isotemp™ Model 282A) at 60°C and a pressure of -94.8kPa (-28in Hg). The dried asphaltenes were weighed by subtracting the empty weights of filter paper and weighing dish from the total weight after drying. The asphaltenes were collected and stored in amber vials for further analyses.

Residual solvent from DAO was removed by rotary evaporation at 55°C and 65 rpm. Heidolph Hei-VAP rotary evaporator was used. 32kPa and 10kPa vacuum were used during evaporation of *n*-hexane and *n*-heptane respectively, while the evaporation of *n*-pentane was performed at atmospheric pressure. The weight of DAO in the flask was recorded and DAO was collected into an amber vial for further analyses. The DAO samples, when observed under a stereomicroscope (SteREO Discovery.V20) at 150 $\times$  magnification, were not found to contain small particulates that could have passed through the filter during filtration.

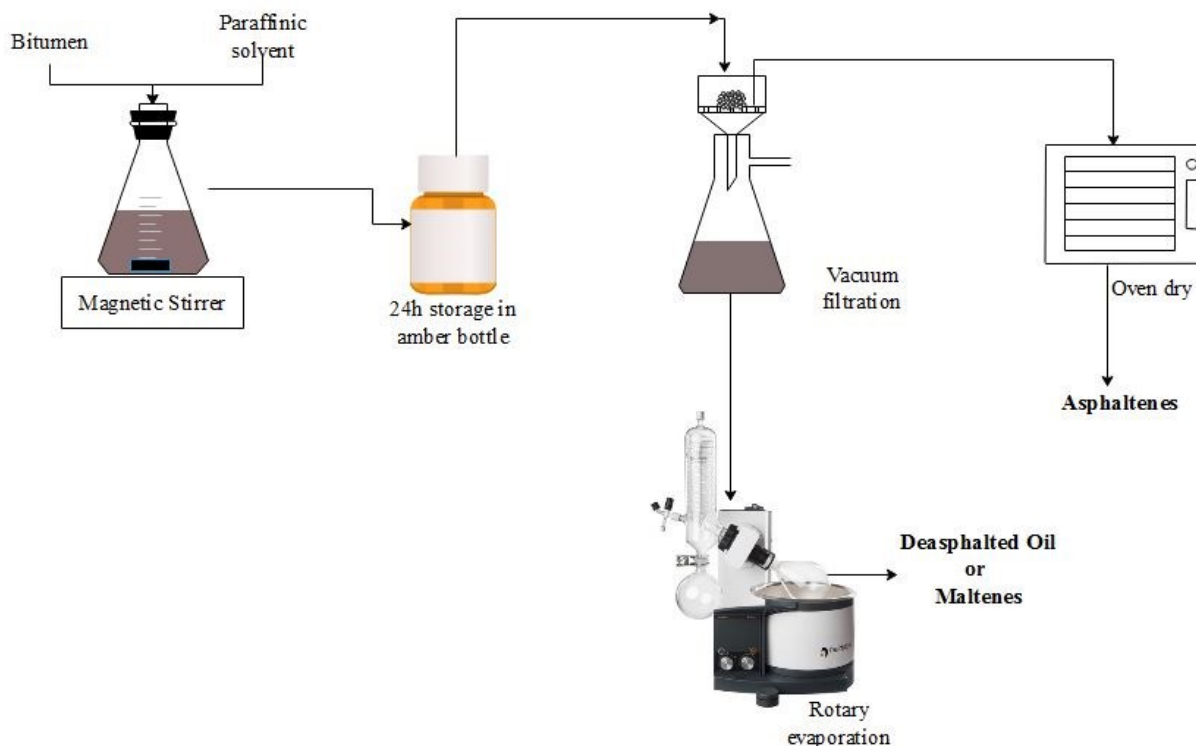


**Figure 3-1.** Process Diagram of Asphaltene Precipitation in this study

### 3.2.2.1 Process Conditions

#### 3.2.2.1.1 Solubility Subfractions

In this study, the asphaltenes produced when *n*-pentane, *n*-hexane and *n*-heptane were used as precipitants are called C<sub>5</sub> asphaltenes, C<sub>6</sub> asphaltenes and C<sub>7</sub> asphaltenes respectively, and the corresponding DAO or maltenes are called C<sub>5</sub> maltenes, C<sub>6</sub> maltenes and C<sub>7</sub> maltenes respectively.

#### 3.2.2.1.2 Solvent to bitumen (S/B) ratios

~10g of bitumen was used in all the experiments. The S/B ratios (ml/g) chosen for this study are 3:1, 4:1, 5:1 and 40:1. The lower S/B ratios represent more practical ratios for industrial practice. The high S/B ratio represent a reference point, since standard methods for asphaltene precipitation recommend S/B ratios of 40:1 and above.<sup>1</sup> Asphaltene precipitation was performed in triplicates for C<sub>5</sub> and C<sub>7</sub> solvents at the above S/B ratios. For C<sub>6</sub>, experiments were performed in triplicates at 3:1 S/B ratio and single experiments were performed at the remaining ratios.

### 3.2.2.1.3 Precipitation Time

The effect of precipitation time on asphaltene precipitation was studied by using two time points: 24h and 330h. In this study, the effect of precipitation time was studied qualitatively by performing one set of experiments (not in triplicates) for C<sub>5</sub> and C<sub>7</sub> solvents at different S/B ratios.

### 3.2.2.1.4 Temperature and Pressure

Asphaltene precipitation experiments were performed at room temperature (~20°C) and atmospheric pressure. The effect of temperature and pressure are not the focus of this study.

### 3.2.3 Analyses

Bitumen feed characterization involved the following analyses:

Density of bitumen at 25°C was measured using Anton Paar Density meter, Model DMA 4500M. The instrument was calibrated using ultra-pure water provided by Anton Paar at 20°C. The density accuracy of the instrument is 0.00005g/cm<sup>3</sup> and the temperature accuracy is 0.03°C. Before injecting into the density meter, the viscosity of bitumen was reduced by heating it to 60°C in a beaker on Heidolph MR Hei-Standard hot plate magnetic stirrer, without stirring.

Anton Paar Abbemat 200 refractometer was used to measure the refractive index of bitumen at 25°C using the sodium D-line (589nm). The range of the instrument is 1.30 to 1.72nD and the accuracy is ± 0.0001nD. Temperature probe accuracy of the instrument is ± 0.05 °C. Equipment was pre-calibrated by the manufacturer using official standards from the National Metrology Institute of Germany. Ethanol check was performed every time before measurements, to check whether the instrument was performing correctly. According to literature, refractive index of ethanol is ~1.3614nD at 20°C.<sup>2</sup>

Mineral content of bitumen was determined by thermogravimetric analysis (TGA) using Mettler Toledo TGA/DSC-1. The equipment contains an MX5 internal microbalance whose capacity and readability are 5.1g and 0.001mg respectively. ~5mg of bitumen was taken into a 70µL alumina crucible and heated in air flowing at a rate of 100ml/min. The gas (air) flow rate was controlled using Mettler Toledo GC 10 gas controller. The sample was heated from 25 to 900°C in the LF 1100 furnace, at a rate of 10°C/min and left for 1h at 900°C. STARe software was used to evaluate the mass loss behavior of the sample.

Microcarbon residue (MCR) of bitumen was determined by TGA analysis using Mettler Toledo TGA/DSC-1. ~5mg of the sample was heated in a 70 $\mu$ L alumina crucible, in the presence of nitrogen gas flowing at the rate of 100ml/min. The flow rate of the nitrogen gas was controlled using the Mettler Toledo GC 10 gas controller. The sample was heated from 25°C to 600°C at a rate of 10°C/min and left for 1h at 600°C.

Elemental Analysis of bitumen was performed by the Analytical laboratory of the Department of Chemistry at University of Alberta using Thermo Flash 2000 CHNS analyzer. Oxygen content was calculated by difference.

The boiling point distribution of bitumen was obtained by simulated distillation (SimDis) analysis, which was performed by following the standard method ASTM D7169-11.<sup>3</sup> The equipment used for this analysis was Agilent 7890B Gas Chromatograph(GC) with DB-HT Simdis column of dimensions 5m x 0.53mm x 0.15 $\mu$ m (length x inner diameter x film thickness) and the detector used was flame ionization detector (FID). Carbon disulfide (Fisher chemical, 99.99% purity) was used as a solvent to dilute the standards and samples. Polywax 655 (Supelco, Neat) was used for retention time calibration. In order to calculate the sample recovery, response factor of the FID detector was determined using ASTM® D6352/D7169 Reference Material 5010 (Supelco) as the external standard. Response factor (RF) is calculated from the net area of the standard ( $A_{STD}$ ), mass of the standard ( $M_{STD}$ ) and mass of the solvent ( $M_{SLSTD}$ ) in the standard solution, using Eq. 3-1.

$$RF = \frac{(M_{STD})}{(M_{STD} + M_{SLSTD})} \times \frac{1}{A_{STD}} \quad \text{Eq. 3-1}$$

Sample recovery (%RC), expressed as a percentage, is calculated using Eq. 3-2

$$\%RC = \frac{(ME)}{\left(\frac{M_{SMP}}{(M_{SMP} + M_{SLSMP})}\right)} \times 100 \quad \text{Eq. 3-2}$$

where, ME is the mass of the sample eluted,  $M_{SMP}$  is the mass of the sample and  $M_{SLSMP}$  is the mass of the solvent in the sample solution. ME is calculated using Eq. 3-3

$$ME = A_{SMP} \times RF \quad \text{Eq. 3-3}$$

where,  $A_{SMP}$  is the net sample area and RF is the response factor of Reference Oil 5010.

Hydrogen (compressed, 99.999% molar purity, Praxair), helium (compressed, 5.0 grade, Praxair) and air (compressed, ZERO grade, Praxair) were used for the operation of GC. OpenLAB GC software was used for operating the GC and acquiring the data, while Dragon Simdis software was used for calibration and reprocessing of the data.  $0.1 \pm 0.005$ g of the sample was weighed and diluted with carbon disulphide to 10ml. The amount of middle distillate, gas oil and residue fractions (wt%) were calculated from the boiling point distribution of bitumen, according to Table 3-1. The sample recovery was 80wt%, i.e. 20wt% of the material is boiling above  $\sim 720^\circ\text{C}$ , as shown in Figure 3-2.

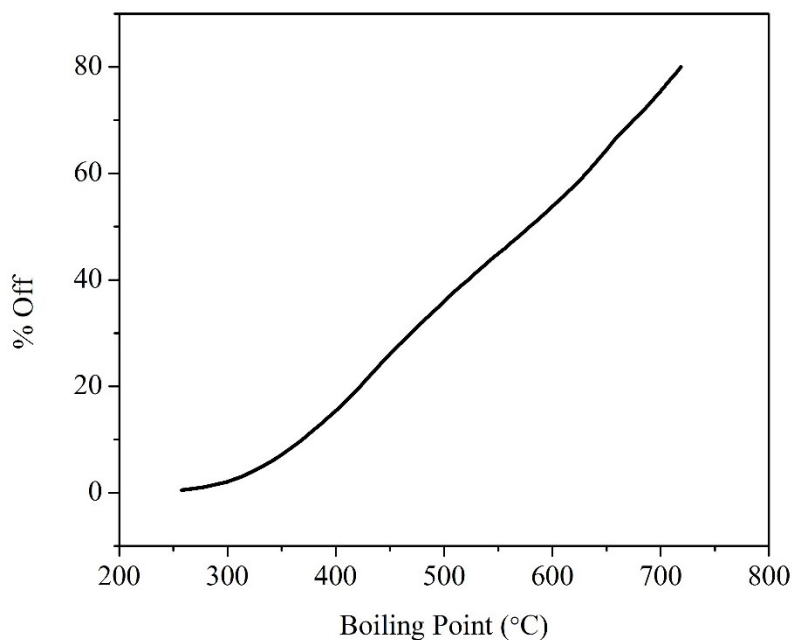


**Figure 3-2.** Simulated Distillation Curve of Athabasca Bitumen

**Table 3-1.** Boiling Ranges of Distillation Fractions used in this study

<b>Distillation Fraction</b>	<b>Boiling Range (°C)</b>
Middle Distillate	Initial Boiling Point - $343^\circ\text{C}$
Gas Oil	$343 - 524^\circ\text{C}$
Residue	$>524^\circ\text{C}$

Metals (Ni,V) were analyzed by X-Ray Fluorescence spectrometry, using Bruker S2 Ranger instrument. The instrument contains a silicon drift detector with Peltier cooling, and a Pd-target X-ray tube. It was calibrated using oil based Ni and V standard solutions (1000 $\mu$ g/g) supplied by Specpure, at different concentrations (1000, 800, 600, 500, 400, 200, 100, 80, 60, 40, 20, 10, 8, 6, 4, 2, 1 ppm) in a mineral oil matrix. The analysis was performed at 40keV and the presence of Ni and V metals was indicated by the  $K_{\alpha 1}$  lines.

The concentration of free radicals in bitumen was measured using Electron Spin Resonance (ESR) spectroscopy. Active Spectrum Micro-ESR was used for this analysis. The sweep range of the instrument is 320 to 9240 Gauss. A 5 mm medium wall precision quartz EPR sample tube, purchased from Wilmad-LabGlass, was used for analysis. Precision quartz tubes are suitable for quantification, and give better results than the standard 5mm quartz tubes. To ensure that the resonator cavity is full, the height of the sample tube was adjusted using an O-ring. DPPH (2, 2-Diphenyl-1-picrylhydrazyl, CAS Number 1898-66-4), supplied by Sigma-Aldrich, was used for calibration of organic free radical. ~280mg of bitumen was diluted to 1ml with toluene. Using the calibration curve, the organic free radical content of bitumen was calculated from the double integral value of the first derivative organic free radical peak of the ESR spectrum. As the instrument was not calibrated for the vanadyl radical, the double integral value of the vanadyl peak of the ESR spectrum was recorded and not quantified. The settings used were: microwave power = 15mW, range of swept magnetic field = 3200-3600G, number of points = 4096, sweep time = 113.9s, number of scans/sweeps = 5, digital gain = 12dB, modulation amplitude = 1.2G. The modulation phase and frequency were automatically set by the instrument. The ESR spectrum of bitumen, which is the first derivative of original absorption spectrum, is shown in Figure 3-3.

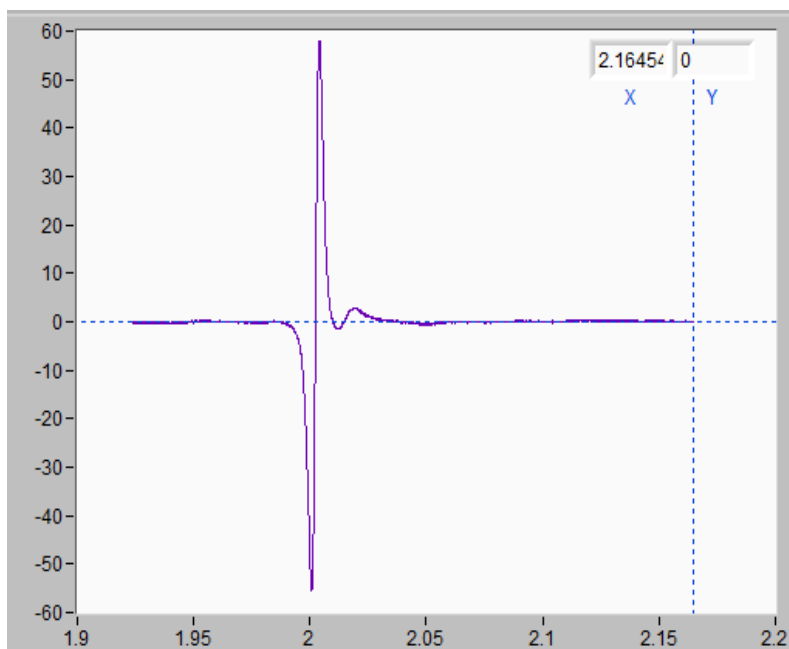


**Figure 3-3.** ESR spectrum of bitumen

Mettler XS105 Dual Range analytical balance was used to weigh bitumen and calibration standards used for analyses.

The characterization of the bitumen feed is shown in Table 3-2.

**Table 3-2.** Characterization of Athabasca Bitumen Feed <sup>a</sup>

Description	Experimental Data	
	x	s
Liquid Density at 25°C (kg/m <sup>3</sup> )	1029.4	3.1
Refractive Index at 25°C (nD)	1.5821	0.0002
Mineral Matter Content (wt%)	1.36	0.10
MCR (wt%)	11.7	1.6
Organic free Radical content (spins/g) g-factor = 2.0025	$4.18 \times 10^{17}$	$7.14 \times 10^{16}$

Vanadyl radical (Double Integral Value) g-factor = 2.0146	5.62×10 <sup>4</sup>	4.78×10 <sup>3</sup>
Elemental Analysis (wt%)		
Carbon	82.83	0.19
Hydrogen	10.02	0.002
Nitrogen	0.56	0.02
Sulfur	4.76	0.20
Oxygen (by difference)	1.83	0.006
Metal Content (ppm)		
Nickel	47.41	0.46
Vanadium	107.25	0.99
SimDis Fractions (wt%)		
Middle Distillate Fraction	6.21	- <sup>b</sup>
Gas Oil Fraction	34.15	- <sup>b</sup>
Residue Fraction	65.85	- <sup>b</sup>

<sup>a</sup> Average (x) and standard deviation (s) of three samples are reported

<sup>b</sup> Analysis was performed on single sample

### 3.2.4 Results

The yields of asphaltenes and DAO (expressed as wt% of bitumen), and associated material losses are shown in Table 3-3 and Table 3-4 for 24h and 330h precipitation times respectively. The material losses were calculated by difference.

The first step where material was lost, was during the transfer of the bitumen-solvent mixture at the end of the contact time to separate the asphaltenes from DAO by filtration. Since it was not possible to use solvent to remove material that stuck to the container wall (S/B ratio was a controlled variable), only mechanical means could be used to assist with this transfer. Losses at low S/B ratios therefore tended to be higher.

The second step where material was lost, was during the transfer of DAO from filtration stage to rotary evaporation stage. The DAO-solvent mixture produced at low S/B ratios was viscous, as the amount of solvent in the mixture was low. Due to high viscosity, material was stuck to the walls of the container used for filtration. It could not be recovered using additional solvent, as the ratio of solvent to DAO could have an impact on solvent recovery.<sup>4</sup>

The third step where material was lost, could have been during the rotary evaporation stage, due to volatilization of light material in DAO along with solvent. However, Figure 3-2 indicates that this amount is negligible, as less than 0.5wt% of bitumen boils below ~258°C.

The losses in the above stages were contributed by one or more of the following components: bitumen, DAO, asphaltenes and solvent. Hence, the material losses were cumulatively calculated by mass balance for each experiment.

**Table 3-3.** Yields of Fractions and Losses from SDA of bitumen with contact time of 24h <sup>a</sup>

Solvent	S/B ratio (v/w)	Asphaltenes Yield (wt%)		DAO Yield (wt%)		Average Material Loss (wt%) (by difference)
		x	s	x	s	
<i>n</i> -pentane	3:1	12.23	2.55	75.66	3.20	12.11
	4:1	14.51	2.39	74.69	3.78	10.80
	5:1	19.38	2.35	72.63	5.04	7.99
	40:1	19.86	1.51	77.61	1.18	2.53
<i>n</i> -hexane	3:1	11.54	1.48	73.82	3.74	14.64
	4:1	13.11	- <sup>b</sup>	76.50	- <sup>b</sup>	10.39
	5:1	17.65	- <sup>b</sup>	73.73	- <sup>b</sup>	8.62
	40:1	18.96	- <sup>b</sup>	80.25	- <sup>b</sup>	0.79
<i>n</i> -heptane	3:1	9.10	1.19	81.53	4.91	9.37
	4:1	12.31	1.40	78.66	3.30	9.03
	5:1	16.35	1.88	77.89	4.27	5.76
	40:1	17.40	2.97	76.05	1.96	6.55

<sup>a</sup> Average (x) and standard deviation (s) of three experiments are reported

<sup>b</sup> Single experiment

**Table 3-4.** Yields of fractions and Losses from SDA of bitumen with contact time of 330h <sup>a</sup>

Solvent	S/B ratio (v/w)	Asphaltene Yield (wt%)	DAO Yield (wt%)	Material Loss (wt%) (by difference)
<i>n</i> -pentane	3:1	20.69	75.26	4.05
	4:1	22.70	68.25	9.05
	5:1	23.79	68.81	7.40
	40:1	21.22	74.13	4.65
<i>n</i> -heptane	3:1	11.40	76.98	11.62
	4:1	15.42	75.6	8.98
	5:1	17.13	77.45	5.42
	40:1	17.57	80.26	2.17

<sup>a</sup> All the experiments were performed for one time

### 3.2.5 Discussion

#### 3.2.5.1 Feed Properties

The measured values of bitumen properties and composition mentioned in Table 3-2 were compared against reported values in literature as shown in Table 3-5. Exact comparison of some properties was not possible, as there are differences in measurement temperature and units.

In Figure 3-3, the central line or signal corresponds to the organic free radical.<sup>5</sup> In the work by Khulbe, et al.<sup>5</sup> the free radical content of Athabasca bitumen was reported to be  $2.5 \times 10^{17}$  spins/g and the g-factor was 2.0023. In their study, the ESR spectrum of Athabasca bitumen contained multiple free radical lines along with the central peak. The paramagnetic VO<sup>+2</sup> ions (V<sup>+4</sup>) produced eight hyperfine lines, due to hyperfine splitting.<sup>5</sup> However, in the present study, only one peak

was observed at  $g=2.0146$ , corresponding to the vanadyl radical. Hyperfine splitting was not observed in the spectral range used in this study. In Figure 3-3, there seems to be an overlap between the organic radical peak and vanadyl peak. Hence, the double integral value, used for quantification of vanadyl radical, was calculated by multiplying the double integral value of the half portion of the vanadyl peak that didn't overlap with the organic radical peak by two.

**Table 3-5.** Comparison of bitumen characterization in this study with values reported in literature

<b>Description</b>	<b>Measured</b>	<b>Literature.<sup>6</sup></b>
Refractive Index (nD)	1.5821	1.57 <sup>a</sup>
Carbon (wt%)	82.83	83.31
Hydrogen (wt%)	10.02	10.59
Nitrogen (wt%)	0.56	0.41
Sulfur (wt%)	4.76	4.78
Oxygen (wt%)	1.83	0.88
H/C ratio	1.45	1.53
<b>Description</b>	<b>Measured</b>	<b>Literature.<sup>7</sup></b>
Liquid Density (kg/m <sup>3</sup> )	1029.4 <sup>b</sup>	1021.7 <sup>c</sup>
Mineral Matter Content (wt%)	1.36	0.24 <sup>d</sup>
MCR (wt%)	11.7	13.6 <sup>e</sup>
Nickel (ppm)	47.41	75
Vanadium (ppm)	107.25	196
Middle Distillate Fraction (wt%, vol%)	6.21 <sup>f</sup>	7.18 <sup>g</sup>
Gas Oil Fraction (wt%, vol%)	34.15 <sup>f</sup>	44.25 <sup>g</sup>
Residue Fraction (wt%, vol%)	65.85 <sup>f</sup>	48.57 <sup>g</sup>

<sup>a</sup> Measurement temperature not reported, <sup>b</sup> Measured at 25°C, <sup>c</sup> Measured at 15.6°C

<sup>d</sup> Toluene insoluble solids which could include coke particles, <sup>e</sup> Solids-free basis

<sup>f</sup> Expressed in wt%, <sup>g</sup> Expressed in volume%

### 3.2.5.2 24h precipitation time

For 24h precipitation time, the yield of asphaltenes decreases from *n*-pentane to *n*-heptane at the observed S/B ratios and it increases with increase in S/B ratio for all the three solvents, as shown in Figure 3-4. These trends are in agreement with literature.<sup>8,9,6</sup> In a study by Luo, et al.<sup>8</sup>, precipitation experiments were performed for 12h using Canadian heavy oil ( $\rho = 975 \text{ kg/m}^3$ ,  $\mu = 9440 \text{ mPa.s}$ ) at room temperature and it was found that the yield of C<sub>5</sub> and C<sub>7</sub> asphaltenes increased with S/B ratio upto 20:1(v/v) and then remained same upto 40:1. Speight, et al.<sup>9</sup> reported that the yield of C<sub>5</sub> asphaltenes from Athabasca bitumen increases with increase in S/B ratio upto 30:1 (ml/g) and remains constant thereafter. The precipitation time in their experiments was 16h. Strausz, et al.<sup>6</sup> reported that the yield of C<sub>5</sub> asphaltenes precipitated at S/B ratio 30:1 (ml/g), reaches a constant at 12h precipitation time, and the value remains unchanged between 12h and 24h precipitation time.

As mentioned in section 2.3.4 of Chapter 2, the amount of asphaltenes precipitated decreases with increase in solubility parameter of the precipitants. Solubility parameter is calculated from the intermolecular forces and molar concentration. In this study, for a given S/B ratio (volume of solvent is constant), the molar concentration of solvents decreases from *n*-pentane (0.0087mol/ml) to *n*-heptane (0.0068mol/ml). However, the intermolecular forces, mainly the dispersion forces increase with increase in carbon number or chain length of the linear paraffinic solvent. Hence, the ability of the solvent to dissolve asphaltenes, represented by the solubility parameter, also increases from *n*-pentane to *n*-heptane, and the amount of asphaltenes precipitated decreases from *n*-pentane to *n*-heptane.

Maltenes have a higher solvent strength for asphaltenes compared to *n*-paraffinic solvents.<sup>6</sup> As the S/B ratio or volume fraction of solvent increases, the solvent strength of the solvent-bitumen mixture decreases, increasing the amount of asphaltenes precipitated.

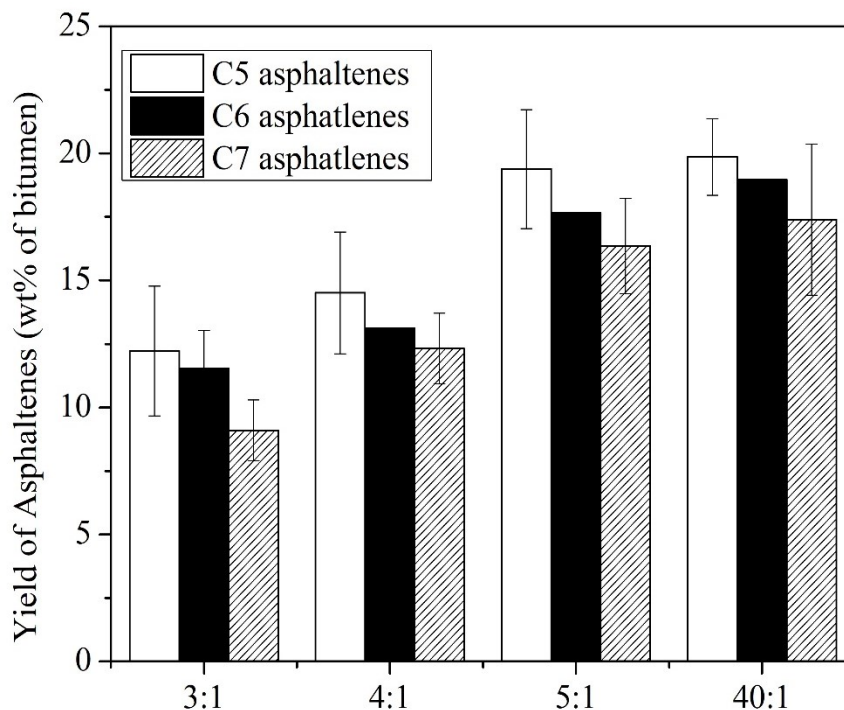


**Figure 3-4.** Yields of C<sub>5</sub>, C<sub>6</sub> and C<sub>7</sub> asphaltenes precipitated at different S/B ratios.

Precipitation Time = 24h

However, such trends could not be observed in the yields of DAO, due to the additional steps during which losses in the experiments could occur and the variability they introduced. Only, in case of *n*-heptane, the yield of DAO decreased with increase in S/B ratio.

The losses varied from 0.79 wt% to 14.64 wt% of bitumen in the experiments. In general, the material losses were more at lower S/B ratios and decreased with increase in S/B ratio. A reason for this behavior could be that the solvent-bitumen mixture and the precipitated asphaltenes are sticky and semi-solid in nature when low S/B ratios are used, contributing to more losses on the surfaces of equipment used for precipitation.

Figure 3-5 shows a comparison of C<sub>5</sub>-asphaltenes precipitated at S/B ratios of 5:1 and 40:1. Though the yields of these two asphaltenes are close, asphaltenes are black, shiny, sticky and have a semi-solid character when precipitated at 5:1, whereas they are brown powdery solids at 40:1. Though C<sub>5</sub>-asphaltenes showed a dominant semi-solid character over C<sub>6</sub> and C<sub>7</sub> asphaltenes, the appearance in C<sub>6</sub> and C<sub>7</sub> asphaltenes transformed in a similar manner with increase in S/B ratio.

According to literature, at S/B ratios  $\leq 20:1$ , asphaltenes retain resin material producing a black, shiny semi-solid precipitate.<sup>9</sup> Hence, the efficiency of separation of asphaltenes from bitumen is greater at higher S/B ratios.

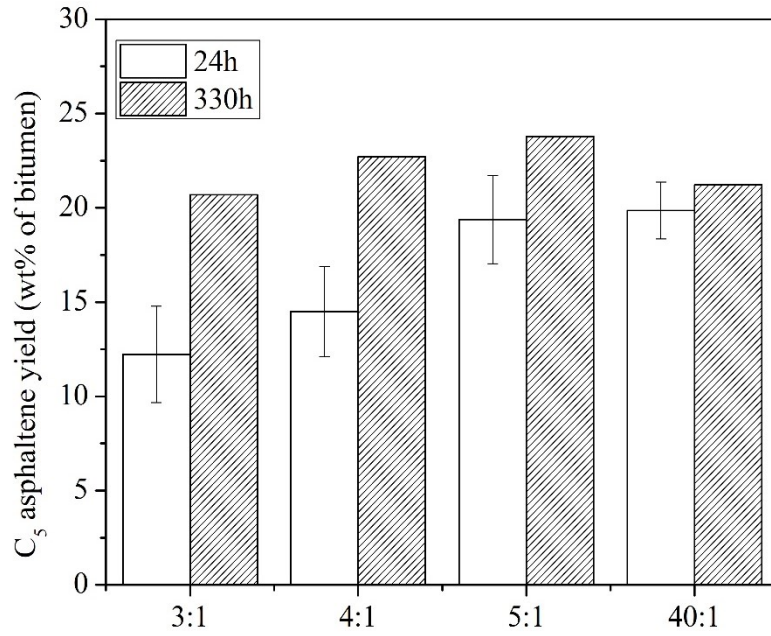


**Figure 3-5.** Appearance of C<sub>5</sub> asphaltenes precipitated at S/B ratios 5:1 and 40:1

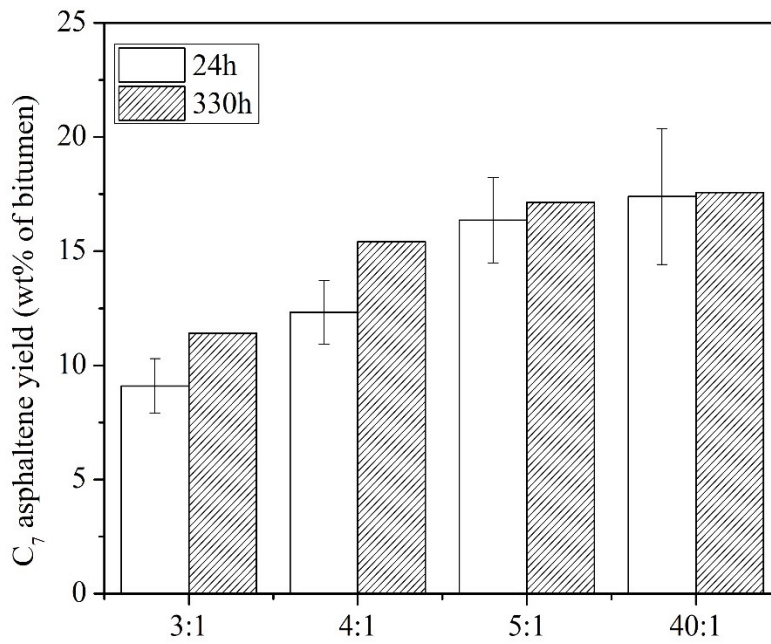
The standard deviations in the yields of asphaltenes and DAO were high. Inhomogeneity in bitumen feed and/or variable losses could be contributing to this variability among the experiments.

### 3.2.5.3 330h precipitation time

The yield of asphaltenes increased with increase in precipitation time, as shown in Figure 3-6.



(a)



(b)

**Figure 3-6.** Effect of precipitation time on the yield of (a) C<sub>5</sub> asphaltenes and (b) C<sub>7</sub> asphaltenes at different S/B ratios

In a study by Shafiee Neistanak,<sup>10</sup> it was observed that the yield of asphaltenes from West Canadian bitumen continued to increase for more than 1000h when precipitation was performed in air. When the same experiments were performed in nitrogen, the asphaltene yield reached a saturation after 48h. Their hypothesis was that oxidation and polymerization reactions catalyzed by oxygen in air contributed to these long term changes in asphaltene yields in the presence of air.

Hydrocarbon auto oxidation mechanisms were reported by Siddiquee,<sup>11</sup> in his work on auto oxidation of oil sands bitumen. Auto oxidation processes go through free radical reactions which can be divided into initiation, propagation and termination reactions.<sup>11</sup> The polarity of bitumen increases due to auto oxidation,<sup>11</sup> which would lead to a decrease in the solubility of bitumen fractions in paraffinic solvents, thus leading to increase in asphaltene content. Free radicals in bitumen, as shown in Table 3-2, which are highly reactive, might also participate in these reactions and initiate low temperature polymerization reactions. The process conditions such as temperature and reaction time could affect the rate of these reactions. Usually, formation of sufficient concentration of free radicals is required for the reactions to proceed at a significant rate. The time required for this is called induction time, and it is commonly observed in auto oxidation processes.<sup>11</sup> In general, presence of metals such as Fe, Co, Mn, Ni could also affect the reactions by offering catalytic activity.<sup>11</sup>

From Figure 3-6 it can be observed that the extent of increase in asphaltene yield with precipitation time was greater for *n*-pentane compared to *n*-heptane and it was greater at lower S/B ratios. At 330h precipitation time, the yield of C<sub>5</sub>-asphaltenes was greater than C<sub>7</sub>-asphaltenes at the observed S/B ratios as shown in Table 3-4. The yield of asphaltenes increases with increase in S/B ratio for both the solvents, with one exception - this increase was not observed in case of C<sub>5</sub>-asphaltenes from 5:1 to 40:1. Thus, in addition to the effect of precipitation time on asphaltenes yield, the difficulty of separating the C<sub>5</sub> asphaltenes from maltenes at lower S/B ratios could have amplified the higher amount of asphaltenes and caused the yield to exceed that found at 40:1 ratio, where this was not a problem. This could be the reason why the yield of C<sub>5</sub> asphaltenes did not monotonously increase with S/B ratio from 3:1 to 40:1.

Again, a specific trend was not observed in the yields of DAO due to variable material losses. The losses varied from 2.17 wt% to 11.62 wt% of bitumen in the experiments.

### 3.2.6 Conclusions

- a) In this chapter, characterization of bitumen feed and material balance calculations in the SDA process at different process conditions were performed. These results will be helpful to interpret the findings related to characterization of asphaltenes and DAO in later chapters.
- b) At 24h precipitation time :
  - The yield of C<sub>5</sub> asphaltenes increased from 12.23 to 19.86 wt% with increase in S/B ratio from 3:1 to 40:1 (ml/g), and that of C<sub>6</sub> and C<sub>7</sub> asphaltenes increased from 11.54 to 18.96wt% and 9.1 to 17.4wt% respectively. The yield of asphaltenes increased with the carbon number of *n*-paraffinic solvent from C<sub>5</sub> to C<sub>7</sub>. These trends in asphaltene yield with solvent and S/B ratio are in agreement with literature.
  - Though the increase in the yield of asphaltenes from 5:1 to 40:1 was not significant, there was a notable difference in their appearance. At 5:1 asphaltenes were black, shiny, sticky and semi-solids whereas at 40:1 they were brown, powdery solids.
- c) The asphaltene yield increased with increase in precipitation time from 24h to 330h at the observed S/B ratios. This effect was more pronounced in the case of C<sub>5</sub> asphaltenes compared to C<sub>7</sub> asphaltenes. However, further experimentation is required to validate these observations.
- d) Material losses occurred at different stages of asphaltene precipitation from bitumen. The losses varied from 0.79 wt% to 14.64 wt% of bitumen in the experiments. The losses decrease with an increase in the S/B ratio from 3:1 to 40:1, indicating that the efficiency of separation of bitumen fractions increases with increase in S/B ratio in the SDA process.

### 3.3 References

1. Ancheyta Juárez, J., *Asphaltenes Chemical Transformation During Hydroprocessing of Heavy Oils*. Taylor & Francis: Boca Raton, 2009; p 461 p.
2. Jiménez Riobóo, R. J., Philipp, M., Ramos, M. A. and Krüger, J. K., Concentration and Temperature Dependence of the Refractive Index of Ethanol-Water Mixtures: Influence of Intermolecular Interactions. *The European Physical Journal E* **2009**, 30 (1), 19.
3. ASTM D7169-11: Standard Test Method for Boiling Point Distribution of Samples with Residues Such as Crude Oils and Atmospheric and Vacuum Residues by High Temperature Gas Chromatography. ASTM International: West Conshohocken, PA, 2011.
4. Lee, J. M., Shin, S., Ahn, S., Chun, J. H., Lee, K. B., Mun, S., Jeon, S. G., Na, J. G. and Nho, N. S., Separation of Solvent and Deasphalted Oil for Solvent Deasphalting Process. *Fuel Processing Technology* **2014**, 119, 204-210.

5. Khulbe, K. C., Chan, B. W., Manoogian, A. and Patmore, D. J., E.s.r of Alberta Tar Sand Bitumen and Thermally Hydrocracked Products. *Fuel* **1986**, 65 (11), 1594-1599.
6. Strausz, O. P. and Lown, E. M., *The Chemistry of Alberta Oil Sands, Bitumens and Heavy Oils*. Alberta Energy Research Institute: Calgary, 2003.
7. Gray, M. R., *Upgrading Oilsands Bitumen and Heavy Oil*. University of Alberta Press: Edmonton, Alberta, 2015.
8. Luo, P., Wang, X. and Gu, Y., Characterization of Asphaltenes Precipitated with Three Light Alkanes under Different Experimental Conditions. *Fluid Phase Equilibria* **2010**, 291 (2), 103-110.
9. Speight, J. G., Long, R. B. and Trowbridge, T. D., Factors Influencing the Separation of Asphaltenes from Heavy Petroleum Feedstocks. *Fuel* **1984**, 63 (5), 616-620.
10. Shafiee Neistanak, M. Kinetics of Asphaltene Precipitation and Flocculation from Diluted Bitumen. University of Calgary, 2014.
11. Siddiquee, M. N. Autoxidation of Oilsands Bitumen: Applied, Model Compounds and Microfluidic Study. University of Alberta, Edmonton, Canada, 2016.

# **CHAPTER 4. CHARACTERIZATION OF ASPHALTENES AND DAO FRACTIONS OF BITUMEN FROM THE SOLVENT DEASPHALTING PROCESS**

## **4.1 Introduction**

In this chapter, some important properties of DAO and asphaltenes that were described briefly in chapter 2, were measured and reported. The DAO and asphaltenes were obtained from bitumen by solvent deasphalting as described in chapter 3. Measurements of free radical content, elemental composition, metal content, Fourier Transform Infrared (FTIR) spectroscopy of DAO and asphaltenes and refractive index of DAO are reported in this chapter.

The chapter begins with a description of the experimental techniques used for these analyses, followed by the results and data analysis to evaluate the role of solvent, S/B ratio and precipitation time of the SDA process on the above mentioned properties of DAO and asphaltenes.

## **4.2 Materials and Methods**

### **4.2.1 Materials**

DAO and asphaltenes produced from SDA of bitumen using C<sub>5</sub>, C<sub>6</sub> and C<sub>7</sub> solvents at S/B ratios 3:1, 4:1, 5:1 and 40:1 (ml/g) and precipitation times 24h and 330h were analyzed.

### **4.2.2 Analyses**

The elemental analysis of DAO and asphaltenes was performed using the same procedure as described in chapter 3 for bitumen analysis.

Fourier Transform Infrared (FTIR) spectroscopy of samples was performed using ABB MB3000 analyzer with deuterated-triglycine sulfate (DTGS) detector. The spectral range of the instrument is 485 to 8500cm<sup>-1</sup>, and the frequency accuracy is <0.06cm<sup>-1</sup>. A PIKE MIRacle™ Reflection Attenuated Total Reflectance (ATR) accessory, containing a diamond crystal plate and high pressure clamping, was used for sampling. Before the sample analysis, a reference background spectrum was collected which contains unwanted IR peaks resulting from the air that fills the sample holder. The instrument automatically subtracts the reference background spectrum from sample spectrum. IR spectrum was obtained for samples over the wavenumber range 4000-600cm<sup>-1</sup> at 4cm<sup>-1</sup> resolution and an average number of scans of 240.

Refractive Index of DAO samples was measured using Anton Paar Abbemat 200 refractometer at using the sodium D-line (589nm) similar to bitumen analysis in chapter 3, at four different temperatures 20°C, 30°C, 40°C and 60°C.

X-ray fluorescence (XRF) spectrometry described in chapter 3 for bitumen was also performed for asphaltenes. XRF calibration for analysis of asphaltenes was performed using Ni(II) Phthalocyanine and V<sub>2</sub>O<sub>5</sub> at different concentrations (5-10-20-50-100-200-300-400-500-600-700 ppm) in a potassium carbonate matrix. The analysis was performed at 40keV and the presence of Ni and V metals was indicated by the K<sub>α1</sub> lines.

Electron spin resonance (ESR) spectroscopy for measurement of free radical content in asphaltenes was performed using Active Spectrum Micro-ESR. A 5 mm medium wall precision quartz EPR sample tube, purchased from Wilmad-LabGlass, was used for analysis. Precision quartz tubes are suitable for quantification, and give better results than the standard 5mm quartz tubes. To ensure that the resonator cavity is full, the height of the sample tube was adjusted using an O-ring. ~6mg of asphaltenes was diluted to 1ml with toluene. The settings used were: microwave power = 10mW, range of swept magnetic field = 3200-3500G, number of points = 53500, sweep time = 150ms, number of scans/sweeps = 8, digital gain = 18dB, modulation amplitude = 0.5G. The modulation phase and frequency were automatically set by the instrument. The instrument was not calibrated at the time when this analysis was performed. The Micro-ESR Signal Processing Software was used to measure the double integral values of organic free radical peak and vanadyl peak, which were used to compare the free radical concentration of samples.

Mettler XS105 Dual Range analytical balance was used to weigh samples for analyses.

## **4.3 Results**

### **4.3.1 Elemental Analysis**

The carbon, hydrogen, nitrogen, sulfur and oxygen contents of C<sub>5</sub> and C<sub>7</sub> asphaltenes, all expressed in wt%, are reported in Table 4-1, Table 4-2, Table 4-3, Table 4-4 and Table 4-5 respectively. Oxygen content was calculated by subtracting the total of carbon, hydrogen, nitrogen and sulfur (in wt%) from 100wt%.

**Table 4-1.** Carbon content (wt%) of asphaltenes obtained with different solvents and S/B ratios by solvent deasphalting when the precipitation time was 24h <sup>a</sup>

S/B ratio	Solvent			
	<i>n</i> -pentane		<i>n</i> -heptane	
	x	s	x	s
3:1	77.69	0.37	74.28	0.01
4:1	78.36	0.32	75.43	0.003
5:1	78.14	0.23	76.30	0.13
40:1	77.54	0.19	76.66	0.06

<sup>a</sup> Analysis of one set of asphaltenes was performed in duplicates. Average (x) and standard deviation (s) of the analysis are reported

**Table 4-2.** Hydrogen content (wt%) of asphaltenes obtained with different solvents and S/B ratios by solvent deasphalting when the precipitation time was 24h <sup>a</sup>

S/B ratio	Solvent			
	<i>n</i> -pentane		<i>n</i> -heptane	
	x	s	x	s
3:1	8.63	0.01	7.80	0.02
4:1	8.44	0.20	7.77	0.003
5:1	8.07	0.01	7.84	0.01
40:1	7.78	0.04	7.70	0.06

<sup>a</sup> Analysis of one set of asphaltenes was performed in duplicates. Average (x) and standard deviation (s) of the analysis are reported

**Table 4-3.** Nitrogen content (wt%) of asphaltenes obtained with different solvents and S/B ratios by solvent deasphalting when the precipitation time was 24h <sup>a</sup>

S/B ratio	Solvent			
	<i>n</i> -pentane		<i>n</i> -heptane	
	x	s	x	s
3:1	0.72	0.01	0.89	0.004
4:1	0.87	0.05	0.97	0.0001
5:1	0.94	0.02	0.96	0.02
40:1	1.07	0.01	1.08	0.03

<sup>a</sup> Analysis of one set of asphaltenes was performed in duplicates. Average (x) and standard deviation (s) of the analysis are reported

**Table 4-4.** Sulfur content (wt%) of asphaltenes obtained with different solvents and S/B ratios by solvent deasphalting when the precipitation time was 24h <sup>a</sup>

S/B ratio	Solvent			
	<i>n</i> -pentane		<i>n</i> -heptane	
	x	s	x	s
3:1	6.37	0.08	6.75	0.06
4:1	6.80	0.22	6.97	0.06
5:1	7.25	0.12	7.15	0.03
40:1	7.65	0.12	7.44	0.14

<sup>a</sup> Analysis of one set of asphaltenes was performed in duplicates. Average (x) and standard deviation (s) of the analysis are reported

**Table 4-5.** Oxygen content (wt%) of asphaltenes obtained with different solvents and S/B ratios by solvent deasphalting when the precipitation time was 24h <sup>a</sup>

S/B ratio	<i>n</i> -pentane		<i>n</i> -heptane	
	x	s	x	s
3:1	6.57	0.46	10.28	0.04
4:1	5.58	0.26	8.85	0.06
5:1	5.59	0.34	7.75	0.11
40:1	5.95	0.11	7.12	0.04

<sup>a</sup> Analysis of one set of asphaltenes was performed in duplicates. Average (x) and standard deviation (s) of the analysis are reported

The carbon, hydrogen, nitrogen, sulfur and oxygen contents of C<sub>5</sub> and C<sub>7</sub> maltenes, all expressed in wt%, are reported in Table 4-6, Table 4-7, Table 4-8, Table 4-9 and Table 4-10 respectively. Oxygen content was calculated by difference.

**Table 4-6.** Carbon content (wt%) of DAO obtained with different solvents and S/B ratios by solvent deasphalting when the precipitation time was 24h <sup>a</sup>

S/B ratio	Solvent			
	<i>n</i> -pentane		<i>n</i> -heptane	
	x	s	x	s
3:1	83.66	0.10	83.06	0.26
4:1	83.81	0.05	83.33	0.28
5:1	83.89	0.05	83.04	0.12
40:1	83.81	0.09	83.48	0.04

<sup>a</sup> Analysis of one set of DAO was performed in duplicates. Average (x) and standard deviation (s) of the analysis are reported

**Table 4-7.** Hydrogen content (wt%) of DAO obtained with different solvents and S/B ratios by solvent deasphalting when the precipitation time was 24h <sup>a</sup>

S/B ratio	Solvent			
	<i>n</i> -pentane		<i>n</i> -heptane	
	x	s	x	s
3:1	10.33	0.06	10.29	0.06
4:1	10.56	0.02	10.37	0.05
5:1	10.58	0.001	10.40	0.07
40:1	10.62	0.01	10.54	0.03

<sup>a</sup> Analysis of one set of DAO was performed in duplicates. Average (x) and standard deviation (s) of the analysis are reported

**Table 4-8.** Nitrogen content (wt%) of DAO obtained with different solvents and S/B ratios by solvent deasphalting when the precipitation time was 24h <sup>a</sup>

S/B ratio	Solvent			
	<i>n</i> -pentane		<i>n</i> -heptane	
	x	s	x	s
3:1	0.41	0.01	0.41	0.007
4:1	0.38	0.03	0.38	0.009
5:1	0.34	0.01	0.37	0.0003
40:1	0.34	0.03	0.33	0.0004

<sup>a</sup> Analysis of one set of DAO was performed in duplicates. Average (x) and standard deviation (s) of the analysis are reported

**Table 4-9.** Sulfur content (wt%) of DAO obtained with different solvents and S/B ratios by solvent deasphalting when the precipitation time was 24h <sup>a</sup>

S/B ratio	Solvent			
	<i>n</i> -pentane		<i>n</i> -heptane	
	x	s	x	s
3:1	4.12	0.05	4.60	0.01
4:1	3.87	0.01	4.33	0.13
5:1	3.75	0.15	4.20	0.05
40:1	3.44	0.06	4.12	0.03

<sup>a</sup> Analysis of one set of DAO was performed in duplicates. Average (x) and standard deviation (s) of the analysis are reported

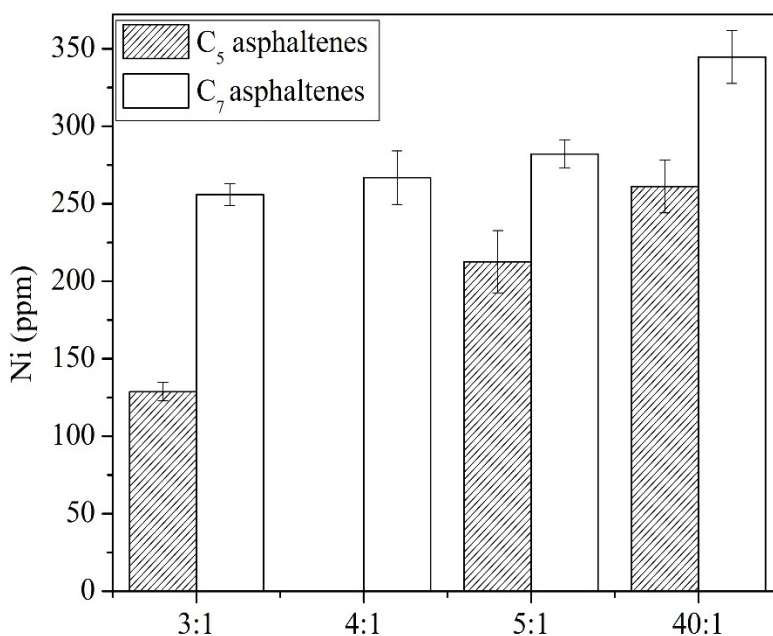
**Table 4-10.** Oxygen content (wt%) of DAO obtained with different solvents and S/B ratios by solvent deasphalting when the precipitation time was 24h <sup>a</sup>

S/B ratio	Solvent			
	<i>n</i> -pentane		<i>n</i> -heptane	
	x	s	x	S
3:1	1.48	0.005	1.65	0.32
4:1	1.38	0.01	1.59	0.19
5:1	1.43	0.11	1.99	0.14
40:1	1.79	0.13	1.52	0.03

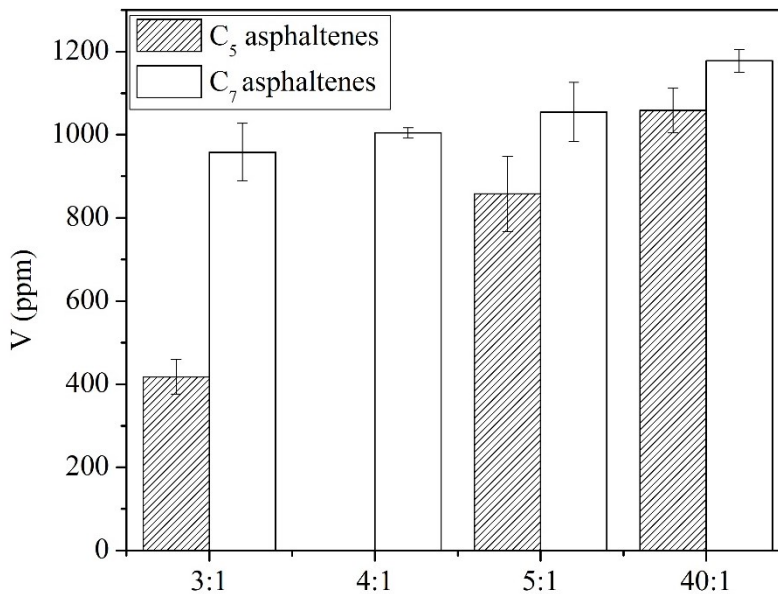
<sup>a</sup> Analysis of one set of DAO was performed in duplicates. Average (x) and standard deviation (s) of the analysis are reported

### 4.3.2 Metal content by X-Ray Fluorescence

Nickel and Vanadium content in asphaltenes was measured using XRF. The measurements are plotted in Figure 4-1. The Ni content in ppm increased from 129 to 261 ppm in C<sub>5</sub> asphaltenes and 256 to 345 ppm in C<sub>7</sub> asphaltenes with increase in S/B ratio from 3:1 to 40:1. The V content in ppm increased from 418 to 1058 ppm in C<sub>5</sub> asphaltenes and 958 to 1178 ppm in C<sub>7</sub> asphaltenes with increase in S/B ratio from 3:1 to 40:1. The Ni and V contents of C<sub>7</sub> asphaltenes were higher than those of C<sub>5</sub> asphaltenes at the observed S/B ratios. The Ni and V content of C<sub>5</sub> asphaltenes at S/B ratio 4:1 was not measured as the quantity of sample required for this analysis was not available.



(a)



(b)

**Figure 4-1.** Metal content in asphaltenes (a) Ni and (b) V expressed in ppm

### 4.3.3 FTIR Spectra

FTIR of asphaltenes and DAO was performed to observe changes in molecular structures when different SDA process conditions are used. Different types of bonds in molecules absorb light at different frequencies of the infrared region and vibrate. Vibrations are accompanied with either stretching (change in bond length) or bending (change in bond angle).<sup>1</sup> The frequency of vibration, which is used to calculate the wavenumber ( $\tilde{\nu}$ ), depends on the strength of the bond and reduced mass of the bonding atoms.<sup>1</sup> Functional groups can mainly be identified using FTIR by observing the peaks that appear at different wavenumbers which correspond to the vibration of specific bonds.

The FTIR spectra of asphaltenes produced using different solvents and S/B ratios in the SDA process with 24h precipitation time are shown in Figure 4-2. In the same figure, spectra of asphaltenes are compared with the IR spectrum of bitumen. Differences among the samples with changes in solvent and S/B ratios could not be identified visually from the graphs.

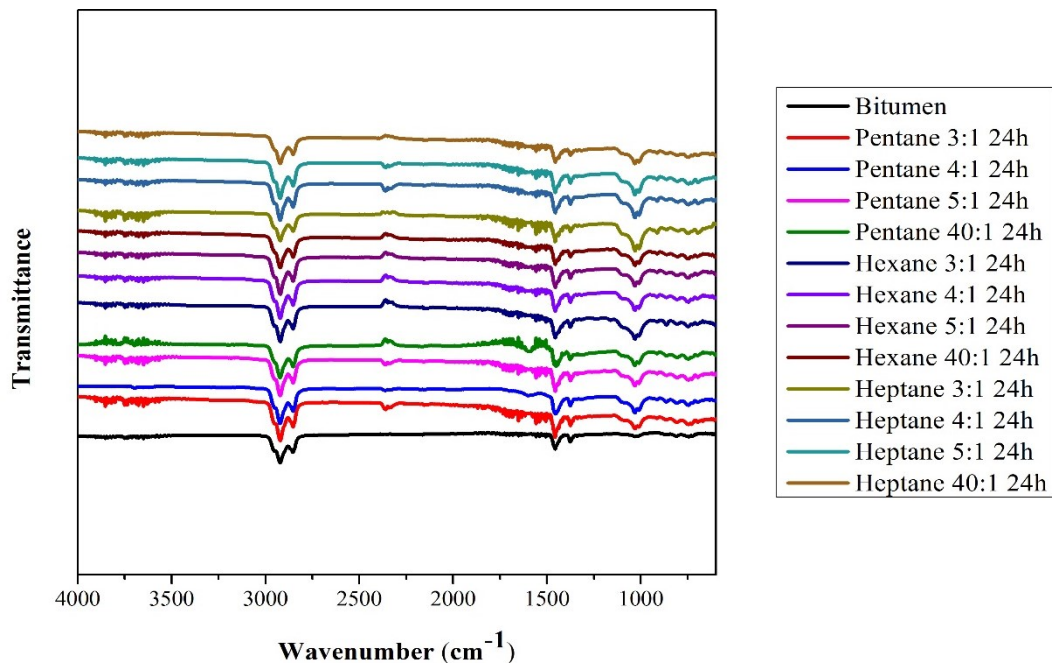


**Figure 4-2.** FTIR spectra of asphaltenes precipitated at different solvents and S/B ratios in the SDA process when the precipitation time = 24h

Changes in asphaltenes with precipitation time can be observed by comparing the FTIR spectra in Figure 4-2 and Figure 4-3. Figure 4-3 contains the FTIR spectra of asphaltenes precipitated after 330h in the SDA process. The absorption bands in Figure 4-3 are similar to those in Figure 4-2, and the differences could not be identified visually among the FTIR spectra with change of precipitation time from 24h to 330h.

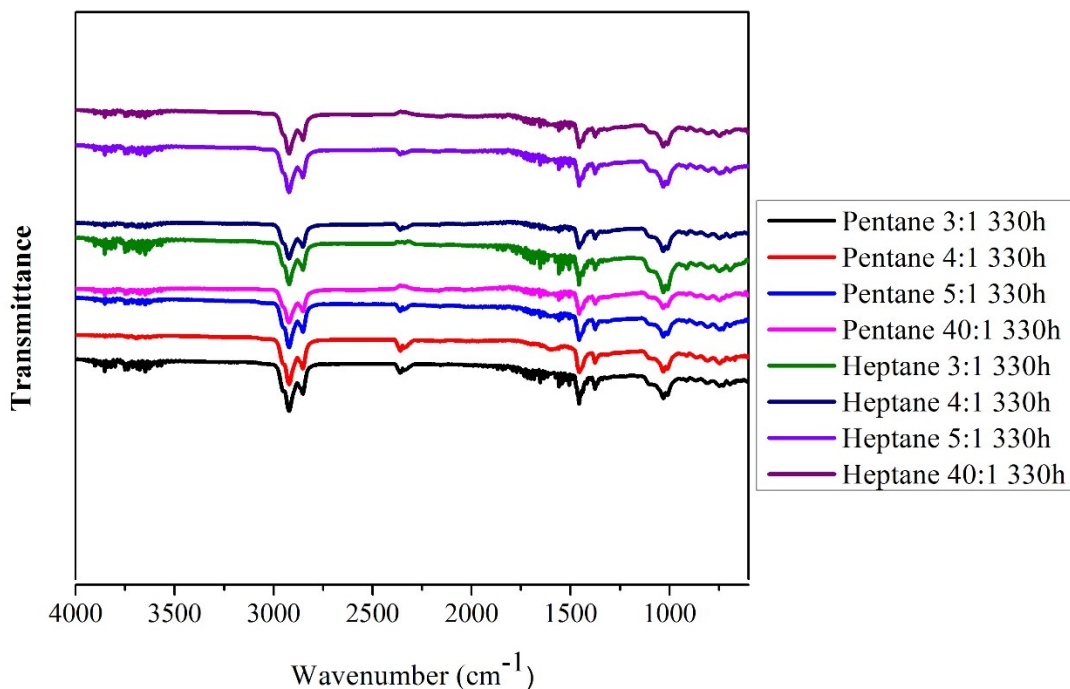


**Figure 4-3.** FTIR spectra of asphaltenes precipitated at different solvents and S/B ratios in the SDA process when the precipitation time = 330h

Figure 4-4 and Figure 4-5 contain IR spectra of DAO precipitated using different solvents and S/B ratios in the SDA process with precipitation time 24h and 330h respectively. They are similar to the FTIR spectrum of bitumen, and visually, no major differences were found with changes in solvent and S/B ratio in the SDA process. The IR peaks between  $\sim 1010$  and  $1030\text{cm}^{-1}$  and at  $\sim 1100\text{cm}^{-1}$ , which were present in the IR spectra of asphaltenes were less intense compared to those in the FTIR spectra of asphaltenes. No visually noticeable differences in DAO were found between 24h and 330h precipitation time by comparing Figure 4-4 and Figure 4-5.

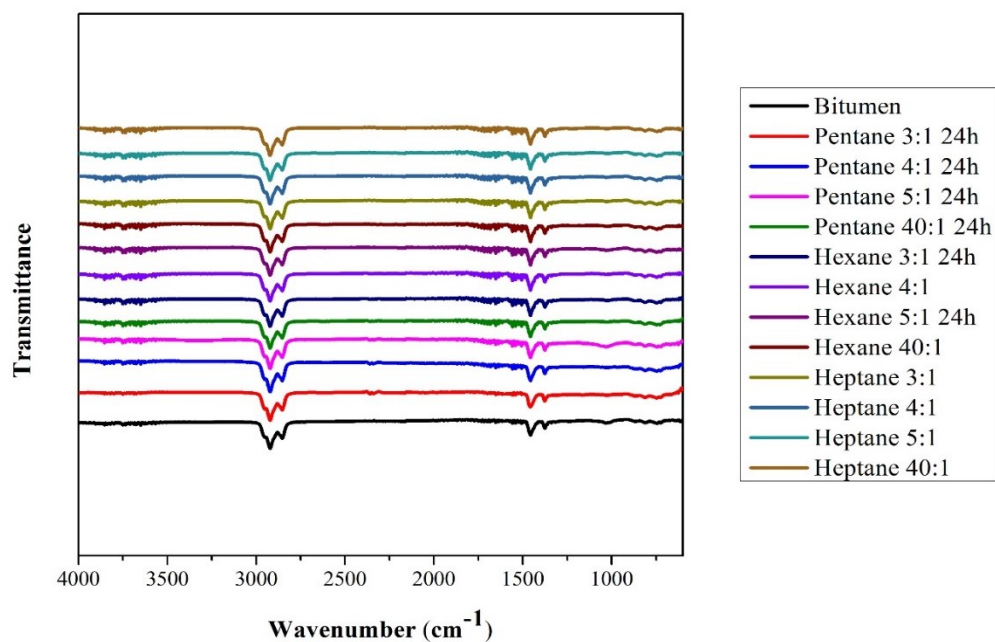


**Figure 4-4.** FTIR spectra of bitumen, and DAO for different solvents and S/B ratios in the SDA process when the precipitation time = 24h

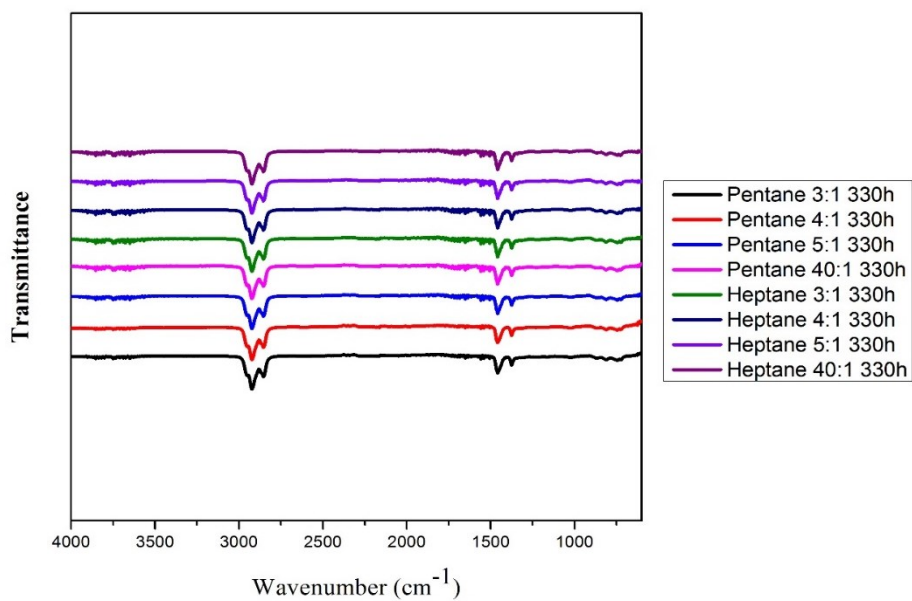


**Figure 4-5.** FTIR spectra of DAO for different solvents and S/B ratios in the SDA process when the precipitation time = 330h

#### 4.3.4 Free Radical Content

In ESR, the first derivative of the absorption signal is recorded as a function of g-factor, as shown in Figure 4-6. To obtain the area under the original absorption spectrum vs. g-factor plot, which is shown in Figure 4-7, a double integration is required. The double integral is proportional to free radical content in the sample.<sup>2</sup> As the same settings and precision tubes were used in the analyses of all the samples, the double integral values of the samples can be compared in order to study qualitatively how the free radical concentration varies among the samples.

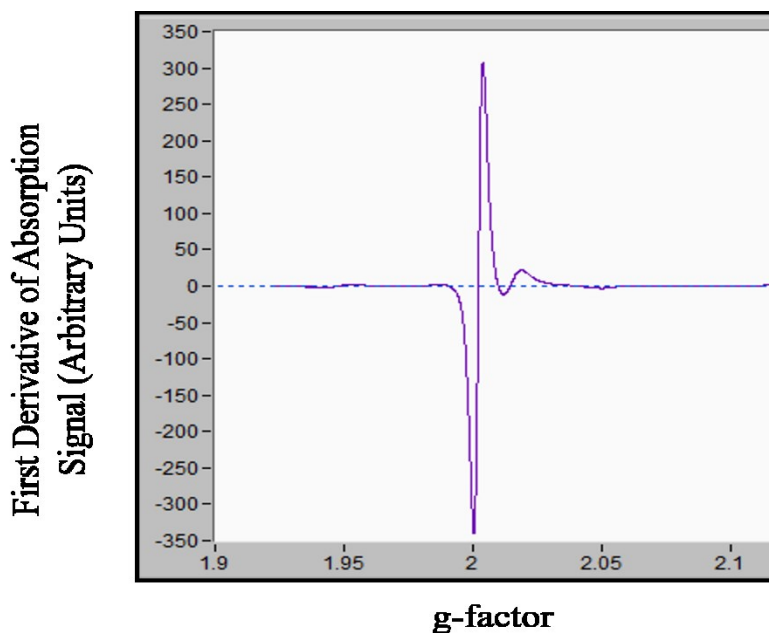


**Figure 4-6.** Graph showing first Derivative of Absorption Spectrum of asphaltenes vs. g-factor in the ESR spectroscopy of asphaltenes

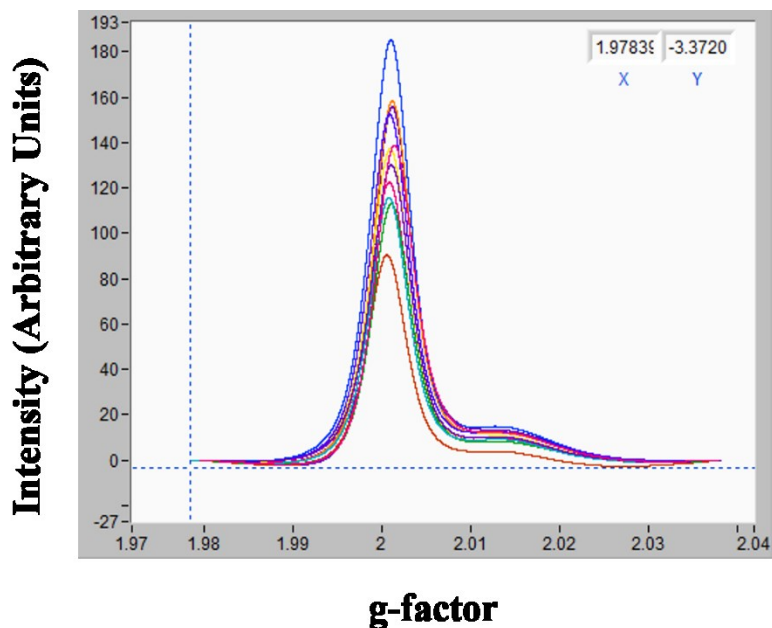


**Figure 4-7.** Absorption spectra of asphaltenes as a function of g-factor obtained in ESR spectroscopic analysis

The central peak in Figure 4-7 is from the organic free radical in asphaltenes. The double integral values of the central peak in C<sub>5</sub>, C<sub>6</sub> and C<sub>7</sub> asphaltenes precipitated at different conditions of the SDA process are plotted in Figure 4-8. The peak at  $g \approx 2.0146$  belongs to the vanadyl radical. Hyperfine splitting of vanadyl radical was not observed in the spectral range used in this study. As shown in Figure 4-7, there seems to be an overlap between the organic radical peak and vanadyl peak. Hence, the double integral value of the vanadyl peak was calculated by multiplying the double integral value of half portion of the vanadyl peak that didn't overlap with the organic radical peak by two. The double integral values of vanadyl radical peak in C<sub>5</sub>, C<sub>6</sub> and C<sub>7</sub> asphaltenes precipitated at different conditions of the SDA process are plotted in Figure 4-9.

The double integral values in both the figures increase from C<sub>5</sub> to C<sub>7</sub> asphaltenes, indicating that the free radical content in asphaltenes increases from C<sub>5</sub> to C<sub>7</sub> asphaltenes at the observed S/B ratios. It can also be observed that the double integral values of asphaltenes increase with increase in S/B ratio from 3:1 to 40:1, indicating that the free radical content in asphaltenes increases with increase in S/B ratio from 3:1 to 40:1.

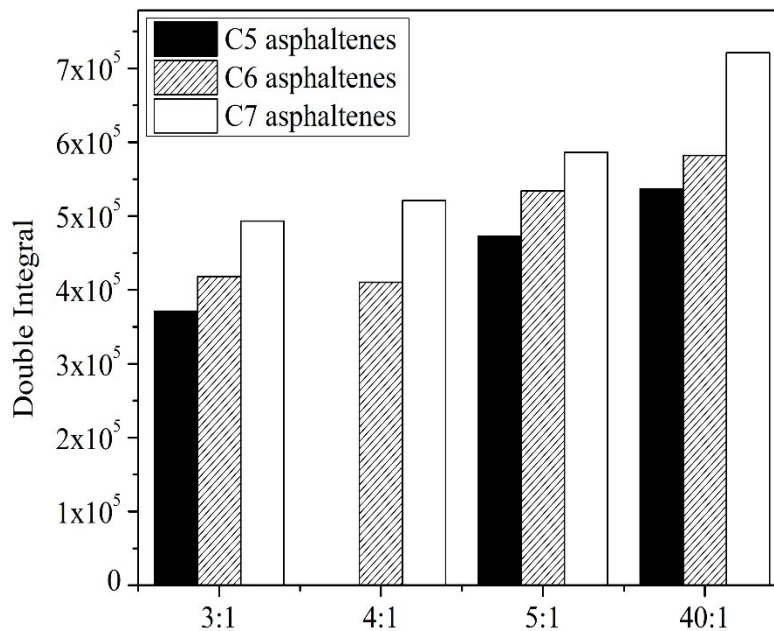


**Figure 4-8.** Double integral values of organic free radical peak in the ESR spectroscopy of C<sub>5</sub>, C<sub>6</sub> and C<sub>7</sub> asphaltenes at different S/B ratios. Precipitation Time = 24h

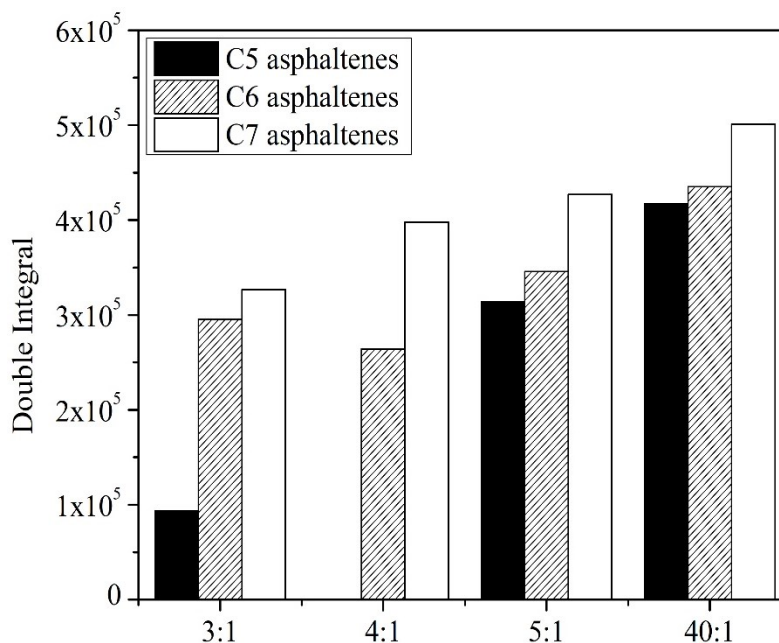


**Figure 4-9.** Double integral values of vanadyl radical peak in the ESR spectroscopy of C<sub>5</sub>, C<sub>6</sub> and C<sub>7</sub> asphaltenes at different S/B ratios. Precipitation Time = 24h

In Figure 4-7, the g-factor of the organic and vanadyl radical peaks appears to be different among the samples. Table 4-11 contains g-factors of organic radical peak in the ESR spectra of C<sub>5</sub>, C<sub>6</sub> and C<sub>7</sub> asphaltenes precipitated using different solvents and S/B ratios in the SDA process. The g-factors changed with the solvent and S/B ratio used in asphaltene precipitation by SDA process.

Table 4-12 contains g-factors of vanadyl peak in the ESR spectra of C<sub>5</sub>, C<sub>6</sub> and C<sub>7</sub> asphaltenes precipitated using different solvents and S/B ratios in the SDA process. The g-factors of C<sub>5</sub>, C<sub>6</sub> increased with increase in S/B ratio from 3:1 to 40:1 in the SDA process used for asphaltene precipitation. Also, the g-factors of vanadyl peak increased from C<sub>5</sub> to C<sub>7</sub> asphaltenes, at the observed S/B ratios.

**Table 4-11.** g-factors of organic free radical signal in the ESR spectra of asphaltenes precipitated using different solvents and at different S/B ratios in the SDA process, with precipitation time = 24h

S/B ratio	g-factor		
	C <sub>5</sub> asphaltenes	C <sub>6</sub> asphaltenes	C <sub>7</sub> asphaltenes
3:1	2.00062	2.00078	2.00139
4:1	- <sup>a</sup>	2.00109	2.001
5:1	2.00078	2.00094	2.00094
40:1	2.00109	2.00011	2.00094

<sup>a</sup> Sample was not available for analysis

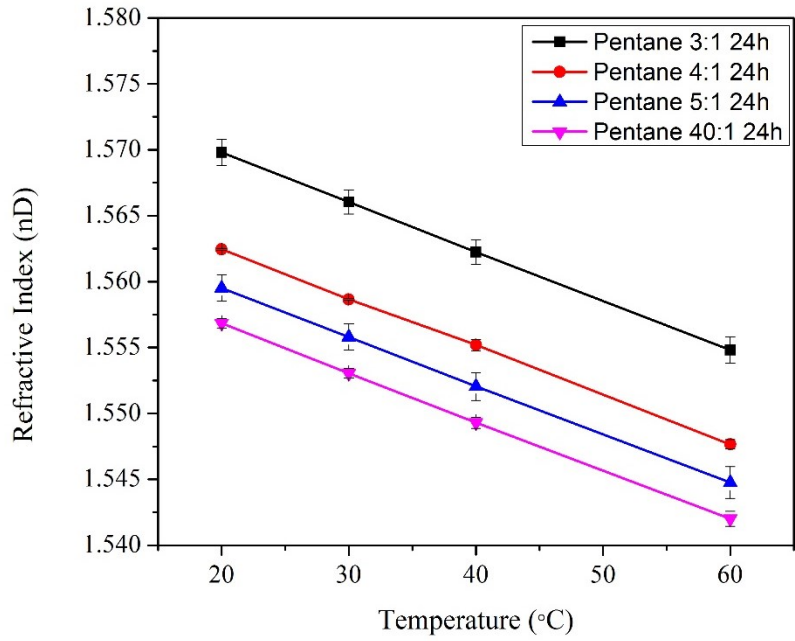
**Table 4-12.** g-factors of vanadyl peak in the ESR spectra of asphaltenes precipitated using different solvents and at different S/B ratios in the SDA process, with precipitation time = 24h

S/B ratio	g-factor		
	C <sub>5</sub> asphaltenes	C <sub>6</sub> asphaltenes	C <sub>7</sub> asphaltenes
3:1	2.01406	2.01453	2.01467
4:1	- <sup>a</sup>	2.01469	2.01487
5:1	2.01437	2.01469	2.015
40:1	2.01469	2.01484	2.01516

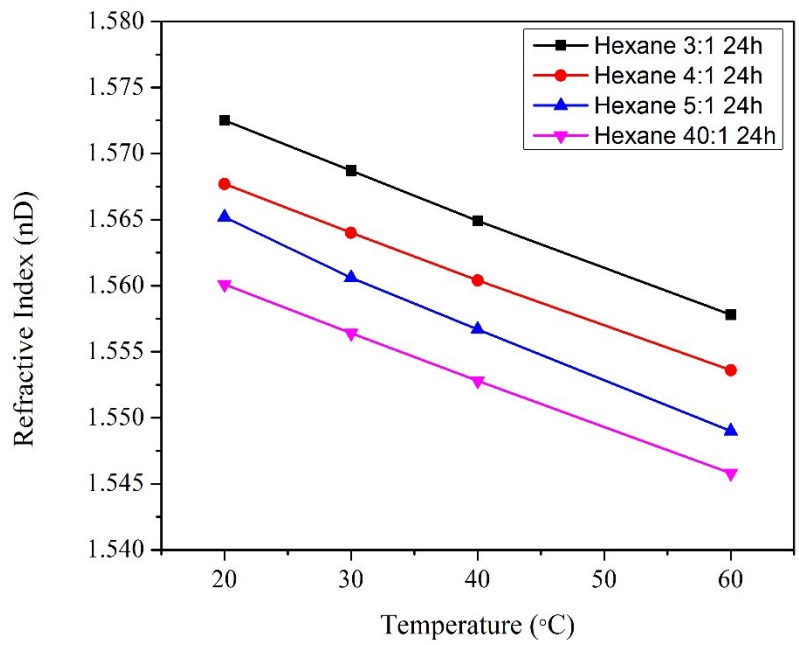
<sup>a</sup> Sample was not available for analysis

#### 4.3.5 Refractive Index of DAO

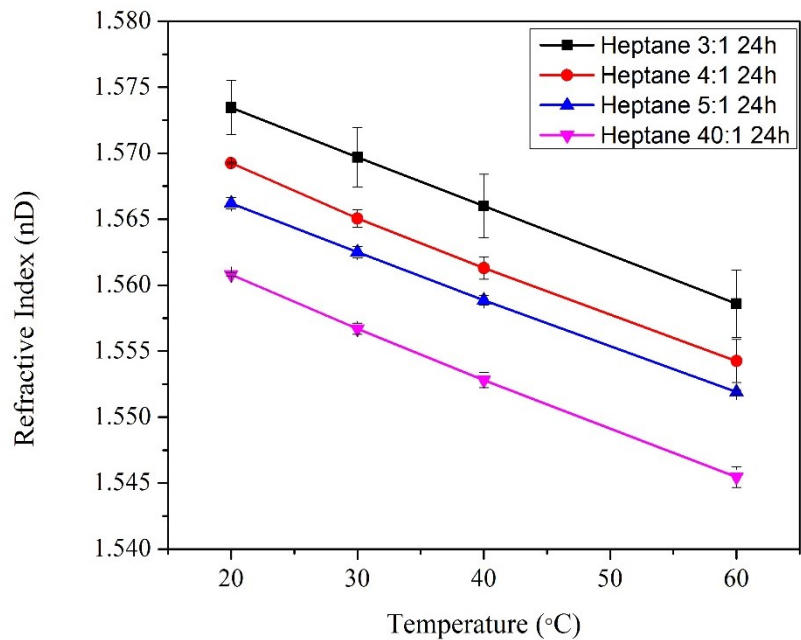
In this study, refractive indexes of DAO samples were measured at different temperatures in the range 20 to 60°C. Changes in refractive indexes of C<sub>5</sub>, C<sub>6</sub> and C<sub>7</sub> maltenes with the S/B ratios used in the SDA process are shown in Figure 4-10. Analysis was performed for three samples of C<sub>5</sub> and C<sub>7</sub> maltenes, and one sample of C<sub>6</sub> maltenes. Refractive index decreased with increase in temperature. The refractive index of maltenes decreased with increase in S/B ratio from 3:1 to 40:1 in the observed temperature range of 20 to 60°C.



(a)



(b)

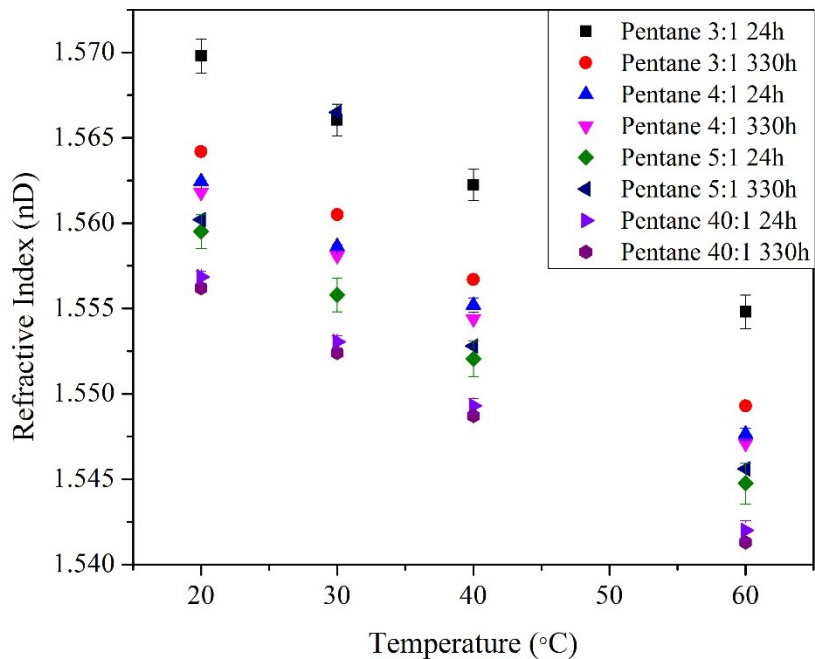


(c)

**Figure 4-10.** Refractive Indexes of DAO with temperature at different S/B ratios and precipitation time = 24h for (a) C<sub>5</sub> maltenes, (b) C<sub>6</sub> maltenes and (c) C<sub>7</sub> maltenes

Changes in refractive index with SDA precipitation time are shown in Figure 4-11. With increase in precipitation time, the refractive index of C<sub>5</sub> and C<sub>7</sub> maltenes decreased at the observed S/B ratios.

(a)



(b)

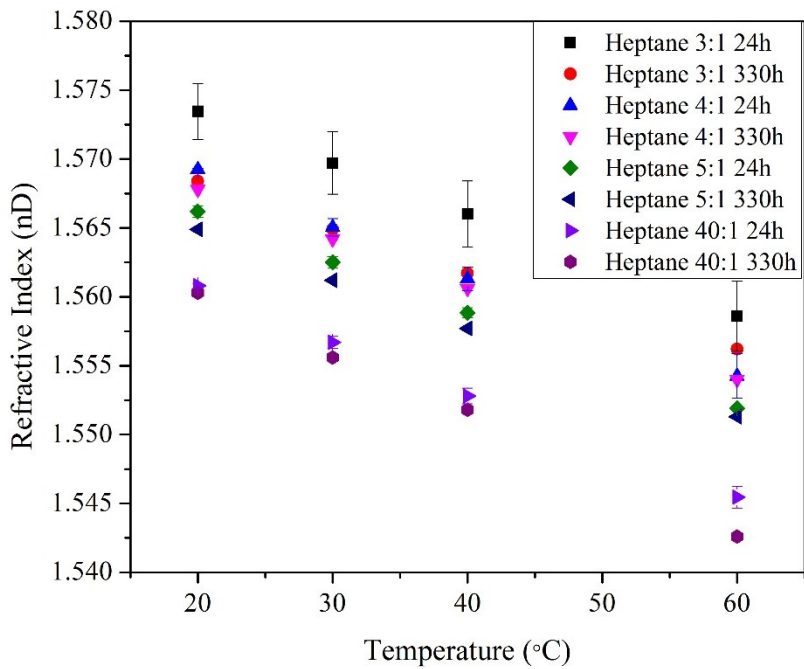


Figure 4-11. Effect of precipitation time in SDA process on the refractive Indexes of DAO

## 4.4 Discussion

### 4.4.1 Effect of SDA process on the chemical composition of asphaltenes and DAO

#### 4.4.1.1 Material balance of elements (C, H, N, S)

The elemental losses of C, H, N, S in the asphaltene precipitation experiments were obtained from material balance calculations (Eq. 4-1) and tabulated in Table 4-13.

$$Z_{loss} = Z_B - \frac{(Z_{Asp} \times Y_{Asp} + Z_{DAO} \times Y_{DAO})}{100} \quad \text{Eq. 4-1}$$

Where

$Z_{loss}$  = Elemental loss in terms of wt% of bitumen

$Z_B$  = wt% of element in bitumen

$Z_{Asp}$  = wt% of element in asphaltenes

$Y_{Asp}$  = yield of asphaltenes in terms of wt% of bitumen

$Z_{DAO}$  = wt% of element in DAO

$Y_{DAO}$  = yield of DAO in terms of wt% of bitumen

**Table 4-13.** Calculated elemental (C, H, N, S) losses during precipitation of asphaltenes using different solvents and S/B ratios

Solvent	S/B ratio	Calculated Elemental Losses (wt% of bitumen)			
		C	H	N	S
<i>n</i> -C <sub>5</sub>	3:1	10.03	1.15	0.16	0.86
	4:1	8.86	0.91	0.15	0.88
	5:1	6.76	0.77	0.13	0.63
	40:1	2.39	0.23	0.08	0.57
<i>n</i> -C <sub>7</sub>	3:1	8.35	0.92	0.14	0.40
	4:1	8.00	0.91	0.14	0.50
	5:1	5.68	0.64	0.11	0.32
	40:1	6.00	0.66	0.12	0.33

#### 4.4.1.2 Hydrogen to carbon (H/C) ratio

As mentioned in chapter 2, H/C ratio is an important quality indicator for petroleum products. Higher the H/C ratio, better is the quality. In general, low H/C ratios indicate high density, aromaticity and high micro carbon residue (MCR) or coking tendency.<sup>3</sup> Correlation of H/C ratio with the solubility parameters of petroleum fractions was reported by Gray.<sup>3</sup>

With the separation of asphaltenes in the SDA process, the H/C ratio increased from 1.45 in bitumen (calculated from Table 3-2 of Chapter 3) to 1.48-1.52 in DAO, as mentioned in Table 4-15.

The changes in H/C ratio of asphaltenes were caused by changes in both the carbon content (wt%) and hydrogen content (wt%), as shown in Table 4-1 and Table 4-2. The H/C ratio of C<sub>5</sub> and C<sub>7</sub> asphaltenes decreased with an increase in the S/B ratio from 3:1 to 40:1, as indicated in Table 4-14. This decrease with S/B ratio was higher for C<sub>5</sub> asphaltenes compared to C<sub>7</sub> asphaltenes, indicating that the effect of S/B ratio on the H/C ratio is more pronounced in the case of C<sub>5</sub> asphaltenes. These trends indicate that with increase in S/B ratio, the aliphatic nature of asphaltenes decreases and/or the cyclic content of the asphaltenes increases. The increase in asphaltene yield with S/B ratio (chapter 3) could be associated with increasing precipitation of the aromatic components of asphaltene fraction in bitumen. The boiling point and coking tendency of the asphaltenes phase should also increase, which could be detected using simulated distillation and thermogravimetric analysis. The results of these additional analyses will be provided in Chapter 5.

The H/C ratio of C<sub>5</sub> asphaltenes is greater than that of C<sub>7</sub> asphaltenes. The difference between the H/C ratios of C<sub>5</sub> and C<sub>7</sub> asphaltenes decreased from 3:1 to 40:1 and the effect of solvent on the H/C ratio of asphaltenes was low at S/B ratios 5:1 and 40:1 compared to 3:1 and 4:1.

**Table 4-14.** H/C ratio of C<sub>5</sub> and C<sub>7</sub> asphaltenes precipitated at different S/B ratios in the SDA process with precipitation time=24h

S/B ratio	H/C ratio	
	C <sub>5</sub> asphaltenes	C <sub>7</sub> asphaltenes
3:1	1.33	1.26
4:1	1.29	1.24
5:1	1.24	1.23
40:1	1.20	1.21

In the study of effect of precipitating conditions on the properties of asphaltenes by Ortega, et al.<sup>4</sup> C<sub>5</sub> and C<sub>7</sub> asphaltenes precipitated from Athabasca vacuum residue at S/B ratios 13:1 and 40:1 were compared. In their results, the H/C ratio of C<sub>5</sub> asphaltenes was greater than C<sub>7</sub> asphaltenes, and the H/C ratio decreased with increase in S/B ratio. The density measurements of solutions of asphaltenes in toluene followed the reverse trend.

In the study by Luo, et al.<sup>5</sup>, it was observed by characterization of C<sub>5</sub> and C<sub>7</sub> asphaltenes precipitated from heavy oil by <sup>1</sup>H NMR and <sup>13</sup>C NMR that C<sub>7</sub> asphaltenes were more aromatic than C<sub>5</sub> asphaltenes.

Asphaltene are characterized by high molecular weight and aromaticity.<sup>6</sup> The intermolecular forces in aromatic structures, which are closely packed, are greater compared to those in aliphatic compounds. Hence, the solvent power required to dissolve the aromatic components of bitumen increases with the aromaticity, indirectly measured by the H/C ratio. This could be the reason behind the decrease in H/C ratio from C<sub>5</sub> to C<sub>7</sub> asphaltenes, and with an increase in S/B ratio from 3:1 to 40:1.

As shown in Table 4-15, changes in the H/C ratio of DAO were much less than those observed among the asphaltenes.

**Table 4-15.** H/C ratio of C<sub>5</sub> and C<sub>7</sub> maltenes precipitated at different S/B ratios in the SDA process with precipitation time=24h

S/B ratio	H/C ratio	
	C <sub>5</sub> maltenes	C <sub>7</sub> maltenes
3:1	1.48	1.49
4:1	1.51	1.49
5:1	1.51	1.50
40:1	1.52	1.51

#### 4.4.1.3 Nitrogen, Sulfur and Oxygen

As mentioned in chapter 2, properties of asphaltenes and DAO depend on their chemical composition. In general, the higher boiling fractions contain higher concentration of nitrogen, sulfur, Ni and V. Density of heavy oils ( $\rho$ ) can be correlated with the elemental composition using Eq. 2-2,<sup>3</sup> at 15.6°C.

$$\rho = 1033 - 13.69H + 13.85S + 115.7N \quad \text{Eq. 4-2}$$

where  $\rho$  is the density of heavy oil in  $\frac{kg}{m^3}$ , and H,S,N are hydrogen, sulfur and nitrogen respectively, all in wt%. In the presence of heavy metals, the density further increases.

The nitrogen and sulfur content (wt%) in asphaltenes increased with increase in S/B ratio used in the SDA process, as shown in Table 4-3 and Table 4-4. The maximum percentage increase in the nitrogen and sulfur content in asphaltenes with increase in S/B ratio was ~20 and ~7% respectively. As mentioned in chapter 2, presence of nitrogen and sulfur containing compounds not only affects the properties of asphaltenes and DAO, but would also affect their processing

Measuring the separation selectivity for heteroatoms from bitumen into the asphaltenes phase at different process conditions is important. It is a fraction and is calculated using Eq. 4-3. For this purpose, the heteroatom content in asphaltenes, expressed as wt% of bitumen, was calculated from the heteroatom content in asphaltenes (wt%), mentioned in Table 4-3, using Eq. 4-4. The extractability of heteroatoms, defined as the amount of nitrogen (wt% of bitumen) present in the DAO, was calculated using Eq. 4-5.

$$\text{Separation Selectivity} = \frac{N'_{Asp}}{N_B} \quad \text{Eq. 4-3}$$

$$N'_{Asp} = \frac{N_{Asp} \times Y_{Asp}}{100} \quad \text{Eq. 4-4}$$

$$E_B = N_B - N'_{Asp} \quad \text{Eq. 4-5}$$

Where

$N_{Asp}$  = wt% of nitrogen in asphaltenes

$N'_{Asp}$  = wt% of nitrogen in asphaltenes in terms of wt% of bitumen

$Y_{Asp}$  = yield % of asphaltenes

$E_B$  = Extractability in terms of wt% of bitumen

$N_B$  = wt% of nitrogen in bitumen

The nitrogen content of asphaltenes, expressed as wt% of bitumen, calculated from Eq. 4-4, and the nitrogen content of bitumen (from chapter3) are plotted in Figure 4-12. The nitrogen content in asphaltenes represents 0.2 to 1 wt% of bitumen at the SDA conditions used in this study. The amount of bitumen represented by the nitrogen content in C<sub>5</sub> and C<sub>7</sub> asphaltenes increased with increase in S/B ratio from 3:1 to 40:1. The values in Figure 4-12 increased by 17 to 47% with increase in S/B ratios, which represents 6 to 10% of the nitrogen content in bitumen. The separation selectivity of C<sub>5</sub> and C<sub>7</sub> asphaltenes for nitrogen increased from 0.16 to 0.38 and 0.15 to 0.34 respectively with increase in S/B ratio from 3:1 to 40:1, as shown in Table 4-16.

The amount of bitumen represented by the nitrogen content of  $C_7$  asphaltenes appears to be lower than that represented by the nitrogen content of  $C_5$  asphaltenes, as shown in Figure 4-12. However, the difference between the two represents less than 5% of nitrogen content in bitumen. The separation selectivity slightly decreases from  $C_5$  to  $C_7$  asphaltenes, as shown in Table 4-16. It is interesting to notice that the nitrogen content of  $C_7$  asphaltenes is higher than that of  $C_5$  asphaltenes, as shown in Table 4-3, though the asphaltene yield and separation selectivities decrease from  $C_5$  to  $C_7$  asphaltenes. However, the effect of solvent on the separation selectivity is much lesser than that of the S/B ratio.

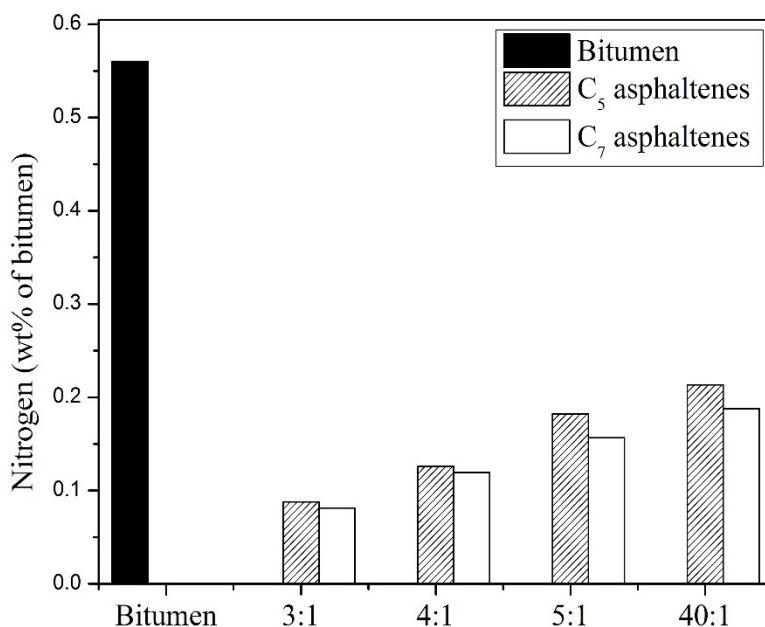


**Figure 4-12.** Nitrogen content of  $C_5$  and  $C_7$  asphaltenes, expressed as wt% of bitumen, at different S/B ratios of SDA process. Precipitation time = 24h

**Table 4-16.** Separation selectivities of C<sub>5</sub> and C<sub>7</sub> asphaltenes for nitrogen in bitumen at different conditions of SDA process. Precipitation Time = 24h

	C <sub>5</sub> asphaltenes	C <sub>7</sub> asphaltenes
3:1	0.16	0.15
4:1	0.22	0.21
5:1	0.33	0.28
40:1	0.38	0.34

The sulfur content of asphaltenes, expressed as wt% of bitumen, was calculated from Eq. 4-4 by replacing nitrogen with sulfur. These values at different conditions of SDA process were plotted along with the sulfur content of bitumen in Figure 4-13. The sulfur content in asphaltenes represents 0.6 to 1.5wt% of bitumen at the SDA conditions used in this study. The amount of bitumen represented by the sulfur content in C<sub>5</sub> and C<sub>7</sub> asphaltenes increased with increase in S/B ratio from 3:1 to 40:1. The values in Figure 4-13 increased by 8 to 40% with increase in S/B ratio, which represents less than 10% of the sulfur content in bitumen.

The separation selectivity for sulfur was calculated from Eq. 4-3, by replacing nitrogen with sulfur. The separation selectivities in C<sub>5</sub> and C<sub>7</sub> asphaltenes for sulfur increased from 0.2 to 0.3 and 0.1 to 0.3 respectively with increase in S/B ratio from 3:1 to 40:1, as shown in Table 4-17. These separation selectivities in C<sub>5</sub> and C<sub>7</sub> asphaltenes for sulfur are similar to those for nitrogen (Figure 4-12) in the range of S/B ratios from 3:1 to 5:1.

The amount of bitumen represented by the sulfur content of C<sub>7</sub> asphaltenes is lower than that represented by the sulfur content of C<sub>5</sub> asphaltenes, as shown in Figure 4-13. However, the difference between the two represents less than 5% of nitrogen content in bitumen. The separation selectivities decrease from C<sub>5</sub> to C<sub>7</sub> asphaltenes, as shown in Table 4-17. It is interesting to notice that the sulfur content of C<sub>7</sub> asphaltenes is higher than that of C<sub>5</sub> asphaltenes, as shown in Table 4-4, though the asphaltene yield and separation selectivities decrease from C<sub>5</sub> to C<sub>7</sub> asphaltenes.

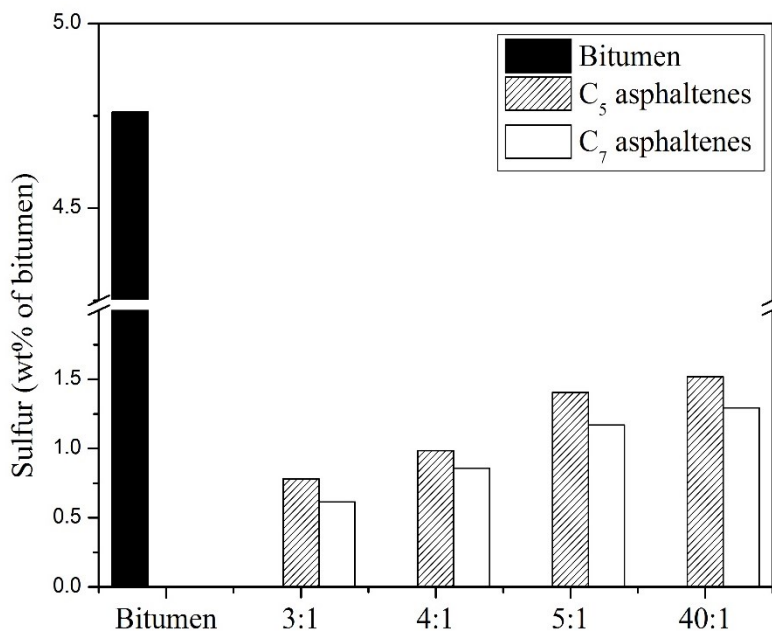


**Figure 4-13.** Sulfur content of C<sub>5</sub> and C<sub>7</sub> asphaltenes, expressed as wt% of bitumen, at different S/B ratios of SDA process. Precipitation time = 24h

**Table 4-17.** Separation selectivities of C<sub>5</sub> and C<sub>7</sub> asphaltenes for sulfur in bitumen at different conditions of SDA process. Precipitation Time = 24h

	C <sub>5</sub> asphaltenes	C <sub>7</sub> asphaltenes
3:1	0.16	0.13
4:1	0.21	0.18
5:1	0.30	0.25
40:1	0.32	0.27

These results indicate that with decrease in asphaltene yield (or increase in the yield of DAO), the separation selectivity for nitrogen and sulfur decreases, thus extracting higher amounts of nitrogen and sulfur from bitumen into the DAO.

The solvent and S/B ratio in SDA process affect the calculated oxygen content in asphaltenes, as shown in Table 4-5. As the oxygen content was calculated by difference, there could inherently be a high uncertainty in the results. The oxygen content of C<sub>5</sub> asphaltenes is lower than that of C<sub>7</sub> asphaltenes at the observed S/B ratios. Though the changes in oxygen content of C<sub>5</sub> asphaltenes with S/B ratio did not follow a regular trend, the oxygen content of C<sub>7</sub> asphaltenes decreased with an increase in S/B ratio.

The oxygen content of asphaltenes, expressed as wt% of bitumen, was calculated from Eq. 4-4 by replacing nitrogen with oxygen. These values at different conditions of SDA process were plotted along with the oxygen content of bitumen in Figure 4-14. The oxygen content in asphaltenes represents 0.8 to 1.3wt% of bitumen at the SDA conditions used in this study. The amount of bitumen represented by the sulfur content in C<sub>5</sub> and C<sub>7</sub> asphaltenes increased with increase in S/B ratio from 3:1 to 40:1 for C<sub>5</sub> asphaltenes and from 3:1 to 5:1 for C<sub>7</sub> asphaltenes. The oxygen content remained similar between 5:1 and 40:1 for C<sub>7</sub> asphaltenes. The values in Figure 4-14 increased by 0.7 to 17% with increase in S/B ratio, which represents less than 10% of the oxygen content in bitumen.

The separation selectivity for oxygen was calculated from Eq. 4-3, by replacing nitrogen with oxygen. The separation selectivities in C<sub>5</sub> and C<sub>7</sub> asphaltenes for oxygen increased from 0.4 to 0.7 and 0.5 to 0.7 respectively with increase in S/B ratio from 3:1 to 40:1, as shown in Table 4-18. The separation selectivities of oxygen are 2 to 4 times higher than those of nitrogen and sulfur. It is interesting to notice that though the separation selectivities and asphaltene yield increased with increase in S/B ratio, the oxygen content in asphaltenes decreased with increase in S/B ratio as shown in Table 4-5.

The amount of bitumen represented by the oxygen content of C<sub>5</sub> asphaltenes is lower than that represented by the oxygen content of C<sub>7</sub> asphaltenes, as shown in Figure 4-14. The difference between the two represents 3 to 15% of the oxygen content in bitumen. The separation selectivities increase from C<sub>5</sub> to C<sub>7</sub> asphaltenes, as shown in Table 4-18.

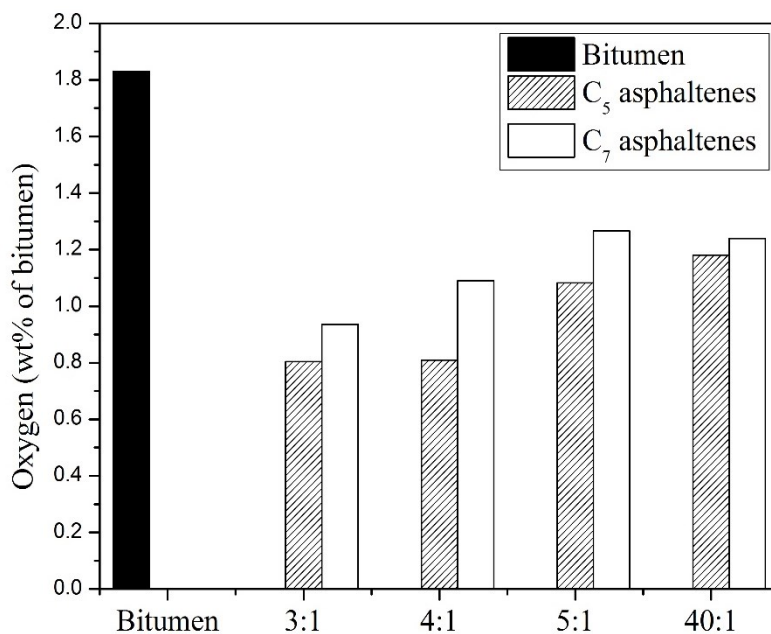


**Figure 4-14.** Oxygen content of C<sub>5</sub> and C<sub>7</sub> asphaltenes, expressed as wt% of bitumen, at different S/B ratios of SDA process. Precipitation time = 24h

**Table 4-18.** Separation selectivities of C<sub>5</sub> and C<sub>7</sub> asphaltenes for oxygen in bitumen at different conditions of SDA process. Precipitation Time = 24h

	C <sub>5</sub> asphaltenes	C <sub>7</sub> asphaltenes
3:1	0.44	0.51
4:1	0.44	0.60
5:1	0.59	0.69
40:1	0.65	0.68

Heteroatoms contribute to the polarity of bitumen, which has an impact on its solubility in organic solvents. Nitrogen and sulfur mainly occur in cyclic, aromatic structures of bitumen.<sup>6</sup> Nitrogen is present in the form of alkyl carbazoles, alkyl quinolines, alkyl pyridines, alkyl metalloporphyrins etc.<sup>6</sup> Sulphur is present in the form of alkyl thiophenes, alkyl dibenzothiophenes, cycloalkano benzo-

thiophones etc.<sup>6</sup> Oxygen is present in the following functions groups of compounds: carboxylic acids, ketones, alcoholic hydroxyl, ethers and esters.<sup>6</sup> These electronegative elements also result in hydrogen bonding interactions in bitumen. As mentioned in chapter 2, in addition to dispersion forces, it is important to consider polar and hydrogen bonding interactions in bitumen, in order to study the solubility of bitumen in solvents more accurately. Hansen solubility parameters of the *n*-paraffin solvents used in this study along with bitumen are given in Table 4-19.  $\delta_D$  corresponds to the dispersion forces between molecules and is nearly equal to the  $\delta_2$  values,  $\delta_P$  corresponds to the polar forces and  $\delta_H$  corresponds to the hydrogen bonding interactions between the molecules.<sup>6</sup>

**Table 4-19.** Hansen solubility parameters of *n*-pentane, *n*-hexane, *n*-heptane and bitumen.<sup>7</sup>

	$\delta_D$	$\delta_P$	$\delta_H$
<i>n</i> -pentane	14.5	0.0	0.0
<i>n</i> -hexane	14.9	0.0	0.0
<i>n</i> -heptane	15.3	0.0	0.0
Bitumen <sup>a</sup>	17.9	4.6	3.2

<sup>a</sup> Average values for 15 different bitumens are reported

Asphaltenes represent the highly polar fraction of bitumen.<sup>7</sup> As shown in Table 4-19, the solvents used in this study are completely non-polar. However, it is difficult to interpret the relative selectivity for partitioning of heteroatoms from bitumen among the solvents, at a given S/B ratio, using the concept of Hansen solubility parameters.

With an increase in the S/B ratio from 3:1 to 40:1, the contribution of polar and hydrogen bonding components, as well as the overall Hansen solubility parameter of the solvent-bitumen mixture decreases. This would have led to increase in the separation selectivity for nitrogen and sulfur in bitumen, with increase in S/B ratio.

#### 4.4.1.4 Nickel and Vanadium

The Nickel and Vanadium content of asphaltenes, expressed as ppm or  $\mu\text{g/g}$  of bitumen, was calculated using Eq. 4-6. These values at different conditions of SDA process were plotted along with the Ni and V content of bitumen in Figure 4-15.

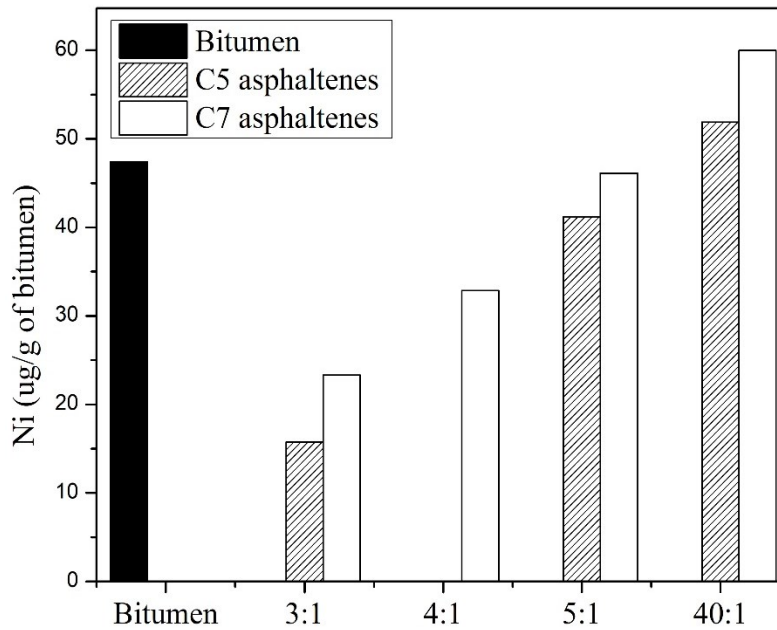
$$X'_{Asp} = \frac{X_{Asp} * Y_{Asp}}{100} \quad \text{Eq. 4-6}$$

Where

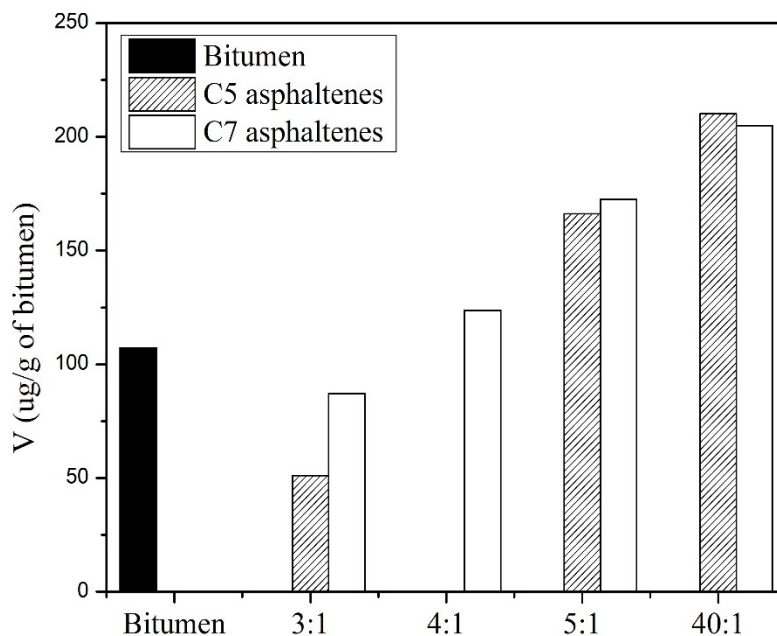
$X_{Asp}$  = Ni or V in asphaltenes in terms of ppm

$X'_{Asp}$  = Ni or V in asphaltenes in terms of ppm of bitumen

$Y_{Asp}$  = yield of asphaltenes in terms of wt% of bitumen



(a)



(b)

**Figure 4-15.** (a) Nickel (Ni) and (b) Vanadium (V) content of C<sub>5</sub> and C<sub>7</sub> asphaltenes, expressed as wt% of bitumen, at different S/B ratios of SDA process. Precipitation time = 24h

As shown in Figure 4-15, the amount of Ni and V in asphaltenes on weight basis of bitumen, increases with increase in S/B ratio. The separation selectivities were calculated from Eq. 4-3, by replacing nitrogen with nickel or vanadium. The separation selectivities in C<sub>5</sub> and C<sub>7</sub> asphaltenes for nickel are shown in Table 4-20. The separation selectivities at 40:1 are greater than one, indicating that the amount of nickel separated into asphaltenes phase is greater than the amount of nickel present in bitumen, which is not possible. However, the trends indicate that the separation selectivity increases with increase in S/B ratio from 3:1 to 40:1. The separation selectivities of nickel in asphaltenes increased from C<sub>5</sub> to C<sub>7</sub> asphaltenes.

**Table 4-20.** Separation selectivities of C<sub>5</sub> and C<sub>7</sub> asphaltenes for nickel in bitumen at different conditions of SDA process. Precipitation Time = 24h

	C <sub>5</sub> asphaltenes	C <sub>7</sub> asphaltenes
3:1	0.33	0.49
4:1	-	0.68
5:1	0.87	0.95
40:1	1.08	1.24

Similar trends were observed in the separation selectivities for vanadium in asphaltenes at different conditions of the SDA process, as shown in Table 4-21. However, most of the values are greater than one, indicating that the mass balance of vanadium in the SDA process is not satisfied by the measurements of XRF analysis.

**Table 4-21.** Separation selectivities of C<sub>5</sub> and C<sub>7</sub> asphaltenes for vanadium in bitumen at different conditions of SDA process. Precipitation Time = 24h

	C <sub>5</sub> asphaltenes	C <sub>7</sub> asphaltenes
3:1	0.48	0.81
4:1	-	1.15
5:1	1.55	1.61
40:1	1.96	1.91

Thus, the extractability of nickel and vanadium into DAO from bitumen decreases with increase in S/B ratio, and decreases from C<sub>5</sub> to C<sub>7</sub> asphaltenes.

As mentioned in chapter 2, it is desired to extract lesser amounts of N, S, Ni and V into DAO in the SDA process. The density of DAO increases with increase in the concentration of heteroatoms and heavy metals. In this study, the extractability of N, O, S, Ni and V, from bitumen into DAO is represented by Eq. 4-5. The extractability decreases with increase in S/B ratio from 3:1 to 40:1.

This indicates that the improvement in the quality of DAO, associated with removal of heteroatoms and heavy metals, can be accomplished by separating higher amount of asphaltenes from bitumen in the SDA process. As mentioned in chapter 1, removal of asphaltenes from bitumen represents a significant loss of material. Hence, there is a trade-off between quality improvement of DAO and losses associated with increased precipitation of asphaltenes.

#### **4.4.2 FTIR Spectra of asphaltenes and DAO at different conditions of SDA process**

The IR peaks observed at  $\sim 2925\text{cm}^{-1}$  and  $2853\text{cm}^{-1}$  in Figure 4-2, Figure 4-3, Figure 4-4 and Figure 4-5 correspond to C-H asymmetric and symmetric stretches respectively, in the CH<sub>2</sub> and CH<sub>3</sub> groups.<sup>8,6</sup> In addition, peaks were observed at  $\sim 1456\text{cm}^{-1}$  and  $\sim 1375\text{cm}^{-1}$ , which correspond to the vibrational bending of methyl and methylene groups.<sup>8,6</sup> The group of peaks between 1800 and  $1600\text{cm}^{-1}$  correspond to the double bond region (C=C and C=O).<sup>9</sup> The peaks between 850 and  $700\text{cm}^{-1}$  are from “the out-of-plane deformation vibration of one isolated aromatic C-H bond ( $870\text{cm}^{-1}$ ), two or three adjacent aromatic C-H bonds ( $814\text{cm}^{-1}$ ) and four aromatic adjacent aromatic bonds ( $750\text{cm}^{-1}$ )”.<sup>8</sup>

Asphaltenes showed additional peaks in FTIR spectroscopy between  $\sim 1010$  and  $1030\text{cm}^{-1}$  and at  $\sim 1100\text{cm}^{-1}$ , as shown in Figure 4-2 and Figure 4-3. The peaks between  $\sim 1010$  and  $1030\text{cm}^{-1}$  correspond to the sulfoxide groups (S=O stretch).<sup>6</sup> The peak at  $\sim 1100\text{cm}^{-1}$  corresponds to C-O stretch in secondary alcohol.<sup>10</sup>

There could be more differences among the FTIR spectra of the samples, which could not be detected visually from the graphs and would require a detailed multivariate modeling analysis. Hence, it cannot be concluded that there is no effect of the SDA process conditions on the chemical structure of asphaltenes and DAO.

#### 4.4.3 Effect of SDA process on free radical content of asphaltenes and DAO

As mentioned in chapter 2, asphaltenes contain a high concentration of free radicals. Free radical reactions occur in upgrading and refining processes and could impact coke formation.<sup>11,12</sup> According to literature, free radicals in asphaltenes also play a role in aggregation and deaggregation of asphaltenes when dissolved in solvents, and vanadium free radicals could lead to catalyst deactivation in upgrading and refining processes.<sup>13</sup> For these reasons, it is important to measure the free radical concentration, in order to develop methods to modify or reduce the free radicals present in asphaltenes.

According to literature, the organic radical peak at  $\sim g=2.003$  in Figure 4-6 and Figure 4-7 is exhibited by the polycyclic aromatic carbocations present in asphaltenes.<sup>11</sup> The presence of paramagnetic  $VO^{+2}$  ions (valency of vanadium = 4) in asphaltenes displays a signal in ESR spectrum of asphaltenes.<sup>11</sup> The g-factor of vanadyl ion is  $\sim 1.96$ .<sup>2</sup> In the previous studies, it was observed that the vanadyl or  $VO^{+2}$  ions generate multiple peaks due to hyperfine splitting in this spectral range.<sup>6,11,13</sup> However, in the present study, only one peak was observed at  $\sim g=2.0145$ , corresponding to the vanadyl radical. This could be due low concentration of vanadium or due to the presence of the solvent toluene. It was previously reported in literature that the nature of solvent and dipole moment of the solvent plays a role in affecting the intensity and g-factor of the peaks in ESR spectroscopy.<sup>13</sup>

The ESR spectroscopic results of asphaltenes in Figure 4-8 and Figure 4-9 indicate that the solvent and S/B ratio used in the SDA process affect the free radical concentration in asphaltenes. Though it is possible that the nature and concentration of free radicals in the precipitated asphaltenes could be different from those of the original asphaltenes present in bitumen, these trends indicate that with increase in asphaltene yield in the SDA process, the free radical concentration of precipitated asphaltenes increases. The increase in free radical content of asphaltenes could also be due to free radical reactions (initiation, hydrogen abstraction, termination reactions) occurring in bitumen-solvent mixture during solvent deasphalting process, leading to formation of new free radicals and asphaltene species. However, the ambient temperature and nature of solvents used in this study may play a role in the free radical reactions.

As shown in Table 4-11 and Table 4-12, the g-factor of asphaltenes varied between 2.00062 and 2.0014 for the organic free radical peak, and between 2.01406 to 2.01516 for the vanadyl radical peak of asphaltenes. These values are different from the g-factor values for bitumen (2.0025 and 2.0146 for organic and vanadyl radical peaks respectively). As mentioned earlier, the g-factors of the ESR peaks of asphaltenes changed with different solvents and S/B ratios used in the precipitation of asphaltenes. These changes in the paramagnetic properties of asphaltenes indicate that not only the concentration of free radicals, but the nature of free radicals in the precipitated asphaltenes phase is different when different conditions of SDA process are used. The g-factor helps to identify different types of samples.<sup>2</sup> Free radical centred on carbon atom has a g-factor 2.0023.<sup>2</sup> The g-factors may vary depending on whether the carbon free radical is a primary, secondary or tertiary radical. Presence of heteroatoms shifts the g-factors.<sup>2</sup> “For example benzosemiquinones, which have significant spin density on oxygens, have  $g \sim 2.004$  and nitroxide radicals which have spin density on a nitrogen and oxygen have  $g \sim 2.006$ . Metal ions have very different g-factors. For example, the vanadyl ion has  $g \sim 1.96$ ”.<sup>2</sup>

As shown in Figure 4-16, the double integral values of vanadyl radical at  $g \sim 2.0145$  were plotted against the vanadium content expressed in ppm from Figure 4-1. A linear correlation was found showing an increase in the double integral values with vanadium content in ppm, indicating that the double integral values of vanadyl radical at  $g \sim 2.0145$  can be used to predict the vanadium content in ppm in asphaltenes and vice versa. The double integral value of bitumen (406.62) at the same settings of ESR, fits to the same correlation with vanadium in ppm, as shown in Figure 4-16. According to literature, “Vanadium atoms in other than the four-valent state have not been detected with certainty in carbonaceous materials”.<sup>6</sup>

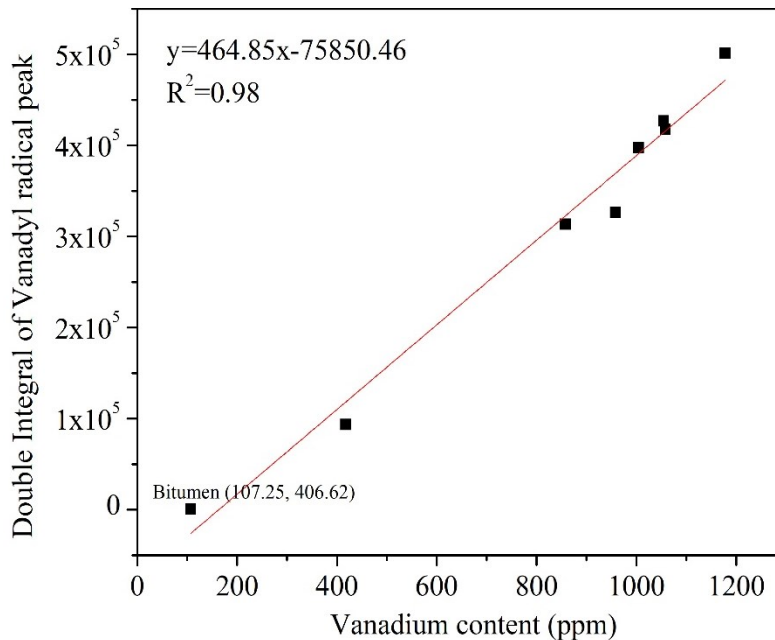


**Figure 4-16.** Correlation between double integral values of vanadyl free radical peak of asphaltenes from ESR spectroscopy and their vanadium content from XRF spectrometry.

#### 4.4.4 Effect of SDA process on the refractive index of DAO

Refractive index provides information about the composition and physical properties of the hydrocarbon liquid. Density and viscosity behave similar to refractive index with respect to temperature. At higher temperature, expansion of the liquid leads to a decrease in density. Refractive index and liquid density are used to estimate the polarizability of liquids, which is related to the strength of intermolecular forces.<sup>14</sup> Changes in refractive index can be attributed to changes in aromatic content, molecular de-aggregation and expansion.<sup>8,15</sup>

A decrease in refractive index of DAO with increase in S/B ratio, as shown in Figure 4-10, could be related to a decrease in the aromatic content of maltenes, due to separation of higher amount of asphaltenes, which are more aromatic, at higher S/B ratios.

In Figure 4-10, refractive index appears to decrease linearly with temperature. Temperature coefficient of refractive index, which is an indication of the change in slope of the refractive index vs temperature plot of the sample with temperature, is given by Eq. 4-7.

$$\frac{dn}{dT} = \frac{n_2 - n_1}{T_2 - T_1} \quad \text{Eq. 4-7}$$

where  $\frac{dn}{dT}$  is the temperature coefficient of refractive index,  $n_2$  and  $n_1$  are the refractive indexes of the sample at temperatures  $T_2$  and  $T_1$  respectively.

The temperature coefficient of the samples is  $\sim 34\text{-}39 \times 10^{-5}/^\circ\text{C}$ , which indicates that the change in refractive index of DAO with change in temperature from 20 to 60°C is nearly constant. Also, the slopes of the lines of different DAO samples are almost similar in the temperature range 20 to 60°C.

The refractive index at different S/B ratios follows the order:  $C_5$  maltenes  $<$   $C_6$  maltenes  $<$   $C_7$  maltenes, and refractive index of  $C_5$  and  $C_7$  maltenes decreased with increase in precipitation time from 24h to 330h. This indicates that  $C_7$  maltenes are more aromatic than  $C_6$  and  $C_5$  maltenes, and that the aromatic content of DAO decreases with increase in precipitation time from 24h to 330h. Though changes in refractive index provide useful information about the changes in the composition, the refractive indexes of DAO at different SDA process conditions could not be meaningfully compared due to the variability in DAO yield and material losses in the SDA process, as mentioned in chapter 3.

## 4.5 Conclusions

- Hydrogen to carbon (H/C) ratio of  $C_5$  asphaltenes decreased from 1.3 to 1.20 and that of  $C_7$  asphaltenes decreased from 1.26 to 1.21 with increase in S/B ratio from 3:1 to 40:1. Changes in both carbon and hydrogen content contributed to changes in H/C ratio with SDA process conditions.
- The nitrogen, sulfur, nickel and vanadium content in asphaltenes increased with increase in S/B ratio from 3:1 to 40:1.  $C_7$  asphaltenes contained higher amount of N, S, Ni and V compared to  $C_5$  asphaltenes.
- The separation selectivity and extractability of nitrogen, sulfur, oxygen, nickel and vanadium were affected by the solvent and S/B ratio used in the SDA process. The separation selectivity increased ( $\uparrow$ ) with increase in S/B ratio from 3:1 to 40:1 in the SDA process, in the following manner:

	N	S	O	Ni	V
C <sub>5</sub>	↑ 0.16 to 0.38	↑ 0.16 to 0.32	↑ 0.44 to 0.65	↑ 0.33 to 1.08	↑ 0.48 to 1.96
C <sub>7</sub>	↑ 0.15 to 0.34	↑ 0.13 to 0.27	↑ 0.51 to 0.68	↑ 0.49 to 1.24	↑ 0.81 to 1.91

- Higher S/B ratios would be required to extract lesser amount of N, S, Ni and V into DAO in the solvent deasphalting process. Density of DAO, which depends on heteroatoms and heavy metals, may be improved by performing solvent deasphalting at higher S/B ratios. There is a trade-off between quality improvement in DAO and the material loss associated with removal of higher yield of asphaltenes from bitumen at higher S/B ratios in the SDA process.
- The double integral values of organic free radical peak and vanadyl peak in ESR spectroscopy of asphaltenes, increased from C<sub>5</sub> to C<sub>7</sub> asphaltenes, and with increase in S/B ratio from 3:1 to 40:1. A linear correlation was observed between the double integral values of vanadyl peak of asphaltenes and their corresponding vanadium content in ppm, measured in XRF spectrometry.
- The solvent and S/B ratio in the solvent deasphalting process not only affected the double integral values of the ESR peaks, but also their g-factors. The g-factor of asphaltenes varied between 2.00062 and 2.0014 for the organic free radical peak, and between 2.01406 to 2.01516 for the vanadyl radical peak of asphaltenes at the solvent deasphalting process conditions used in this study. The g-factor increased with increase in S/B ratio from 3:1 to 40:1.
- Visual observation of FTIR spectra of asphaltenes and DAO did not indicate any noticeable changes with SDA process conditions, except that the FTIR spectra of asphaltenes, precipitated after 24h and 330h precipitation time in the SDA process, contained additional peaks between ~1010 cm<sup>-1</sup> and 1030 cm<sup>-1</sup>, and at 1100cm<sup>-1</sup>, which, according to literature correspond to the sulfoxide (S=O) groups and C-O of secondary alcohol respectively. A detailed multivariate analysis of the FTIR spectra would be required to determine the changes in the spectra with SDA process conditions.

- Refractive Index of DAO decreased with temperature ranging from 20 to 60°C. The temperature coefficient of DAO samples was  $\sim 34\text{-}39 * 10^{-5}/^{\circ}\text{C}$ , indicating that the slope of the refractive index vs. temperature plot of DAO samples is nearly constant with change in temperature from 20 to 60 °C, and the slopes for all the DAO samples used in this study were nearly similar.

## 4.6 References

1. Stuart, B., *Infrared Spectroscopy Fundamentals and Applications*. J. Wiley: Chichester, West Sussex, England, 2004.
2. Eaton, G. R., Eaton, S. S., Barr, D. P. and Weber, R. T., *Quantitative EPR*. Springer Science & Business Media: 2010.
3. Gray, M. R., *Upgrading Oilsands Bitumen and Heavy Oil*. University of Alberta Press: Edmonton, Alberta, 2015.
4. Ortega, L. C., Rogel, E., Vien, J., Ovalles, C., Guzman, H., Lopez-Linares, F. and Pereira-Almao, P., Effect of Precipitating Conditions on Asphaltene Properties and Aggregation. *Energy & Fuels* **2015**, *29* (6), 3664-3674.
5. Luo, P., Wang, X. and Gu, Y., Characterization of Asphaltenes Precipitated with Three Light Alkanes under Different Experimental Conditions. *Fluid Phase Equilibria* **2010**, *291* (2), 103-110.
6. Strausz, O. P. and Lown, E. M., *The Chemistry of Alberta Oil Sands, Bitumens and Heavy Oils*. Alberta Energy Research Institute: Calgary, 2003.
7. Hansen, C. M., *Hansen Solubility Parameters a User's Handbook*. 2nd ed.; CRC Press: Boca Raton, 2007.
8. Yanez Jaramillo, L. M. Visbreaking of Oilsands Bitumen between 150° and 300°C. MSc Thesis, University of Alberta, Edmonton, AB, Canada, 2016.
9. Borrego, A. G., Blanco, C. G., Prado, J. G., Díaz, C. and Guillén, M. D., 1h NMR and FTIR Spectroscopic Studies of Bitumen and Shale Oil from Selected Spanish Oil Shales. *Energy & Fuels* **1996**, *10* (1), 77-84.
10. Coates, J., Interpretation of Infrared Spectra, a Practical Approach. In *Encyclopedia of Analytical Chemistry*, John Wiley & Sons, Ltd: 2006.
11. Niizuma, S., Steele, C. T., Gunning, H. E. and Strausz, O. P., Electron Spin Resonance Study of Free Radicals in Athabasca Asphaltene. *Fuel* **1977**, *56* (3), 249-256.
12. Peraza, A., Sánchez, M. and Ruetter, F., Modeling Free-Radical Reactions, Produced by Hydrocarbon Cracking, with Asphaltenes. *Energy & Fuels* **2010**, *24* (7), 3990-3997.

13. Khulbe, K. C., Mann, R. S., Lu, B. C. Y., Lamarche, G. and Lamarche, A. M., Effects of Solvents on Free Radicals of Bitumen and Asphaltenes. *Fuel Processing Technology* **1992**, 32 (3), 133-141.
14. George, A. K. and Singh, R. N., Correlation of Refractive Index and Density of Crude Oil and Liquid Hydrocarbon. *International Journal of Chemical, Environmental & Biological Sciences (IJCEBS)* **2015**, 3 (5), 420-422.
15. Evdokimov, I. N. and Losev, A. P., Effects of Molecular De-Aggregation on Refractive Indices of Petroleum-Based Fluids. *Fuel* **2007**, 86 (15), 2439-2445.

## **CHAPTER 5. EFFECT OF SDA PROCESS ON THE THERMAL PROPERTIES OF ASPHALTENES AND DAO**

### **5.1 Introduction**

Transportation and processing of bitumen and its fractions are performed over a range of temperatures. At low temperatures, phase separation of solids can lead to fouling and plugging of process equipment.<sup>1</sup> In many upgrading processes, reactions are performed at temperatures as high as 500°C.<sup>2</sup> Thermal properties of asphaltenes and DAO such as melting, boiling, cracking and coking tendency are important to monitor, as they impact the design, flexibility, chemistry, and efficiency of the processes. In this chapter, the thermal behavior of asphaltenes and DAO obtained from bitumen at different conditions of the SDA process was studied.

The boiling point profile of the samples was obtained by Simulated Distillation (SimDis). Hot Stage Microscopy (HSM) was used to visually observe the changes in asphaltenes upon heating. The microcarbon residue (MCR), which is a measure of the coking tendency of the substance, was measured for asphaltenes and DAO using thermogravimetric analysis (TGA). The data obtained from these analyses was analyzed by calculations and correlations, to interpret the effect of the SDA process conditions on the thermal properties of DAO and asphaltenes.

### **5.2 Materials and Methods**

#### **5.2.1 Materials**

DAO and asphaltenes produced from SDA of bitumen using C<sub>5</sub>, C<sub>6</sub> and C<sub>7</sub> solvents at S/B ratios 3:1, 4:1, 5:1 and 40:1 (ml/g) and precipitation times 24h and 330h were analyzed.

#### **5.2.2 Analyses**

SimDis analysis and MCR measurement by TGA performed in Chapter 3 for bitumen, were also performed for asphaltenes and DAO.

Hot stage microscopy was used to visually observe the liquefying behavior of asphaltenes. An Olympus BX50 microscope with a camera attachment and coupled with Mettler FP84HT thermal analysis cell was used for this analysis. Asphaltenes (<1mg) were heated from 25 to 300°C at 10°C/min in a glass crucible and videos were captured at 10x magnification with the aid of the

Studio Capture software. In addition to the images taken from the videos, light intensity values from the same instrument also provided information on the liquefaction of asphaltenes.

DSC was used to study the phase transitions in asphaltenes with temperature. The analysis was performed under nitrogen atmosphere at atmospheric pressure using Mettler Toledo DSC 1. The DSC setup contains an FRS-5 sensor with 56 thermocouples, 400 W power amplifier, and Haake intracooler. Nitrogen gas flow rate was maintained at 100ml/min using a Mettler Toledo GC 10 gas controller. Cole Palmer PMR1-010750 gas flow meter was used to control the flow rate of nitrogen gas purged at 100ml/min. The instrument was calibrated for heat flow and temperature with In and Zn standards. ~10 mg of sample was taken into a 40 $\mu$ L aluminum crucible. The lid of the crucible was placed on a rubber surface, and a hole was pierced into it with a needle. The crucible was sealed with the lid with the aid of Mettler crucible sealing press. Changes in heat flow were recorded as the sample was heated from 25 to 300°C at a rate of 10°C/min, cooled back to 25°C at the same rate and heated again to 300°C at the same rate.

Mettler XS105 Dual Range analytical balance was used to weigh DAO and asphaltenes for analyses. The readability of the balance is 0.01mg and 0.1mg at a maximum capacity of 41g and 120g respectively.

SimDis, HSM and DSC were performed on one set of asphaltenes and maltenes, whereas TGA analysis was performed for three sets of asphaltenes and maltenes. The details of the preparation of asphaltenes and maltenes were described in Chapter 3.

## **5.3 Results**

### **5.3.1 Boiling Point Distribution by Simdis**

Determination of true boiling point (TBP) curves of petroleum feed and products using methods based on physical distillation is very time-consuming (~48h) and is labor intensive.<sup>3</sup> The analysis time can be reduced and the process of distillation can be automated by simulation using gas chromatography, called GC SimDis.

SimDis curves of C<sub>5</sub> and C<sub>7</sub> asphaltenes precipitated at S/B ratio 4:1 are shown in Figure 5-1 as examples. The amount of material that volatilizes upon distillation, represented as ‘%Off’ (wt% of the sample) is plotted as a function of temperature. The boiling point distribution of samples up

to a temperature of  $\sim 720^{\circ}\text{C}$  was obtained. At any given temperature, the amount of volatiles or low boiling point material in  $\text{C}_5$  asphaltenes is greater than that of  $\text{C}_7$  asphaltenes.

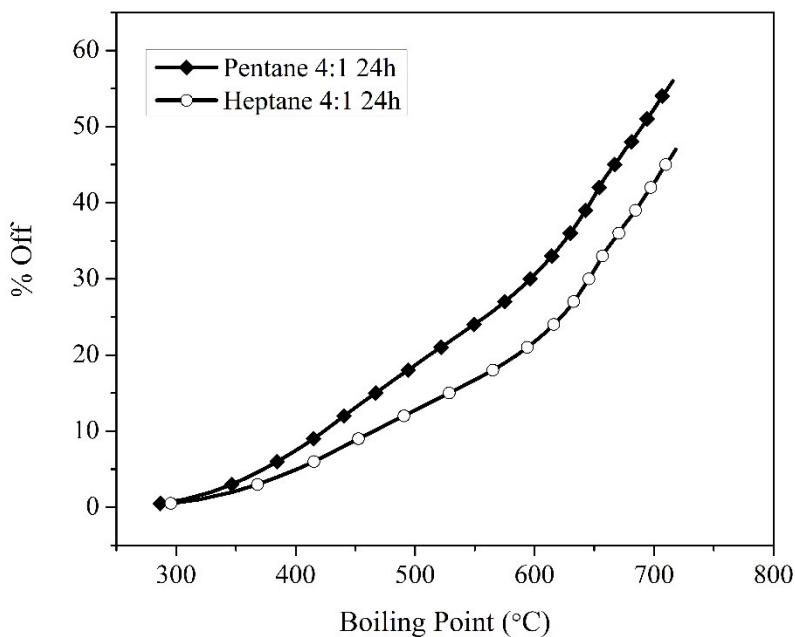


**Figure 5-1.** SimDis curves of  $\text{C}_5$  and  $\text{C}_7$  asphaltenes precipitated at S/B ratio 4:1 and with precipitation time = 24h

Figure 5-2 contains distillation curves of  $\text{C}_5$  asphaltenes precipitated at different S/B ratios in the SDA process. At any given temperature, the amount of volatile material lost by distillation decreases with increase in S/B ratio. Similar curves were obtained for other asphaltenes.

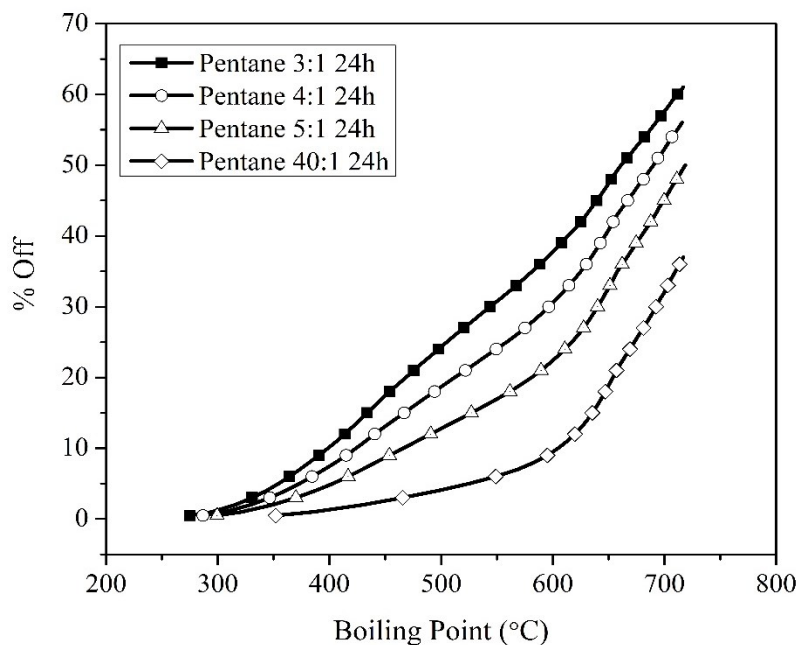


**Figure 5-2.** SimDis curves of C<sub>5</sub> asphaltenes precipitated at different S/B ratios and with precipitation time = 24h

The amounts of middle distillate, gas oil and residue fractions in the asphaltenes, expressed as wt%, were calculated and tabulated in Table 5-1, Table 5-2 and Table 5-3. The boiling ranges used in Table 3-1 of Chapter 3 for SimDis of bitumen were applied.

The middle distillate fraction of asphaltenes decreases with increase in S/B ratio used in the SDA process, for C<sub>5</sub>, C<sub>6</sub> and C<sub>7</sub> solvents. It decreases from C<sub>5</sub> to C<sub>7</sub> at S/B ratios 3:1 to 5:1. At 40:1, the amount of middle distillate fraction is <0.5 wt% for C<sub>5</sub>, C<sub>6</sub> and C<sub>7</sub> asphaltenes. Similar to the middle distillate fraction, the amount of vacuum gas oil fraction decreases with increase in S/B ratio for C<sub>5</sub>, C<sub>6</sub> and C<sub>7</sub> asphaltenes, and decreases from C<sub>5</sub> to C<sub>7</sub> at the observed S/B ratios. The amount of residue (+524°C), shown in Table 5-3, in C<sub>5</sub>, C<sub>6</sub> and C<sub>7</sub> asphaltenes increases with increase in S/B ratio, and increases from C<sub>5</sub> to C<sub>7</sub> at the observed S/B ratios. However, with increase in S/B ratio from 3:1 to 40:1, the effect of solvent selected for precipitation on the distribution of boiling fractions in asphaltenes decreases. The effect of solvent at S/B ratios 5:1 and 40:1 is insignificant.

**Table 5-1.** Middle distillate fraction (wt%) of C<sub>5</sub>, C<sub>6</sub> and C<sub>7</sub> asphaltenes precipitated at different S/B ratios in the SDA process, Precipitation time = 24h

	C <sub>5</sub>	C <sub>6</sub>	C <sub>7</sub>
3:1	3.95	3.72	2.05
4:1	2.79	2.00	1.85
5:1	1.77	1.69	1.71
40:1	<0.5	<0.5	<0.5

**Table 5-2.** Gas Oil fraction (wt%) of C<sub>5</sub>, C<sub>6</sub> and C<sub>7</sub> asphaltenes precipitated at different S/B ratios in the SDA process, Precipitation time = 24h

	C <sub>5</sub>	C <sub>6</sub>	C <sub>7</sub>
3:1	23.49	22.19	13.83
4:1	18.45	18.43	12.79
5:1	12.97	12.91	11.80
40:1	4.97	4.17	3.12

**Table 5-3.** Residue fraction (wt%) of C<sub>5</sub>, C<sub>6</sub> and C<sub>7</sub> asphaltenes precipitated at different S/B ratios in the SDA process, Precipitation time = 24h

	C <sub>5</sub>	C <sub>6</sub>	C <sub>7</sub>
3:1	72.55	74.09	84.12
4:1	78.76	79.57	85.36
5:1	85.25	85.40	86.49
40:1	95.03	95.05	96.09

The amounts of middle distillate, gas oil and residue fractions of DAO are shown in Table 5-4, Table 5-5 and Table 5-6 respectively. The middle distillate and gas oil fractions appear to increase with an increase in S/B ratio from 3:1 to 40:1 for C<sub>5</sub>, C<sub>6</sub> and C<sub>7</sub> maltenes, and the residue fraction decreases with increase in S/B ratio. These trends in DAO are opposite to the trends observed in asphaltenes.

**Table 5-4.** Middle distillate fraction (wt%) of C<sub>5</sub>, C<sub>6</sub> and C<sub>7</sub> maltenes precipitated at different S/B ratios in the SDA process, Precipitation time = 24h

	C <sub>5</sub>	C <sub>6</sub>	C <sub>7</sub>
3:1	7.29	7.27	7.18
4:1	7.79	7.41	7.30
5:1	7.94	7.52	7.67
40:1	8.69	7.88	7.62

**Table 5-5.** Gas Oil fraction (wt%) of C<sub>5</sub>, C<sub>6</sub> and C<sub>7</sub> maltenes precipitated at different S/B ratios in the SDA process, Precipitation time = 24h

	C <sub>5</sub>	C <sub>6</sub>	C <sub>7</sub>
3:1	36.55	36.01	35.92
4:1	39.72	37.43	36.28
5:1	40.15	38.43	36.70
40:1	41.49	40.06	38.59

**Table 5-6.** Residue fraction (wt%) of C<sub>5</sub>, C<sub>6</sub> and C<sub>7</sub> maltenes precipitated at different S/B ratios in the SDA process, Precipitation time = 24h

	C <sub>5</sub>	C <sub>6</sub>	C <sub>7</sub>
3:1	56.16	56.72	55.90
4:1	52.49	54.66	55.43
5:1	51.92	54.05	54.63
40:1	49.82	51.57	52.80

The amount of middle distillate, gas oil and residue fractions of C<sub>5</sub> and C<sub>7</sub> asphaltenes precipitated after 330h in the SDA process are tabulated in Table 5-7, Table 5-8 and Table 5-9. The amount of middle distillate and gas oil fractions of C<sub>5</sub> and C<sub>7</sub> asphaltenes numerically increases with increase in precipitation time from 24h to 330h, but it is a small difference and unlikely to be a meaningful. The amount of residue fraction numerically decreases with increase in precipitation time for C<sub>5</sub> and C<sub>7</sub> asphaltenes. However, these changes are insignificant.

**Table 5-7.** Effect of precipitation time in SDA process on the Middle distillate fraction of asphaltenes

	C <sub>5</sub>		C <sub>7</sub>	
	24h	330h	24h	330h
3:1	3.95	4.14	2.05	2.43
4:1	2.79	2.95	1.85	2.67
5:1	1.77	2.14	1.71	2.10
40:1	0.00	0.49	0.79	1.03

**Table 5-8.** Effect of precipitation time in SDA process on the Gas Oil fraction of asphaltenes

	C <sub>5</sub>		C <sub>7</sub>	
	24h	330h	24h	330h
3:1	23.49	24.20	13.83	14.44
4:1	18.45	18.64	12.79	13.02
5:1	12.97	14.94	11.80	12.08
40:1	4.97	5.42	3.12	4.52

**Table 5-9.** Effect of precipitation time in SDA process on the Residue fraction of asphaltenes

	C <sub>5</sub>		C <sub>7</sub>	
	24h	330h	24h	330h
3:1	72.55	71.65	84.12	83.13
4:1	78.76	78.41	85.36	84.31
5:1	85.25	82.92	86.49	85.82
40:1	95.03	94.09	96.09	94.45

The effect of precipitation time on the boiling point distribution of DAO is indicated in Table 5-10, Table 5-11 and Table 5-12. The changes in the fractions of DAO with change in precipitation time from 24h to 330h are insignificant.

**Table 5-10.** Effect of precipitation time in SDA process on the Middle distillate fraction of DAO

	C <sub>5</sub>		C <sub>7</sub>	
	24h	330h	24h	330h
3:1	7.29	6.91	8.18	8.27
4:1	7.79	8.01	8.30	8.55
5:1	7.94	8.00	8.67	8.47
40:1	8.69	8.39	8.62	8.53

**Table 5-11.** Effect of precipitation time in SDA process on the Gas Oil fraction of DAO

	C <sub>5</sub>		C <sub>7</sub>	
	24h	330h	24h	330h
3:1	36.55	35.73	35.92	35.92
4:1	39.72	39.68	36.28	36.48
5:1	40.15	39.21	36.70	37.15
40:1	41.49	41.46	38.59	37.09

**Table 5-12.** Effect of precipitation time in SDA process on the Residue fraction of DAO

	C <sub>5</sub>		C <sub>7</sub>	
	24h	330h	24h	330h
3:1	56.16	57.36	55.90	55.81
4:1	52.49	52.31	55.43	54.97
5:1	51.92	52.80	54.63	54.39
40:1	49.82	50.15	52.80	54.39

### 5.3.2 Thermogravimetric Analysis

TGA is defined as “a technique in which the mass change of a substance is measured as a function of temperature whilst the substance is subjected to a controlled temperature programme”.<sup>4</sup> TGA is used to monitor mass loss and gain. Mass loss occurs due to mechanisms such as decomposition, evaporation, reduction and desorption. Mass gain occurs due to mechanisms such as oxidation and

absorption. TGA can be used to study reaction kinetics, characterize materials, analyze composition, measure residue content and study thermal stability of materials.<sup>4</sup>

Shown in Figure 5-3 are the TGA curves of bitumen, C<sub>5</sub> asphaltenes and C<sub>5</sub> maltenes precipitated at S/B ratio 40:1. The mass loss until 200°C was 2.4, 0.1 and 3.1 wt% for bitumen, asphaltenes and maltenes respectively. A significant loss in mass takes place in two temperature ranges, 200-400°C and 400-480°C. In these temperature ranges, the slope of the curves indicates the rate of mass loss. Between 200 and 400°C, the rate of mass loss was much faster for maltenes compared to asphaltenes. Between 400°C and 480°C, the slope of the curves appears to be similar for bitumen, maltenes, and asphaltenes. Above 600°C, the mass reaches a constant value. The residue (proportional to coke) that remained after 600°C was greater in amount for asphaltenes, followed by bitumen and maltenes.

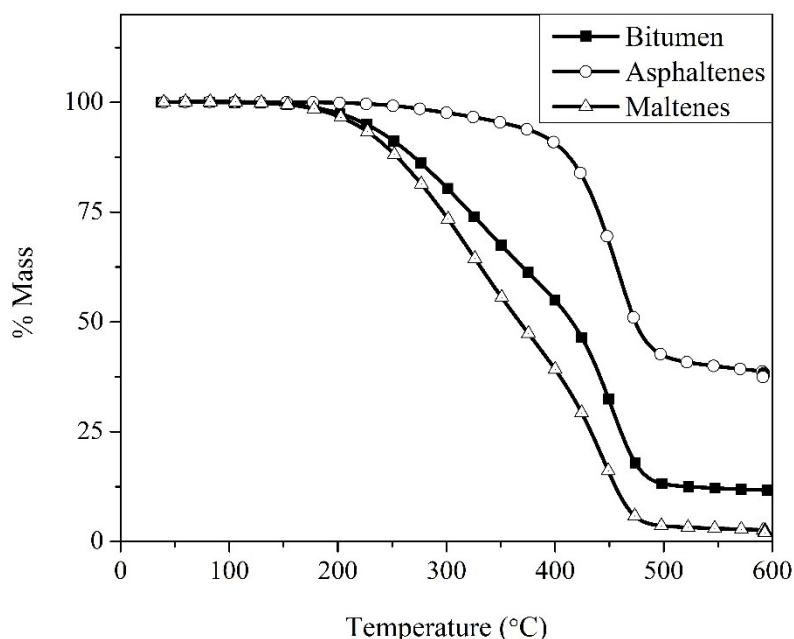


**Figure 5-3.** TGA curves of Bitumen, C<sub>5</sub> asphaltenes and C<sub>5</sub> maltenes, precipitated at S/B ratio 40:1 and with precipitation time = 24h

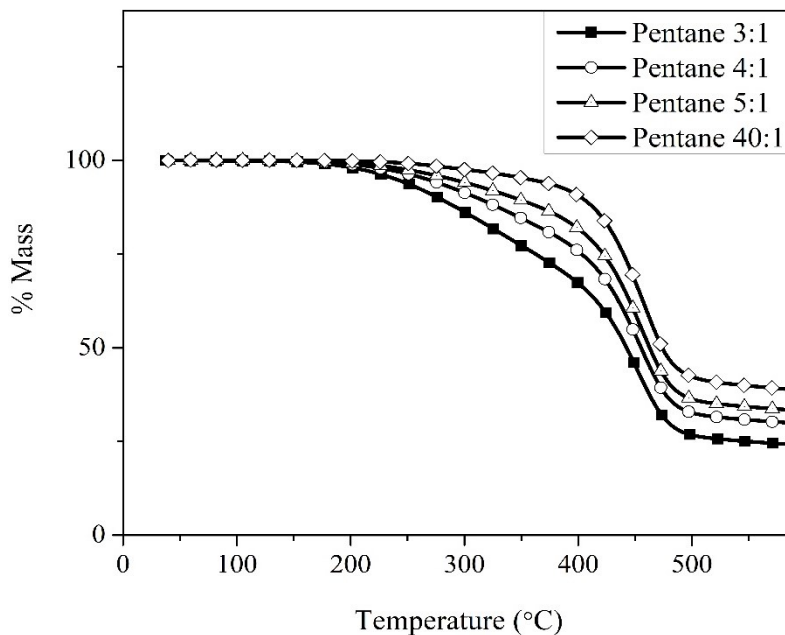
Mass loss in TGA occurs due to volatilization and cracking. To decouple them, the TGA results of bitumen, C<sub>5</sub> asphaltenes and maltenes were compared with the SimDis results, as shown in Table 5-13. The temperature range 200-400°C was further divided into two ranges 200-300°C and

300-400°C. Mass of the residue remaining after heating the samples to 600°C is also mentioned in Table 5-13. All the masses were expressed in wt% of the sample.

**Table 5-13.** Comparison of mass loss of bitumen, C<sub>5</sub> asphaltenes and maltenes in TGA and SimDis analyses in different ranges of temperature

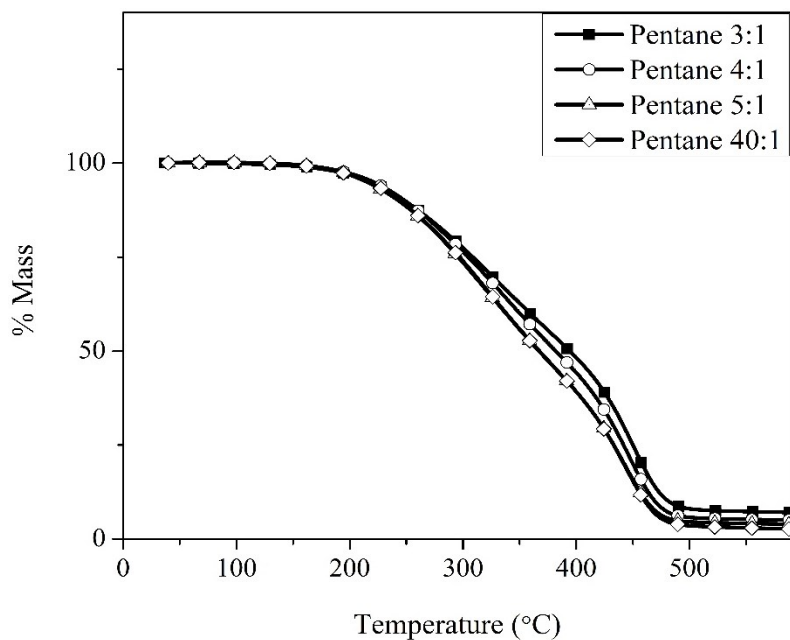
Temperature Range (°C)	Analysis	Mass Loss <sub>bit</sub> <sup>a</sup> (wt%)	Mass Loss <sub>asp</sub> <sup>b</sup> (wt%)	Mass Loss <sub>mal</sub> <sup>c</sup> (wt%)
200-300°C	TGA	17.0	2.3	23.0
	SimDis	~1.6	~0.0	2.6
300-400°C	TGA	25.7	7.0	34.8
	SimDis	13.3	~0.82	16.7
400-480°C	TGA	39.1	43.7	34.5
	SimDis	16.7	2.2	20.2
480-600°C	TGA	4.2	9.5	2.7
	SimDis	21.7	6	25.6
Temperature Range (°C)	Analysis	Mass Resid <sub>bit</sub> <sup>d</sup> (wt%)	Mass Resid <sub>asp</sub> <sup>e</sup> (wt%)	Mass Resid <sub>mal</sub> <sup>f</sup> (wt%)
+600°C	TGA	11.7	37.45	1.96
	SimDis	46.2	90.5	34.1
<sup>a</sup> Mass Loss in bitumen, <sup>b</sup> Mass Loss in asphaltenes, <sup>c</sup> Mass Loss in maltenes <sup>d</sup> Mass of residue in bitumen, <sup>e</sup> Mass of residue in asphaltenes, <sup>f</sup> Mass of residue in maltenes				

Figure 5-4 contains TGA curves of C<sub>5</sub> asphaltenes at different S/B ratios. With the increase in S/B ratio, the amount of residue increases. The rate of mass loss between 200°C and 400°C increases with a decrease in S/B ratio. And the rate of mass loss between 400°C and 480°C appears to increase with an increase in S/B ratio. Similar curves were obtained for C<sub>6</sub> and C<sub>7</sub> asphaltenes.



**Figure 5-4.** TGA curves of C<sub>5</sub> asphaltenes precipitated at different S/B ratios and with precipitation time = 24h

In the case of C<sub>5</sub> maltenes (shown in Figure 5-5), the amount of residue decreased with increase in S/B ratio. Though the TGA curves of maltenes were very close, the rate of mass loss between 200°C and 400°C increases with increase in S/B ratio. And the rate of mass loss between 400°C and 480°C appears to be similar at the observed S/B ratios. Similar results were obtained for C<sub>6</sub> and C<sub>7</sub> maltenes.



**Figure 5-5.** TGA curves of  $C_5$  maltenes precipitated at different S/B ratios and with precipitation time = 24h

Table 5-14 and Table 5-15 contain MCR of asphaltenes produced at different conditions of the SDA process. The MCR of asphaltenes increases with increase in S/B ratio for  $C_5$ ,  $C_6$  and  $C_7$  asphaltenes at both 24h and 330h precipitation time. It increases from  $C_5$  to  $C_7$  at the observed S/B ratios. The MCR decreased with increase in precipitation time, though the change can be considered to be insignificant.

**Table 5-14.** MCR of Asphaltenes (wt%), Precipitation Time = 24h <sup>a</sup>

S/B ratio	C <sub>5</sub> asphaltenes		C <sub>6</sub> asphaltenes		C <sub>7</sub> asphaltenes	
	x	s	x	s	x	S
3:1	23.5	0.7	24.9	- <sup>b</sup>	35.0	1.6
4:1	29.9	0.2	30.4	- <sup>b</sup>	35.2	0.8
5:1	32.2	0.1	34.1	- <sup>b</sup>	35.5	0.8
40:1	37.7	0.4	40.7	- <sup>b</sup>	41.0	1.3

<sup>a</sup> Average (x) and standard deviation (s) of three samples is reported

<sup>b</sup> Single sample was analyzed

**Table 5-15.** MCR of Asphaltenes (wt%), Precipitation Time = 330h

	C <sub>5</sub> asphaltenes	C <sub>7</sub> asphaltenes
3:1	22.2	34.9
4:1	28.7	35.1
5:1	29.6	35.2
40:1	37.0	40.3

The MCR of maltenes is shown in Table 5-16 and Table 5-17 for precipitation time of 24h and 330h respectively. It can be observed that the MCR of maltenes decreases with increase in S/B ratio for C<sub>5</sub>, C<sub>6</sub> and C<sub>7</sub> solvents at both 24h and 330h precipitation times. MCR of maltenes increased from C<sub>5</sub> to C<sub>7</sub> at the observed S/B ratios and at both precipitation times. The MCR

increased with increase in precipitation time, though the change can be considered to be insignificant.

**Table 5-16.** MCR of maltenes (wt%), Precipitation Time = 24h <sup>a</sup>

S/B ratio	C <sub>5</sub> maltenes		C <sub>6</sub> maltenes		C <sub>7</sub> maltenes	
	x	s	x	s	x	S
3:1	6.4	0.1	8.0	- <sup>b</sup>	8.0	0.7
4:1	4.6	0.3	6.3	- <sup>b</sup>	6.4	1.3
5:1	3.4	0.1	5.8	- <sup>b</sup>	6.2	0.4
40:1	2.0	0.1	4.3	- <sup>b</sup>	4.4	0.7

<sup>a</sup> Average (x) and standard deviation (s) of three samples is reported

<sup>b</sup> Single sample was analyzed

**Table 5-17.** MCR of maltenes (wt%), Precipitation Time = 330h

	C <sub>5</sub> asphaltenes	C <sub>7</sub> asphaltenes
3:1	7.0	8.2
4:1	4.9	6.8
5:1	3.7	6.1
40:1	2.9	4.4

### 5.3.3 Liquefying Point of Asphaltenes

#### 5.3.3.1 Hot Stage Microscopy (HSM)

HSM was used to visually observe the changes in asphaltenes upon heating. Asphaltenes appear as black, opaque solid particles at the beginning, which slowly transform into liquid droplets with an increase in temperature. As heating progresses, the liquid droplets grow in size and merge to form a continuous liquid phase. The microscopic images of C<sub>5</sub> and C<sub>7</sub> asphaltenes precipitated at S/B ratio 5:1 are shown in Figure 5-6 as examples. Similar behavior was shown by other asphaltene samples but with different temperatures of liquefaction.

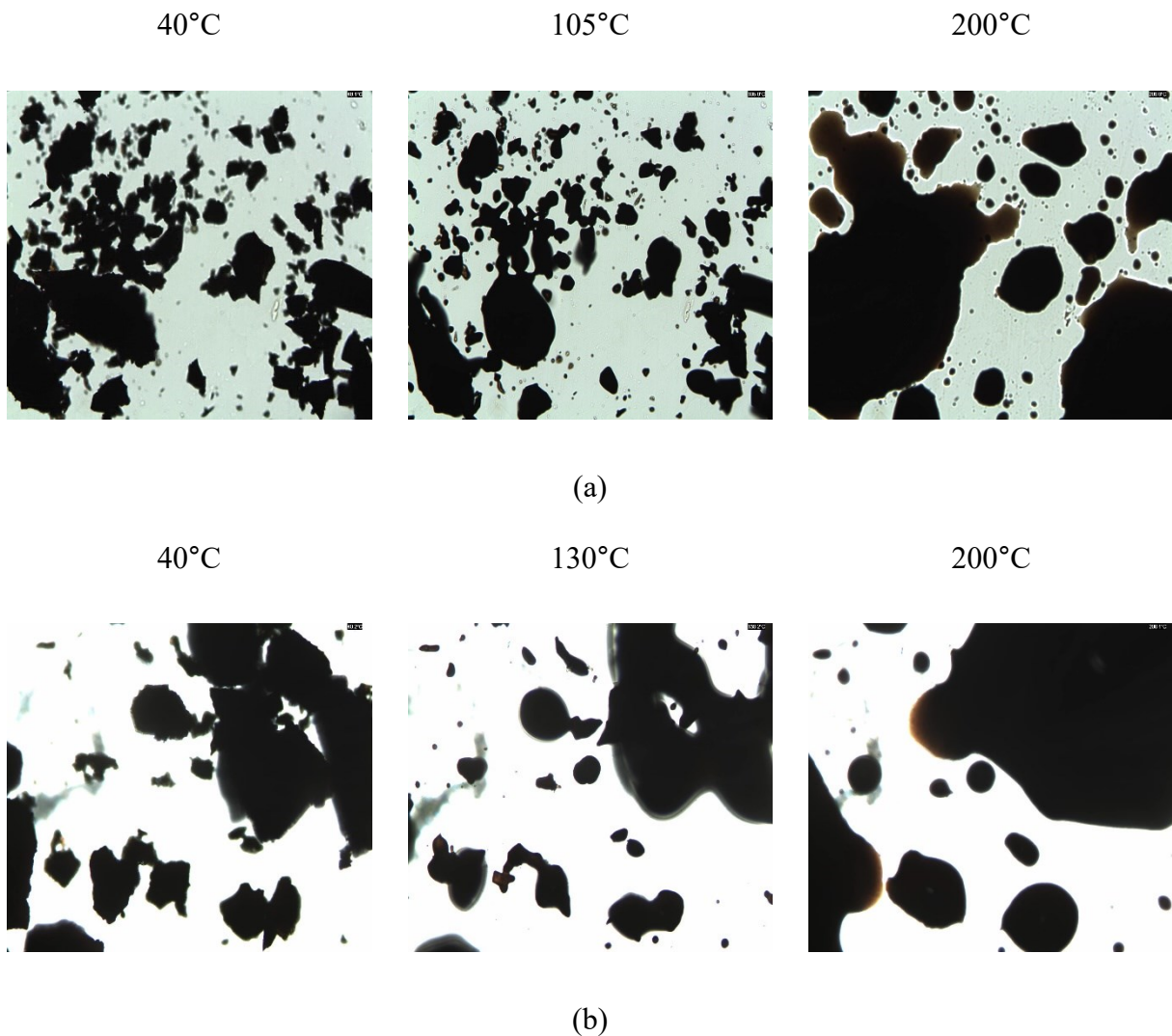


**Figure 5-6.** Microscopic Images of (a) C<sub>5</sub> asphaltenes and (b) C<sub>7</sub> asphaltenes precipitated at S/B ratio 5:1

In the video's fast forward mode, it was seen that asphaltenes begin to liquefy at a certain temperature, called liquefying point. The liquefying points of asphaltenes at different S/B ratios that were obtained by visual inspection of the video are mentioned in Table 5-18. However, as the changes in the initial stages of liquefaction were very slow, it was difficult to reliably capture the onset temperature from the images. The liquefying point of asphaltenes, mentioned in Table 5-18 is lower than the corresponding temperatures mentioned in Figure 5-6.

**Table 5-18.** Liquefying Point of C<sub>5</sub> and C<sub>7</sub> asphaltenes at different S/B ratios by Visual Observation

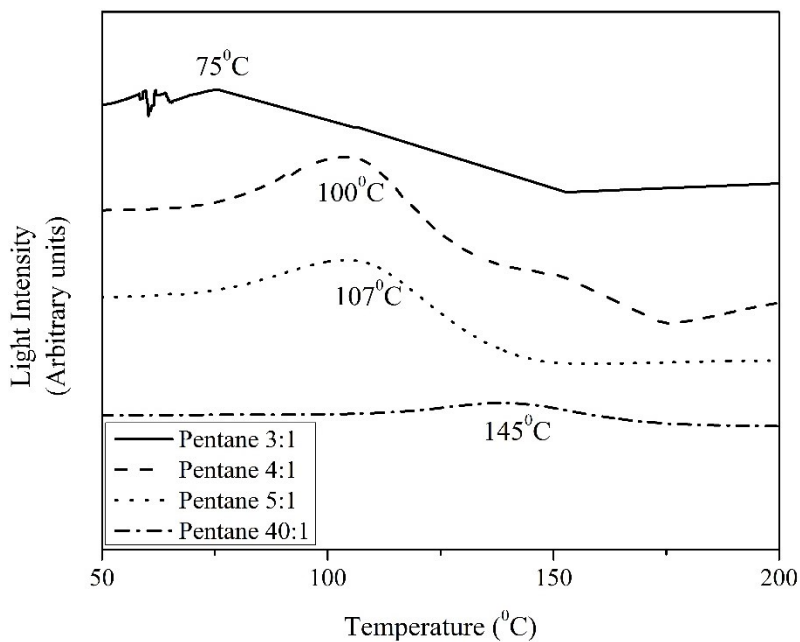
Solvent	S/B ratio	Liquefying Point (°C)
<i>n</i> -pentane	3:1	66
	4:1	78
	5:1	88
	40:1	121
<i>n</i> -heptane	3:1	77
	4:1	90
	5:1	102
	40:1	125

The results in Table 5-18 indicate that the liquefying point of the C<sub>5</sub>-asphaltenes is consistently lower than that of the C<sub>7</sub>-asphaltenes. The liquefying point increases with increase in the S/B ratio for both solvents.

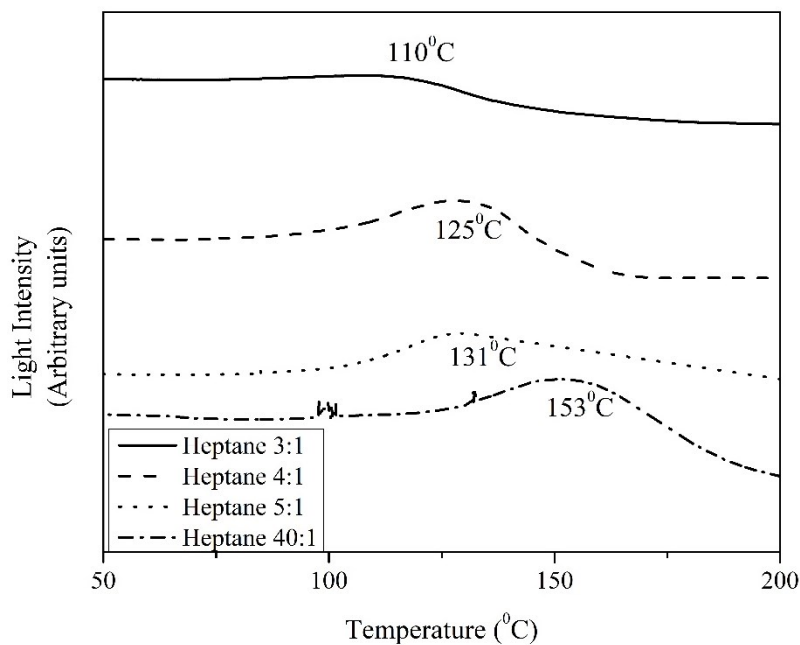
Reflected light intensity values of C<sub>5</sub> and C<sub>7</sub> asphaltenes were plotted against temperature as shown in Figure 5-7. Reflected light microscopy is ideal for opaque substances which cannot transmit light through them. Changes in light intensity with temperature indicate changes in color, refractive index, texture or expansion.<sup>5</sup> The magnitude of light intensity seems to depend on the mass of the sample under observation, which in this case could not be quantified as it was below 1mg and

dependent on the area of the sample under observation. Hence, the absolute light intensity of the curves in Figure 5-7 does not provide any information.

The temperature at which the maximum light intensity was observed for  $C_5$  asphaltenes was lower than that of the  $C_7$  asphaltenes at each of the studied S/B ratios. The shift in the peak of the curves to lower temperatures with a decrease in the S/B ratio also gives a similar trend as in Table 5-18.



(a)



(b)

**Figure 5-7.** Reflected light intensity against temperature for (a) C<sub>5</sub>-asphaltenes and (b) C<sub>7</sub>-asphaltenes at different S/B ratios

### 5.3.3.2 Differential Scanning Calorimetry (DSC)

DSC is defined as “a technique in which the heat-flow rate (power) to the sample is monitored against time or temperature while the temperature of the sample, in a specified atmosphere, is programmed.”<sup>6</sup> Changes in heat flow represent thermal transitions in substances. DSC is used for the study of phase behavior, measurement of heat capacities, determination of the phase diagram and degree of crystallinity of substances, determination of heats of reactions and reaction mechanisms and characterization of materials. It is used to observe transitions such as melting, polymorphism and glass transition of materials.<sup>6</sup>

The energy change associated with asphaltenes heating is illustrated by the calorigram of one of the samples in Figure 5-8. The asphaltenes does not exhibit a clear onset of melting (indicated by endothermic peak pointing downwards) and the enthalpy change associated with liquefying the asphaltenes is too low to represent a typical liquid–solid phase transition.

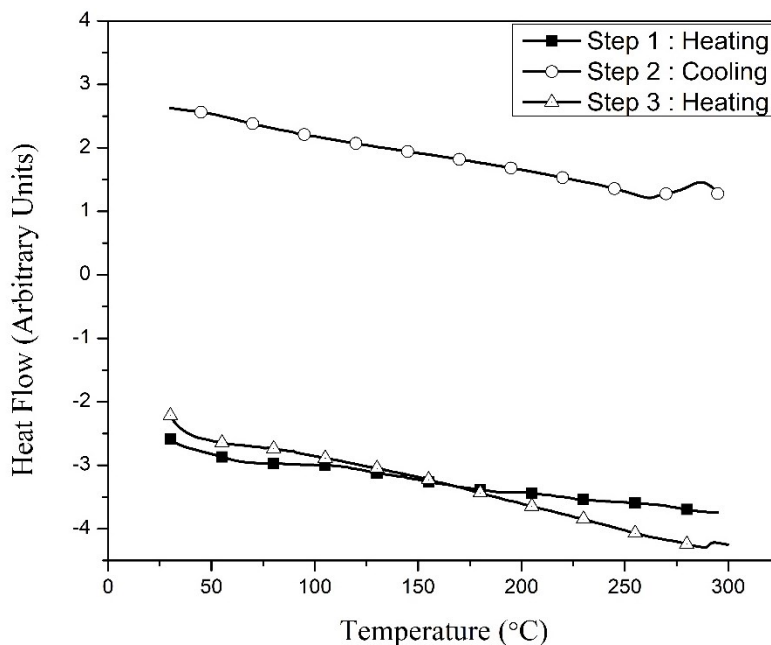


**Figure 5-8.** DSC curves of  $C_7$  asphaltenes precipitated at S/B ratio 5:1

## 5.4 Discussion

### 5.4.1 Boiling Point distribution of asphaltenes and DAO

The boiling point of a fraction can be correlated with the average molar mass of the fraction.<sup>2</sup> The higher the molar mass, higher is the boiling point of the fraction. According to Speight,<sup>7</sup> generally speaking, the proportion of aliphatic compounds in crude oils decreases with increase in boiling point or molecular weight.

From SimDis results shown in Figure 5-1, Table 5-1, Table 5-2 and Table 5-3, it can be expected that  $C_5$  asphaltenes are lighter and more aliphatic compared to  $C_7$  asphaltenes. As mentioned in chapter 2, it is reported in literature that with increase in the carbon number of  $n$ -alkane solvent, the molecular weight and aromaticity of the precipitated asphaltenes increase.

SimDis results shown in Figure 5-2, Table 5-1, Table 5-2 and Table 5-3 indicate that asphaltenes precipitated from bitumen at lower S/B ratios are lighter and more aliphatic, and the concentration of heavier and aromatic components increases with increase in S/B ratio. Though the asphaltene yields at S/B ratios 5:1 and 40:1 were similar (chapter 3), a significant difference in the proportion of boiling fractions was observed.

The results in Table 5-7 to Table 5-12 indicate that changes in the amount of boiling fractions of asphaltenes and DAO with the change in precipitation time from 24h to 330h are insignificant. Thus, the effect of precipitation time on boiling point distribution of asphaltenes and DAO is very less or insignificant compared to that of solvent and S/B ratio at the SDA process conditions used in this study.

#### 5.4.2 Selectivity of the SDA process at different process conditions for the extraction of boiling fractions of bitumen

Section 5.4.1 compared the nature of asphaltenes precipitated at different conditions of the SDA process in terms of the boiling point distribution. However, from the process point of view, it is important to determine the separation selectivity and extractability of different boiling fractions in bitumen at different SDA process conditions. The boiling fractions of asphaltenes in Table 5-1, Table 5-2 and Table 5-3, expressed as wt% of asphaltenes were converted into wt% of bitumen using Eq. 5-1 and plotted in comparison to boiling fractions in bitumen, as shown in Figure 5-9. The separation selectivity for different boiling fractions from bitumen into the asphaltenes phase is represented as a percentage, and calculated using Eq. 4-3. The separation selectivities are listed in Table 5-19. The extractability is defined as the percentage of boiling fraction in bitumen that remains in the DAO after asphaltene precipitation. It is represented by Eq. 5-3.

$$\begin{aligned}
 & \text{Boiling fraction in asphaltenes (wt\% of bitumen)} \\
 & \text{Boiling fraction in asphaltenes (wt\% of asphaltenes)} \times \\
 = & \frac{\% \text{Yield of asphaltenes}}{100}
 \end{aligned}
 \tag{Eq. 5-1}$$

$$\begin{aligned}
 & \text{Separation Selectivity (\%)} = \\
 & \frac{\text{Weight of boiling fraction in asphaltenes (wt\% of bitumen)}}{\text{Weight of boiling fraction in bitumen (wt\% of bitumen)}} \times 100
 \end{aligned}
 \tag{Eq. 5-2}$$

$$\text{Extractability (\%)} = 100 - \text{Separation Selectivity (\%)}
 \tag{Eq. 5-3}$$

Following are the observations from Figure 5-9 and Table 5-19:

0.09 to 0.48wt% of bitumen belongs to the middle distillate fraction of asphaltenes at the SDA process conditions used in this study, with precipitation time = 24h. Bitumen contains ~6.21wt% of middle distillate fraction as mentioned in Chapter 3. This indicates that the separation selectivity of middle distillate fraction varies from ~1.4 to 8%, and the extractability into DAO varies from 92 to 98.6%.

0.02 to 2.87wt% of bitumen belongs to the gas oil fraction of asphaltenes at the SDA process conditions used in this study, with precipitation time = 24h. Bitumen contains ~34wt% of gas oil fraction as mentioned in Chapter 3. This indicates that the separation selectivity of gas oil fraction varies from ~0.05 to 8.4%, and the extractability into DAO varies from 92 to 99.95%.

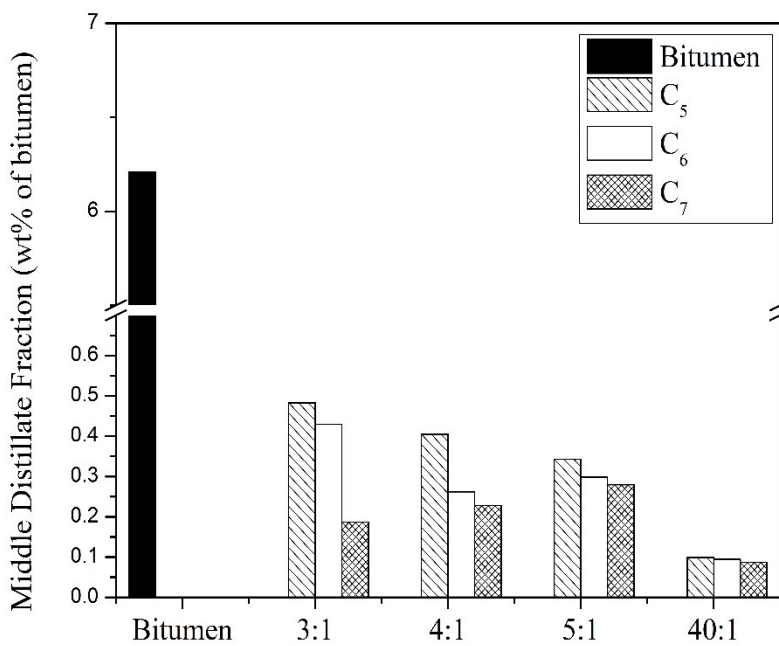
7.65 to 18.87wt% of bitumen belongs to the residue fraction of asphaltenes at the SDA process conditions used in this study, with precipitation time = 24h. Bitumen contains ~66wt% of residue fraction as mentioned in Chapter 3. This indicates that the separation selectivity of residue fraction varies from ~12 to 29%, and the extractability into DAO varies from 71 to 89%.

From Figure 5-9, it appears that the decrease in asphaltene yield from C<sub>5</sub> to C<sub>7</sub> asphaltenes at the observed S/B ratios is accompanied by a decrease in the separation selectivity for all the three boiling fractions of bitumen. Thus, the extractability of the boiling fractions increases when the solvent is varied from *n*-C<sub>5</sub> to *n*-C<sub>7</sub>. Although the nature of asphaltenes changes from lighter and aliphatic to heavier and aromatic from C<sub>5</sub> to C<sub>7</sub> asphaltenes (section 5.4.1), the selectivity for separation of heavier, aromatic components from bitumen, on a weight basis, gradually decreases when the solvent is varied from *n*-C<sub>5</sub> to *n*-C<sub>7</sub> in the SDA process.

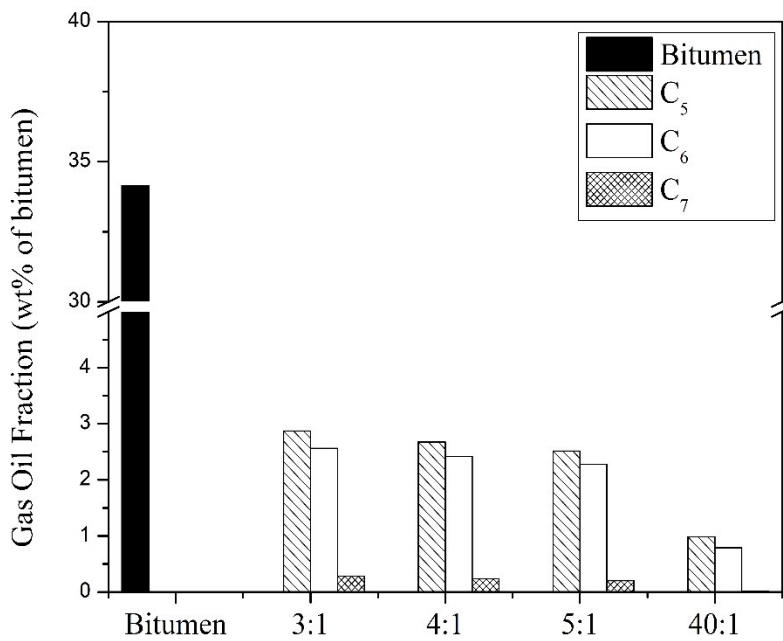
As mentioned earlier, the boiling point of a fraction can be directly correlated with its molecular weight. According to Strausz, et al.<sup>8</sup> fractionation of molecular weight takes place during asphaltene precipitation from bitumen using paraffinic solvents of varying linear chain length. When C<sub>5</sub> asphaltenes are dissolved in *n*-hexane, the lower molecular weight components dissolve, precipitating out the higher molecular weight or the least soluble portion of the C<sub>5</sub> asphaltenes as C<sub>6</sub> asphaltenes. The same occurs when C<sub>6</sub> asphaltenes are dissolved into *n*-heptane, and so on. Thus, the separation selectivity which represents the ‘quantity’ of the boiling fractions separated

into asphaltenes from bitumen decreases when the solvent used in the SDA process is varied from  $n\text{-C}_5$  to  $n\text{-C}_7$ . Differently put, the the fraction of lighter boiling material retained by the DAO increases from  $n\text{-C}_5$  to  $n\text{-C}_7$ .

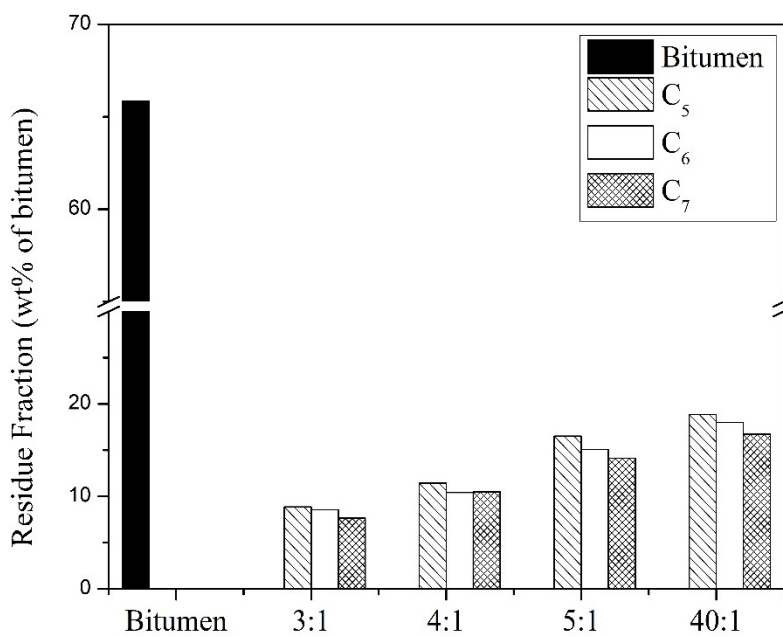
The increase in asphaltene yield with increase in S/B ratio is accompanied by an increase in the separation selectivity for residue fraction and decrease in the separation selectivity for gas oil fraction of bitumen. In other words, increasing the volume or the number of moles of paraffinic solvent in the solvent-bitumen mixture in the SDA process, results in increased precipitation of higher molecular weight components present in bitumen, while also leading to increased solubility of lower molecular weight components of bitumen in the solvent. This indicates the effect of number of moles of the solvent on the interactions between the solvent molecules and the solute molecules of different boiling fractions of bitumen, which impacts the mixing. At S/B ratio 40:1, the extractability of gas oil fraction is maximum and that of residue fraction is minimum. On the other hand, the separation selectivity of middle distillate fraction of bitumen in  $\text{C}_6$  and  $\text{C}_7$  asphaltenes doesn't follow a regular decreasing trend with increase in S/B ratio, indicating that in some cases with increase in asphaltene yield, the retention of lighter and aliphatic components belonging to middle distillate fraction of bitumen by the asphaltenes fraction increases.



(a)



(b)



(c)

**Figure 5-9.** (a) Middle Distillate (b) Gas Oil (c) Residue fractions of asphaltenes on bitumen weight basis, Precipitation time = 24h

**Table 5-19.** Separation selectivities of C<sub>5</sub>, C<sub>6</sub> and C<sub>7</sub> asphaltenes for middle distillate, gas oil and residue fractions in bitumen at different conditions of SDA process. Precipitation Time = 24h

		Separation Selectivity (%)		
	S/B ratio	C <sub>5</sub> asphaltenes	C <sub>6</sub> asphaltenes	C <sub>7</sub> asphaltenes
Middle Distillate Fraction	3:1	7.78	6.91	3.00
	4:1	6.52	4.22	3.67
	5:1	5.52	4.80	4.50
	40:1	1.60	1.53	1.40
Gas Oil Fraction	3:1	8.41	7.50	0.83
	4:1	7.84	7.08	0.69
	5:1	7.36	6.67	0.59
	40:1	2.89	2.32	0.05
Residue Fraction	3:1	13.47	12.98	11.62
	4:1	17.35	15.84	15.96
	5:1	25.09	22.89	21.47
	40:1	28.66	27.37	25.39

### 5.4.3 Cracking behavior of asphaltenes and DAO

Studies by Liu, et al.<sup>9</sup>, Trejo, et al.<sup>10</sup> and Shin, et al.<sup>11</sup> on pyrolysis and TGA of bitumen, asphaltenes and maltenes were used to interpret the results in Table 5-13.

Between 200 and 300°C, 17.0, 2.3, 23.0wt% of mass was lost from bitumen, asphaltenes and maltenes respectively in the TGA analysis. From the SimDis results, ~1.6, 0.0 and 2.6wt% of material volatilized before 300°C from bitumen, asphaltenes and maltenes respectively. This indicates that cracking reactions take place in bitumen and maltenes before 300°C leading to formation of lighter volatile hydrocarbons from heavier components.

Between 300 and 400°C, 25.7, 7.0, 34.8wt% of mass was lost from bitumen, asphaltenes and maltenes respectively in the TGA analysis. From the SimDis results, 13.3, ~0.82 and 16.7wt% of material volatilized between 300 and 400°C from bitumen, asphaltenes and maltenes respectively. The cracking reactions are more pronounced in maltenes and bitumen compared to asphaltenes between 300 and 400°C.

39.1, 43.7 and 34.5wt% of mass were lost from bitumen, asphaltenes, and maltenes respectively between 400°C and 480°C. From the SimDis results, 16.7, 2.2 and 20.2wt% of material volatilized from bitumen, asphaltenes and maltenes respectively, indicating that significant cracking reactions occur in all the three samples.

A mass loss of 4.2, 9.5 and 2.7wt% was obtained for bitumen, asphaltenes and maltenes respectively between 480°C and 600°C. From SimDis results, 21.7, 6 and 25.6wt% of material volatilized in this temperature range, most of which would have undergone cracking during pyrolysis at lower temperatures.

The residue (proportional to coke) that remained after 600°C was greater in amount for asphaltenes (37.45wt%), followed by bitumen (11.7wt%) and maltenes (1.96wt%). According to literature, maltenes transform into asphaltenes during pyrolysis leading to coke formation.<sup>9,12,13</sup> From SimDis results, 53.8, 9.5, 65.9wt% of bitumen, asphaltenes and maltenes respectively, volatilizes below 600°C, leaving behind 46.2, 90.5, 34.1wt% which continues to vaporize at higher temperatures.

Table 5-20 compares the composite or effective mass loss ( $Mass\ Loss_{eff}$ ) of C<sub>5</sub> asphaltenes and C<sub>5</sub> maltenes, precipitated at S/B ratio 40:1 and precipitation time 24h, on a bitumen basis with mass loss in bitumen.  $Mass\ Loss_{eff}$  was calculated in different temperature zones between 200 and 600°C for both TGA and SimDis analyses using the following equation:

$$\begin{aligned}
 & \text{Mass Loss}_{eff} = \text{Eq. 5-4} \\
 & = \frac{(\text{Mass Loss}_{asp} \times \% \text{Yield of asphaltenes} + \text{Mass Loss}_{mal} \times \% \text{Yield of maltenes})}{100}
 \end{aligned}$$

where  $\text{Mass Loss}_{asp}$  and  $\text{Mass Loss}_{mal}$  are the mass losses in asphaltenes and maltenes respectively. The yield of asphaltenes and maltenes mentioned in Chapter 3, were applied in this equation.

The composite mass of residue ( $\text{Mass Resid}_{eff}$ ) of asphaltenes and maltenes, calculated in similar manner is also mentioned in Table 5-20. The purpose of these calculations is to determine whether the distillation versus temperature profiles for the separated fractions are different to that of the bitumen as a whole.

**Table 5-20.** Comparison of ‘effective’ mass loss and mass of residue from asphaltenes and DAO on bitumen basis with the mass loss and mass of residue from bitumen

Temperature Zone (°C)	Analysis	Mass Loss <sub>bit</sub> (wt%)	Mass Loss <sub>eff</sub> (wt%)
200-300°C	TGA	17.0	18.3
	SimDis	~1.6	2.0
300-400°C	TGA	25.7	28.4
	SimDis	13.3	13.1
400-480°C	TGA	39.1	35.5
	SimDis	16.7	16.1
480-600°C	TGA	4.2	4.0
	SimDis	21.7	21.1
Temperature Zone (°C)	Analysis	Mass Resid <sub>bit</sub> (wt%)	Mass Resid <sub>eff</sub> (wt%)
+600°C	TGA	11.7	9.0
	SimDis	46.2	44.4

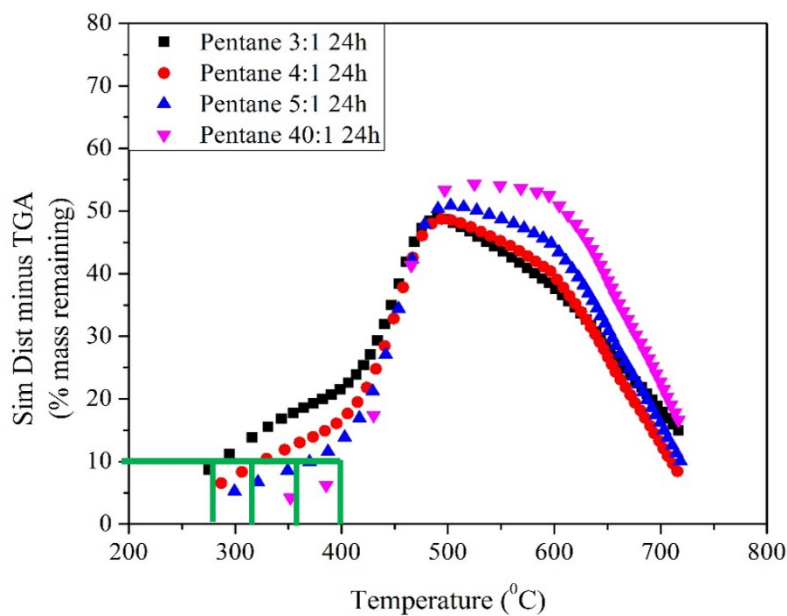
According to Table 5-20, there is a smaller difference between effective mass loss or effective residue of asphaltenes and maltenes, and mass loss or residue of bitumen in SimDis analysis. This means that solvent deasphalting doesn’t alter the boiling point distribution (on weight basis) of asphaltene and maltene fractions originally present in bitumen, when separated.

The effective mass loss in TGA analysis is greater than mass loss in bitumen by 4wt% between 200 and 400°C, and it is lesser than mass loss in bitumen by 3.6wt% between 400 and 480°C. The effective mass of residue is lesser than mass of residue from bitumen by 2.7wt%. It appears that the cracking behavior of asphaltenes and/or maltenes below 400°C is affected by separating these fractions and processing them individually. However, this finding needs further investigation, by taking into account the 2.53wt% of material lost from bitumen in asphaltene precipitation process (from chapter 3).

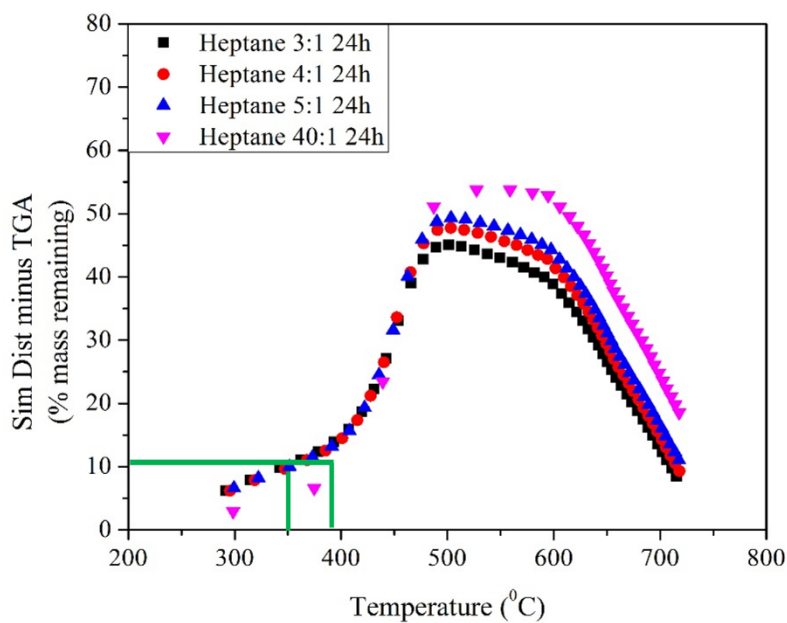
The distillation and reactive components of asphaltenes were separated by subtracting the TGA curves from SimDis curves. This approach allows to study the effect of solvent and S/B ratio in the SDA process on the reactivity of asphaltenes as a function of temperature. Figure 5-10 shows the subtraction of TGA curve from SimDis curve of C<sub>5</sub> and C<sub>7</sub> asphaltenes. The difference in the mass (wt%) remaining when heated in SimDis and TGA is plotted against temperature. The constructions in green color made on Figure 5-10 indicate the onset temperature for meaningful cracking of the C<sub>5</sub> and C<sub>7</sub> asphaltenes. The threshold for meaningful cracking was assumed to be 10wt% in the plot shown in Figure 5-10. From the constructions, it can be read that the onset temperature increases with increase in S/B ratio from 3:1 to 40:1. For example, the onset temperature for meaningful cracking of C<sub>5</sub> asphaltenes increases from 275°C to 400°C with increase in S/B ratio from 3:1 to 40:1.

The GC-SimDis oven was heated up to a temperature of 425°C at the rate of 15°C/min in this study. Thus, at those high temperatures, it is possible that cracking reactions can occur in the GC column. Carbognani, et al.<sup>14</sup> investigated on-column thermal cracking in high temperature simulated distillation of Athabasca vacuum residua components. In their paper, previous literature evidence of cracking of asphaltenes even at temperatures as low as 100°C were presented. The role of heating rate, time and temperature, on the cracking of petroleum compounds was emphasized in their literature review. The appearance of a second chromatographic peak or mode in the high temperature simulated distillation (HTSD) of resins and asphaltenes at temperatures above 320°C in their study, led to the hypothesis that secondary cracking of components could be occurring on HSTD columns. The column heating rate used in their study was 15°C/min up to a maximum temperature of 425°C, which is same as the heating method used in the present study.

The relationship between the GC oven temperature and the distillation temperature in SimDis analysis used in this study is shown in Figure 5-11.



(a)



(b)

**Figure 5-10.** Subtraction of TGA curve from Simdis Curve of (a) C<sub>5</sub> asphaltenes (b) C<sub>7</sub> asphaltenes precipitated at different S/B ratios with precipitation time = 24h

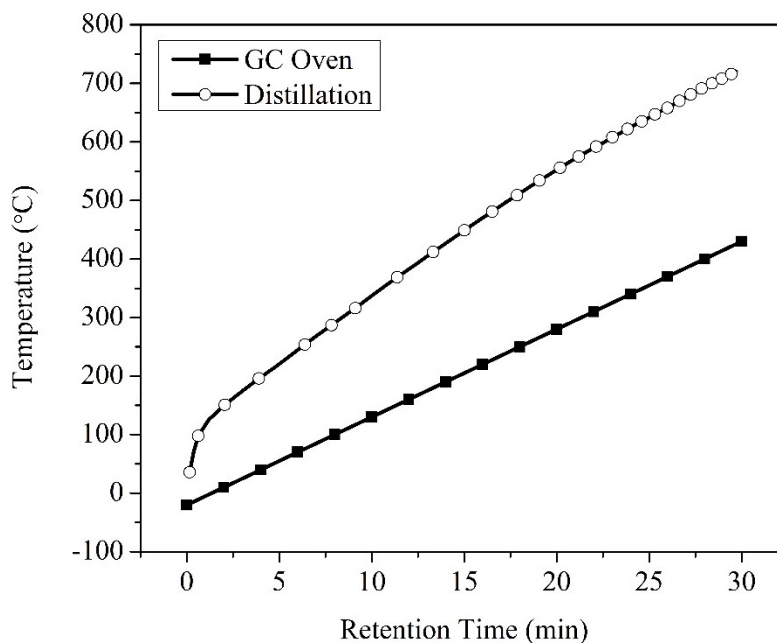


**Figure 5-11.** Relationship between GC Oven temperature and Distillation Temperature in SimDis

In Figure 5-10, the curves rise upto 480°C, indicating that mass loss in TGA is faster than the mass loss in SimDis. From Figure 5-11, distillation upto a boiling point of 480°C required heating of the GC column upto ~230°C. As on-column cracking is insignificant at column temperatures below 230°C, it can be assumed that SimDis curve represents only distillation of asphaltenes below 480°C. Thus, the difference between TGA and SimDis curve upto 480°C represents the cracking reaction component that occurs in TGA of asphaltenes.

At temperatures below 400°C, cracking was more prominent as the S/B ratio decreased from 40:1 to 3:1. Between 400 and 480°C, the curves of all the samples overlap because the rate of mass loss due to cracking reactions increases with increase in S/B ratio. Above 480°C, the mass loss during TGA of all the samples was insignificant, indicating that cracking has subsided.

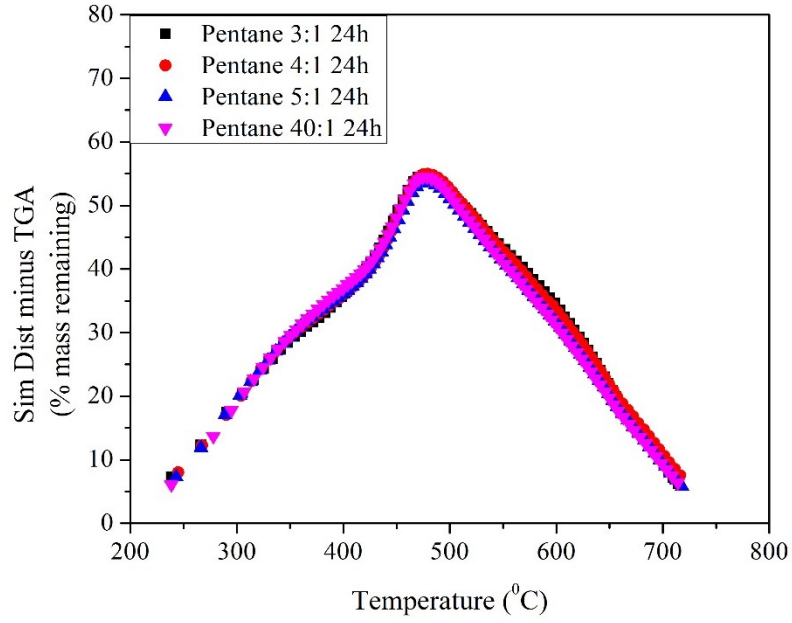
The hypothesis behind the decrease in rate of cracking reactions with temperature is that chemical structures being cracked at higher temperatures are stronger and require higher energy for cracking, leading to an increase in the activation energy required for cracking of unconverted material with an increase in conversion. Thermodynamic reactivity and reaction kinetics depend on factors such as bond dissociation energies and molecular weight.<sup>15,16</sup> The assumption of

uniform cracking kinetics that works well for decomposition of polymers, needs careful examination in the case of asphaltenes, as asphaltenes are a complex, heterogeneous mixture with a wide distribution of bond strengths and molecular weight.<sup>16</sup>

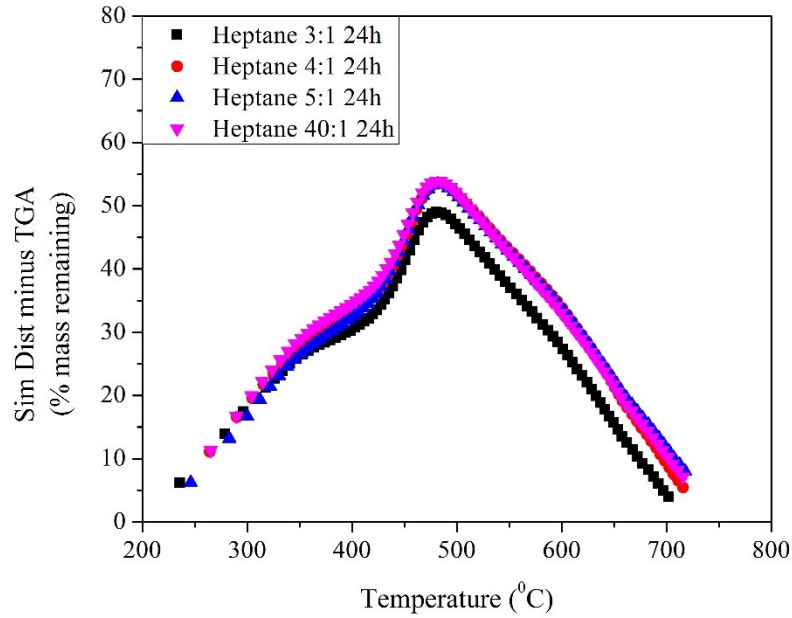
In Figure 5-10, the curve starts to fall after 480°C, indicating that the rate of cracking of asphaltenes decreases above 480°C. From earlier discussion, significant on-column cracking is likely to occur above column temperatures of 275°C in SimDis of asphaltenes depending on the SDA conditions used in this study for precipitation of asphaltenes. From Figure 5-11, a column temperature of 275°C corresponds to a distillation temperature of ~540°C, which means that the SimDis curve of C<sub>5</sub> asphaltenes precipitated at S/B ratio 3:1, above 540°C, represents both distillation and on-column cracking of asphaltenes. Thus, for C<sub>5</sub> asphaltenes precipitated at S/B ratio 3:1, this method to decouple distillation and reactivity components by subtracting SimDis curve from TGA curve becomes invalid above 540°C, as a combination of distillation and chemical reactions (cracking and/or addition) occur in both TGA and SimDis analyses.

For C<sub>5</sub> asphaltenes precipitated at S/B ratio 40:1, on-column cracking is significant at column temperatures above 400°C, which correspond to boiling point of 680°C and above. Thus, this method is valid upto ~680°C in Figure 5-10. Above 600°C, the shape of the curve in Figure 5-10 is similar to the shape of SimDis curve, in which the mass remaining decreases with increase in temperature due to the distillation of components. The mass remaining in SimDis also increases with increase in S/B ratio from 3:1 to 40:1, as lighter components are present in asphaltenes precipitated at lower ratios compared to those precipitated at higher ratios (section 5.4.1).

The curves obtained by subtraction of TGA from SimDis results for C<sub>5</sub> and C<sub>7</sub> maltenes, as shown in Figure 5-12, have a shape similar to the curves obtained for asphaltenes. The curves overlap in the case of C<sub>5</sub> maltenes. For C<sub>7</sub> maltenes, the cracking increases with increase in S/B ratio up to 480°C, above which the shape is similar to the shape of the SimDis curve. Though lighter components are present in maltenes produced at higher S/B ratios, the difference in the mass remaining in SimDis and the mass remaining in TGA (residue) increased with increase in S/B ratio. The curve falls with an increase in temperature due to the distillation of components. Again, this method of comparison between TGA and SimDis curves becomes invalid at temperatures above which on-column cracking of maltenes occurs in the SimDis analysis. From Figure 5-12, the onset of cracking of maltenes is ~265°C, which corresponds to a boiling temperature of 535°C.



(a)



(b)

**Figure 5-12.** Subtraction of TGA curve from Simdis Curve of (a) C<sub>5</sub> maltenes (b) C<sub>7</sub> maltenes precipitated at different S/B ratios with precipitation time = 24h

#### 5.4.4 Microcarbon residue (MCR)

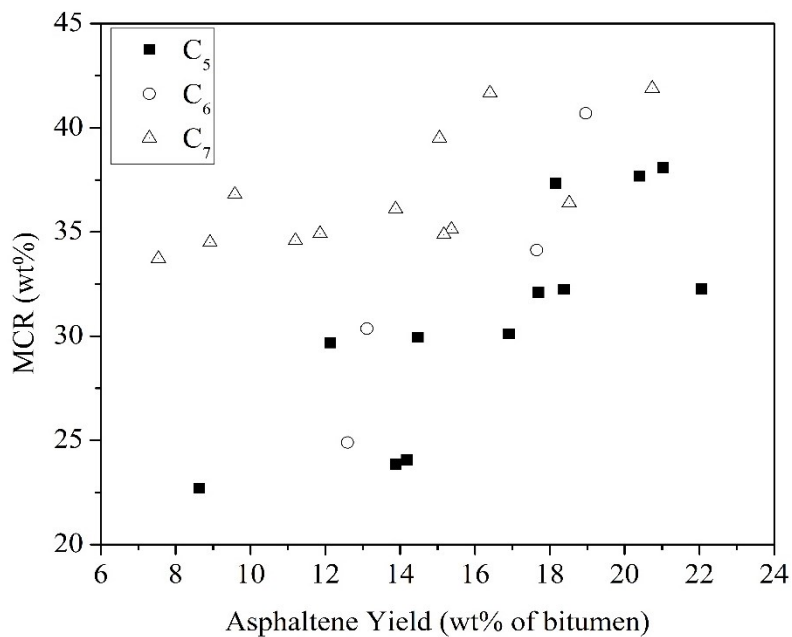
As mentioned earlier, MCR is an indicator of the coke forming tendency. According to Table 5-14, Table 5-15, Table 5-16 and Table 5-17, the coke forming tendency of asphaltenes increases from C<sub>5</sub> to C<sub>7</sub> and increases with increase in S/B ratio. Though the increase in asphaltene yield from S/B ratios 5:1 to 40:1 was not very high, a notable increase in MCR of samples was found, which explains the difference in the nature of asphaltenes at S/B ratios 5:1 and 40:1. The coke forming tendency of asphaltenes appears to slightly decrease with increase in precipitation time from 24h to 330h. However, the changes with precipitation time are not significant.

According to literature, asphaltenes contribute to coke formation.<sup>13</sup> When MCR of asphaltenes was plotted against asphaltene yield, as shown in Figure 5-13, a scattered plot was obtained, with no correlation between MCR and asphaltene yield for C<sub>5</sub>, C<sub>6</sub> and C<sub>7</sub> asphaltenes. When the average MCR was plotted against average asphaltene yield in Figure 5-13, MCR of C<sub>5</sub>, C<sub>6</sub> and C<sub>7</sub> asphaltenes independently increased with increase in their yield. However, from Table 5-14, MCR of C<sub>7</sub> asphaltenes > C<sub>6</sub> asphaltenes > C<sub>5</sub> asphaltenes, at a given S/B ratio, even though the yield of C<sub>5</sub> asphaltenes > C<sub>6</sub> asphaltenes > C<sub>7</sub> asphaltenes (chapter 3). Also, even though the increase in asphaltene yield from S/B ratios 5:1 to 40:1 was not very high (chapter 3), a notable increase in MCR of samples was found in Table 5-14, indicating that asphaltene yield is not a good indicator of coke forming tendency.

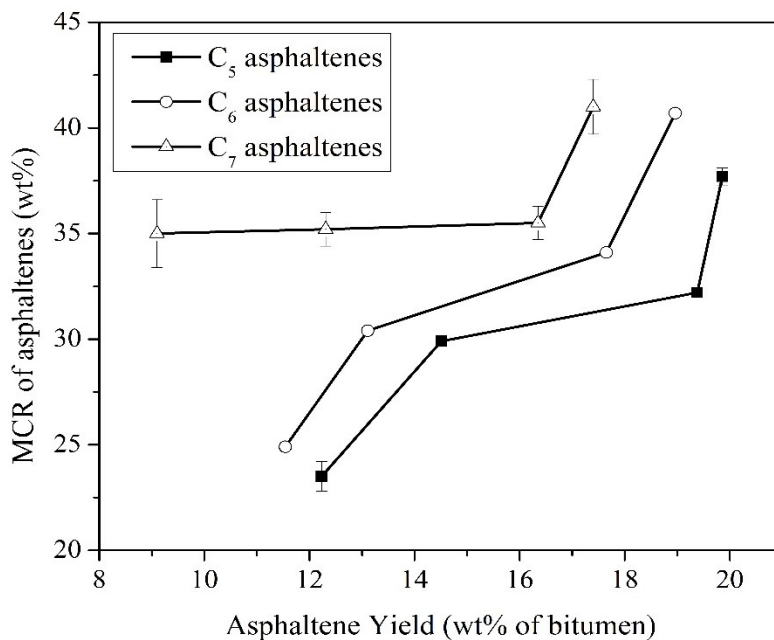
Also shown in Figure 5-13 is the relation between MCR of C<sub>5</sub>, C<sub>6</sub> and C<sub>7</sub> asphaltenes and the corresponding amount of residue (+524°C) fraction obtained in the SimDis analysis. With the increase in residue content, the MCR increases. The MCR decreases with an increase in H/C ratio, as shown in Figure 5-13. In general, feeds with higher molecular weight and aromaticity produce more coke.<sup>2</sup>

According to literature, coke formation from asphaltenes takes place by a series of reactions that lead to increase in molecular weight and decrease in aromaticity.<sup>2</sup> Insolubility and hydrogen depletion lead to the formation of mesophase or any other second liquid or solid phase, which ultimately leads to coke formation. In a study by Rahimi, et al.<sup>12</sup> the MCR of different fractions of Athabasca bitumen vacuum residue correlated well with the H/C ratio and aromatic carbon

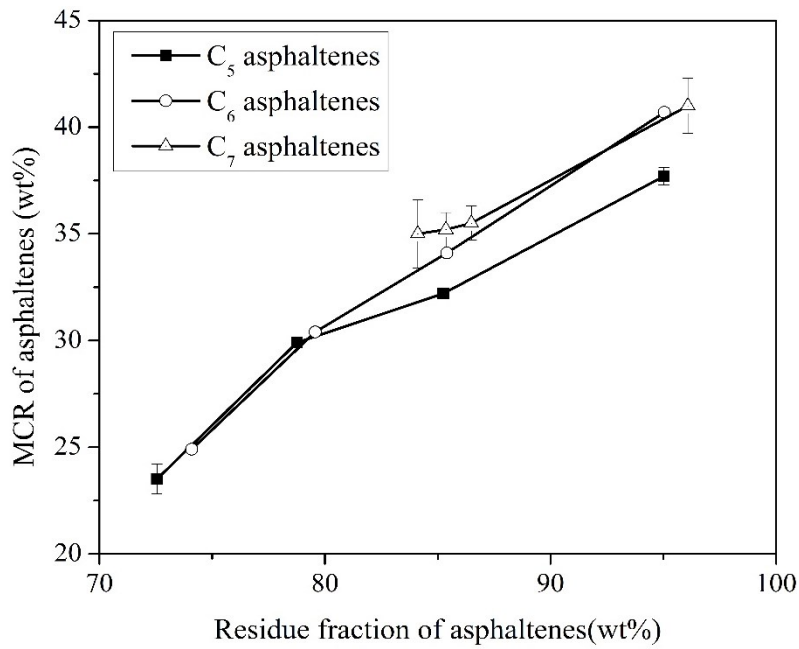
content. The mesophase was found to form sooner when the MCR, molecular weight and aromaticity of the fractions were higher.



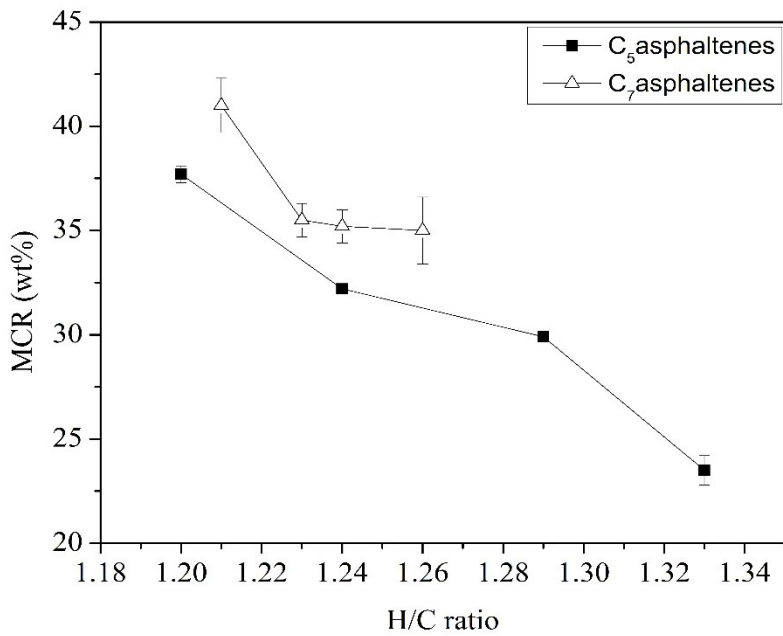
(a)



(b)



(c)



(d)

**Figure 5-13.** (a) Correlation between MCR of asphaltenes and their yields

(b) Correlation between average MCR and average asphaltene yield

(c) Correlation between MCR of asphaltenes and residue fraction of asphaltenes

(d) Correlation between MCR of asphaltenes and their H/C ratio

#### **5.4.5 Liquefaction of asphaltenes**

The results in Table 5-18 indicate that a higher temperature is required to maintain asphaltenes in a fluid state when high carbon number linear paraffinic solvents or high S/B ratios are used in the SDA process.

Melting transition in asphaltenes was not observed in the DSC calorigram (Figure 5-8) at the temperatures where liquefaction was found to occur in the HSM results (Table 5-18). A possible reason for liquefaction of asphaltenes at the temperatures observed in this study could be that a portion of asphaltenes that contains lighter material melts upon heating. The liquid phase thus formed then dissolves the heavier material, leading to the formation of a continuous liquid phase. Thus, the solid to liquid transformation of asphaltenes could be due to self-dissolution.

The reason why the liquefying point of C<sub>5</sub> asphaltenes is lower than C<sub>7</sub> asphaltenes could be that C<sub>5</sub> asphaltenes contain greater amount of low molecular weight material compared to C<sub>7</sub> asphaltenes. Asphaltenes precipitated at lower S/B ratios contain greater amount lighter material or more components that are not asphaltenes (e.g. resins), which are trapped in the precipitates due to inefficient phase separation. This in turn leads to a decrease in the liquefying point of the asphaltenes fraction.

From the SimDis results in Table 5-1, Table 5-2 and Table 5-3, significant differences were observed among the gas oil and residue fractions of asphaltenes precipitated using different solvents and S/B ratios in the SDA process. Thus, the liquefying point can be considered to be mainly related to the gas oil and residue fractions in asphaltenes. However, the low amounts of gas oil fraction, especially in C<sub>7</sub> asphaltenes, and at S/B ratios 5:1 and 40:1 indicates that liquefaction of C<sub>7</sub> asphaltenes at higher S/B ratios is reflective of the residue fraction of asphaltenes.

The correlation between the maximum point of intensity curve versus temperature for a fixed area of observation (Figure 5-7) and the liquefaction of asphaltenes (Table 5-18) indicates that reflected light intensity can be used as a tool to study the liquefaction or thermal behavior of asphaltenes. This correlation could be due to changes in optical properties of asphaltenes as they physically transform upon heating.

### **5.5 Conclusions**

- The solvent (*n*-pentane, *n*-hexane and *n*-heptane) and S/B ratio (3:1 to 5:1 compared to 40:1) in the SDA process affect the boiling point distribution, separation selectivity and extractability of boiling fractions in bitumen, cracking behavior and MCR of asphaltenes and DAO. They also affect the liquefying point of asphaltenes.
- The trends in the simulated distillation curves and boiling fractions of asphaltenes indicate that precipitated asphaltenes become heavier with increase in the carbon number of linear paraffinic solvent and with increase in S/B ratio.
- The changes in the boiling point distribution of asphaltenes and DAO were insignificant with change in precipitation time from 24h to 330h in the SDA process.
- The separation selectivity for middle distillate, gas oil and residue fractions of bitumen decreased from C<sub>5</sub> to C<sub>7</sub> asphaltenes, and the extractability into DAO correspondingly increased with the change in solvent.
- With increase in S/B ratio, the separation selectivity for the residue fraction of bitumen increased and the separation selectivity for gas oil fraction decreased. The extractability of residue and gas oil fractions from bitumen into DAO thus followed the opposite trend.
- MCR of asphaltenes, which is a measure of coking tendency, increased from C<sub>5</sub> to C<sub>7</sub>, and with increase in S/B ratio. MCR increased with increase in the residue fraction of asphaltenes and with decrease in the H/C ratio of asphaltenes. It was found that asphaltene yield is not a good indicator of coke forming tendency, indirectly measured by MCR.
- The changes in MCR of asphaltenes and DAO with change in precipitation time from 24h to 330h were insignificant.
- The onset temperature of cracking reactions in asphaltenes increases with increase in S/B ratio. S/B ratios used in the precipitation of asphaltenes in the SDA process also affect the rate of cracking reactions occurring in asphaltenes with respect to temperature.
- The liquefying point of C<sub>5</sub> asphaltenes was lower than that of C<sub>7</sub> asphaltenes, and it increased with increase in S/B ratio. This indicates that the asphaltenes precipitated at higher S/B ratios and using higher carbon number linear paraffinic solvent, require higher temperatures to maintain them in fluid state.
- A correlation was found between reflected light intensities and liquefaction of asphaltenes, indicating that reflected light intensity can be used as a measurement tool to monitor thermal behavior of asphaltenes.

- Enthalpy change corresponding to a typical melting transition was not observed in differential scanning calorimetric analysis of asphaltenes, at the temperatures where liquefaction of asphaltenes was visually observed in the hot stage microscopic analysis. The hypothesis behind liquefaction of asphaltenes is that they undergo self-dissolution instead of melting.
- In this study, significant differences in the studied thermal properties were observed between the asphaltenes precipitated at S/B ratios 5:1 and 40:1, which indicates that even though their yields are similar, their nature is different.

## 5.6 References

1. Speight, J. G., Chapter 9 - Fouling During Deasphalting and Dewaxing. In *Fouling in Refineries*, Gulf Professional Publishing: Boston, 2015; pp 209-235.
2. Gray, M. R., *Upgrading Oilsands Bitumen and Heavy Oil*. University of Alberta Press: Edmonton, Alberta, 2015.
3. Espinosa-Peña, M., Figueroa-Gómez, Y. and Jiménez-Cruz, F., Simulated Distillation Yield Curves in Heavy Crude Oils: A Comparison of Precision between ASTM D-5307 and ASTM D-2892 Physical Distillation. *Energy & Fuels* **2004**, *18* (6), 1832-1840.
4. *Principles of Thermal Analysis and Calorimetry*. Edited by P.J. Haines, Royal Society of Chemistry: Cambridge, 2002.
5. Haines, P. J. and Skinner, G. A., Simultaneous Differential Scanning Calorimetry and Reflected Light Intensity Measurements in Polymer Studies. *Thermochimica Acta* **1988**, *134*, 201-206.
6. Höhne, G. W. H., Hemminger, W. and Flammersheim, H.-J., *Differential Scanning Calorimetry: An Introduction for Practitioners*. Springer Berlin Heidelberg: 1996.
7. Speight, J. G., *Handbook of Petroleum Analysis*. Wiley-Interscience: New York, 2001.
8. Strausz, O. P. and Lown, E. M., *The Chemistry of Alberta Oil Sands, Bitumens and Heavy Oils*. Alberta Energy Research Institute: Calgary, 2003.
9. Liu, P., Zhu, M., Zhang, Z., Wan, W., Yani, S. and Zhang, D., Thermogravimetric Studies of Characteristics and Kinetics of Pyrolysis of Buton Oil Sand. *Energy Procedia* **2014**, *61*, 2741-2744.
10. Trejo, F., Rana, M. S. and Ancheyta, J., Thermogravimetric Determination of Coke from Asphaltenes, Resins and Sediments and Coking Kinetics of Heavy Crude Asphaltenes. *Catalysis Today* **2010**, *150* (3), 272-278.

11. Shin, S., Im, S. I., Kwon, E. H., Na, J.-G., Nho, N. S. and Lee, K. B., Kinetic Study on the Nonisothermal Pyrolysis of Oil Sand Bitumen and Its Maltene and Asphaltene Fractions. *Journal of Analytical and Applied Pyrolysis* **2017**, *124*, 658-665.
12. Rahimi, P., Gentzis, T., Dawson, W. H., Fairbridge, C., Khulbe, C., Chung, K., Nowlan, V. and DelBianco, A., Investigation of Coking Propensity of Narrow Cut Fractions from Athabasca Bitumen Using Hot-Stage Microscopy. *Energy & Fuels* **1998**, *12* (5), 1020-1030.
13. Wiehe, I. A., *Process Chemistry of Petroleum Macromolecules*. CRC Press: Boca Raton, 2008.
14. Carbognani, L., Lubkowitz, J., Gonzalez, M. F. and Pereira-Almao, P., High Temperature Simulated Distillation of Athabasca Vacuum Residue Fractions. Bimodal Distributions and Evidence for Secondary “on-Column” Cracking of Heavy Hydrocarbons. *Energy & Fuels* **2007**, *21* (5), 2831-2839.
15. Carey, F. A. and Sundberg, R. J., Structural Effects on Stability and Reactivity. In *Advanced Organic Chemistry: Part A: Structure and Mechanisms*, Springer US: Boston, MA, 2007; pp 253-388.
16. Zhao, Y., Gray, M. R. and Chung, K. H., Molar Kinetics and Selectivity in Cracking of Athabasca Asphaltenes. *Energy & Fuels* **2001**, *15* (3), 751-755.

## CHAPTER 6. CONCLUSIONS

### 6.1 Background

The objective of this project is to study the effect of solvent, solvent to bitumen (S/B) ratio and precipitation time in solvent deasphalting process on the chemical composition and properties of asphaltenes and DAO fractions of bitumen. Solvent deasphalting (SDA) is the precipitation of asphaltenes from bitumen by addition of an *n*-paraffin solvent such as *n*-pentane and *n*-heptane. Industries employ low S/B ratios between 3:1 and 10:1 in the SDA process due to high cost of solvent recovery. The type of solvent, S/B ratio, precipitation time, temperature and pressure used in the SDA process affect the yield and nature of DAO and asphaltenes. The DAO produced in the SDA process is thermally cracked to improve its properties and processed to valuable liquid products. The conversion of DAO in the thermal cracking stage and properties of the resultant products are impacted by the chemical composition and physical properties of DAO, which in turn are affected by the process conditions used in the SDA process. Examples of properties that could be affected by the solvent deasphalting process are: 1. the coking tendency of DAO in the thermal cracking process, which limits the conversion to useful products, 2. the density of DAO which should be within the limits of pipeline specification, 3. the presence of free radicals in asphaltenes, which play a role in upgrading and refining processes and 4. the fluidity of asphaltenes, which needs to be maintained to avoid plugging and fouling of process equipment. Asphaltenes produced in the SDA process have a lower value compared to DAO. As bitumen contains 14-20 wt% of asphaltenes, removal of all the asphaltenes from bitumen represents a significant loss. Thus, it is desired to achieve quality improvement in DAO, while minimizing the yield of asphaltenes in the SDA process at the same time.

### 6.2 Experimental Approach

In this study, asphaltenes were precipitated from Athabasca bitumen. *n*-pentane, *n*-hexane and *n*-heptane were used as precipitants in the SDA process at S/B ratios 3:1, 4:1, 5:1 and 40:1 (ml/g). The effect of changing the precipitation time from 24h to 330h was studied. Experiments were performed at room temperature and atmospheric pressure. The yield of asphaltenes and DAO, and the associated material losses at different conditions of SDA process were measured (chapter 3). Chemical characteristics (chapter 4) and thermal properties (chapter 5) of asphaltenes and DAO

produced at different conditions of SDA process were studied using various characterization techniques.

### **6.3 Major Conclusions**

The major conclusions of this study are divided into three parts, chapter-wise:

1. Asphaltene yield and material balance in SDA process
2. Chemical characterization of asphaltenes and DAO
3. Thermal properties of asphaltenes and DAO

#### **6.3.1 Asphaltene yield and material balance in the solvent deasphalting process**

- a) The solvent, S/B ratio and precipitation time used in the solvent deasphalting of bitumen showed an impact on asphaltene yield and recovery of material after separation.
- b) The effect of solvent and S/B ratio on the yield of asphaltenes found in this study was similar to that reported in literature. At 24h precipitation time, the yield of C<sub>5</sub> asphaltenes increased from 12.23 to 19.86 wt% with increase in S/B ratio from 3:1 to 40:1 (ml/g), and that of C<sub>6</sub> and C<sub>7</sub> asphaltenes increased from 11.54 to 18.96wt% and 9.1 to 17.4wt% respectively. The yield of asphaltenes increased with the carbon number of *n*-paraffinic solvent from C<sub>5</sub> to C<sub>7</sub>.
- c) The yield of asphaltenes precipitated at S/B ratios 5:1 and 40:1 were similar. However, their appearance was significantly different, indicating that their characteristics are different.
- d) Loss of material occurred during precipitation of asphaltenes. The recovery of material was low when lower S/B ratios were used. The increase in losses at lower S/B ratios are attributed to the sticky and thick nature of the solvent-bitumen mixture at lower S/B ratios. Material balance calculations indicated that the losses varied from 0.79wt% to 14.64wt% in the asphaltene precipitation experiments.

#### **6.3.2 Chemical characterization of asphaltenes and DAO**

- e) The solvent and S/B ratio in the SDA process affected the H/C ratio, nitrogen, sulfur, nickel and vanadium content of precipitated asphaltenes. The H/C ratio of C<sub>5</sub> asphaltenes was greater than that of C<sub>7</sub> asphaltenes at the observed S/B ratios. The H/C ratio decreased with an increase in S/B ratio from 3:1 to 40:1. The nitrogen, sulfur, nickel and vanadium content in asphaltenes

increased with increase in S/B ratio from 3:1 to 40:1. C<sub>7</sub> asphaltenes contained higher amount of N, S, Ni and V compared to C<sub>5</sub> asphaltenes. These findings are in accordance with literature.

- f) The separation selectivity (fraction of the element in bitumen separated into asphaltenes phase) and extractability (fraction of the element in bitumen extracted into DAO) of nitrogen, sulfur, nickel and vanadium were affected by the solvent and S/B ratio used in the SDA process. The separation selectivity increased with increase in S/B ratio from 3:1 to 40:1 in the SDA process. Thus, higher S/B ratios are required to extract lesser amount of N, S, Ni and V into DAO in the solvent deasphalting process.
- g) The double integral values of organic free radical peak and vanadyl peak in ESR spectroscopy of asphaltenes, increased from C<sub>5</sub> to C<sub>7</sub> asphaltenes, and with increase in S/B ratio from 3:1 to 40:1. A linear correlation was observed between the double integral values of vanadyl peak of asphaltenes and their corresponding vanadium content in ppm, measured in XRF spectrometry. Changes in g-factors of the organic and vanadyl radical peaks were observed with changes in solvent and S/B ratios. The g-factor increased with increase in S/B ratio from 3:1 to 40:1.
- h) Significant differences were observed in the chemical characteristics of asphaltenes precipitated at S/B ratios 5:1 and 40:1, indicating that asphaltene yield is not a reliable indicator of the effects of fractionation on bitumen fractions in solvent deasphalting process

### **6.3.3 Thermal properties of asphaltenes and DAO**

- i) The precipitated asphaltenes become heavier with increase in the carbon number of linear paraffinic solvent and with increase in S/B ratio. The separation selectivity for middle distillate, gas oil and residue fractions of bitumen decreased from C<sub>5</sub> to C<sub>7</sub> asphaltenes. With increase in S/B ratio, the separation selectivity for the residue fraction of bitumen increased and the separation selectivity for gas oil fraction decreased.
- j) MCR of asphaltenes, which is a measure of coking tendency, increased from C<sub>5</sub> to C<sub>7</sub> asphaltenes, and with increase in S/B ratio from 3:1 to 40:1. MCR increased with increase in the residue fraction of asphaltenes and with decrease in the H/C ratio of asphaltenes. It was found that asphaltene yield is not a good indicator of coke forming tendency, indirectly measured by MCR.

- k) The onset temperature of cracking reactions in asphaltenes increases with increase in S/B ratio. S/B ratios used in the precipitation of asphaltenes in the SDA process also affect the rate of cracking reactions occurring in asphaltenes with respect to temperature.
- l) The liquefying point of  $C_5$  asphaltenes was lower than that of  $C_7$  asphaltenes, and it increased with increase in S/B ratio. This indicates that the asphaltenes precipitated at higher S/B ratios and using higher carbon number linear paraffinic solvent, require higher temperatures to maintain them in fluid state. A correlation was found between reflected light intensities and liquefaction of asphaltenes, indicating that reflected light intensity can be used as a measurement tool to monitor thermal behavior of asphaltenes.
- m) In this study, significant differences in the studied thermal properties were observed between the asphaltenes precipitated at S/B ratios 5:1 and 40:1, which indicates that even though their yields are similar, their nature is different.
- n) Changes in boiling point distribution and micro carbon residue of asphaltenes with change in precipitation time from 24h to 330h were insignificant.

#### **6.4 Recommendations for future work**

- a) In the present study, solvent deasphalting experiments were performed at room temperature and atmospheric pressure. While the results of this study are instructive and form the basis for understanding the effect of solvent deasphalting process conditions on bitumen fractions, it is recommended to perform further experimentation at the industrial process conditions.
- b) This study focused on the effect of linear paraffin solvents of varying chain length on the properties of asphaltenes and DAO in the solvent deasphalting process. However, it is worthwhile to extend the investigation beyond linear paraffin solvents, by incorporating the usage of branched-chain alkanes, cycloalkanes etc. as precipitants in the solvent deasphalting process, and studying the effect of structural and stereoisomerism of these solvents on the fractionation of bitumen.

## BIBLIOGRAPHY

1. *Asphaltenes and Asphalts*, 2. Edited by Yen, T.F. and Chilingar, G.V., Elsevier Science: Amsterdam, 2000.
2. *Principles of Thermal Analysis and Calorimetry*. Edited by P.J. Haines, Royal Society of Chemistry: Cambridge, 2002.
3. ASTM D7169-11: Standard Test Method for Boiling Point Distribution of Samples with Residues Such as Crude Oils and Atmospheric and Vacuum Residues by High Temperature Gas Chromatography. ASTM International: West Conshohocken, PA, 2011.
4. Standard Test Method for Characteristic Groups in Rubber Extender and Processing Oils and Other Petroleum-Derived Oils by the Clay-Gel Absorption Chromatographic Method. ASTM International: 2016.
5. Abivin, P., Taylor, S. D. and Freed, D., Thermal Behavior and Viscoelasticity of Heavy Oils. *Energy & Fuels* **2012**, 26 (6), 3448-3461.
6. Ancheyta Juárez, J., *Asphaltenes Chemical Transformation During Hydroprocessing of Heavy Oils*. Taylor & Francis: Boca Raton, 2009; p 461 p.
7. Asprino, O. J., Elliott, J. A. W., McCaffrey, W. C. and Gray, M. R., Fluid Properties of Asphaltenes at 310–530 °C. *Energy & Fuels* **2005**, 19 (5), 2026-2033.
8. Barman, B. N., Hydrocarbon-Type Analysis of Base Oils and Other Heavy Distillates by Thin-Layer Chromatography with Flame-Ionization Detection and by the Clay—Gel Method. *Journal of Chromatographic Science* **1996**, 34 (5), 219-225.
9. Barneto, A. G. and Carmona, J. A., Thermogravimetric Description of Visbreaker Streams in an Oil Refinery. *Thermochimica Acta* **2016**, 642, 1-9.

10. Bazyleva, A., Fulem, M., Becerra, M., Zhao, B. and Shaw, J. M., Phase Behavior of Athabasca Bitumen. *Journal of Chemical & Engineering Data* **2011**, *56* (7), 3242-3253.
11. Bockrath, B. C. and Schweighardt, F. K., Coal-Derived Asphaltenes. In *Chemistry of Asphaltenes*, American Chemical Society: 1982; Vol. 195, pp 29-38.
12. Borrego, A. G., Blanco, C. G., Prado, J. G., Díaz, C. and Guillén, M. D., <sup>1</sup>H NMR and FTIR Spectroscopic Studies of Bitumen and Shale Oil from Selected Spanish Oil Shales. *Energy & Fuels* **1996**, *10* (1), 77-84.
13. Carbognani, L., Lubkowitz, J., Gonzalez, M. F. and Pereira-Almao, P., High Temperature Simulated Distillation of Athabasca Vacuum Residue Fractions. Bimodal Distributions and Evidence for Secondary “on-Column” Cracking of Heavy Hydrocarbons. *Energy & Fuels* **2007**, *21* (5), 2831-2839.
14. Carbonezi, C. A., de Almeida, L. C., Araujo, B. C., Lucas, E. F. and González, G., Solution Behavior of Naphthenic Acids and Its Effect on the Asphaltenes Precipitation Onset. *Energy & Fuels* **2009**, *23* (3), 1249-1252.
15. Carey, F. A. and Sundberg, R. J., Structural Effects on Stability and Reactivity. In *Advanced Organic Chemistry: Part A: Structure and Mechanisms*, Springer US: Boston, MA, 2007; pp 253-388.
16. Cherney, D. P., Wu, C., Thorman, R. M., Hegner, J. L., Yeganeh, M. S., Ferrughelli, D. and Ulysse, E., Investigating the Impact of Crude Oil Solubility on Water-in-Oil Emulsion Stability and Its Relation to Molecular Composition of Crude Oil at the Oil–Water Interface. *Energy & Fuels* **2015**, *29* (6), 3616-3625.
17. Coates, J., Interpretation of Infrared Spectra, a Practical Approach. In *Encyclopedia of Analytical Chemistry*, John Wiley & Sons, Ltd: 2006.

18. Eaton, G. R., Eaton, S. S., Barr, D. P. and Weber, R. T., *Quantitative EPR*. Springer Science & Business Media: 2010.
19. Espinosa-Peña, M., Figueroa-Gómez, Y. and Jiménez-Cruz, F., Simulated Distillation Yield Curves in Heavy Crude Oils: A Comparison of Precision between ASTM D-5307 and ASTM D-2892 Physical Distillation. *Energy & Fuels* **2004**, *18* (6), 1832-1840.
20. Evdokimov, I. N. and Losev, A. P., Effects of Molecular De-Aggregation on Refractive Indices of Petroleum-Based Fluids. *Fuel* **2007**, *86* (15), 2439-2445.
21. Friesen, W. I., Michaelian, K. H., Long, Y. and Dabros, T., Effect of Solvent-to-Bitumen Ratio on the Pyrolysis Properties of Precipitated Athabasca Asphaltenes. *Energy & Fuels* **2005**, *19* (3), 1109-1115.
22. George, A. K. and Singh, R. N., Correlation of Refractive Index and Density of Crude Oil and Liquid Hydrocarbon. *International Journal of Chemical, Environmental & Biological Sciences (IJCEBS)* **2015**, *3* (5), 420-422.
23. Gray, M. R., *Upgrading Oilsands Bitumen and Heavy Oil*. University of Alberta Press: Edmonton, Alberta, 2015.
24. Haines, P. J. and Skinner, G. A., Simultaneous Differential Scanning Calorimetry and Reflected Light Intensity Measurements in Polymer Studies. *Thermochimica Acta* **1988**, *134*, 201-206.
25. Haines, P. J. and Skinner, G. A., Simultaneous Differential Scanning Calorimetry and Reflected Light Intensity Measurements in Polymer Studies. *Thermochimica Acta* **1988**, *134*, 201-206.

26. Haji-Akbari, N., Teeraphakul, P., Balgoa, A. T. and Fogler, H. S., Effect of *n*-Alkane Precipitants on Aggregation Kinetics of Asphaltenes. *Energy & Fuels* **2015**, *29* (4), 2190-2196.
27. Hamidi Zirasefi, M., Khorasheh, F., Ivakpour, J. and Mohammadzadeh, A., Improvement of the Thermal Cracking Product Quality of Heavy Vacuum Residue Using Solvent Deasphalting Pretreatment. *Energy & Fuels* **2016**, *30* (12), 10322-10329.
28. Hansen, C. M., *Hansen Solubility Parameters a User's Handbook*. 2nd ed.; CRC Press: Boca Raton, 2007.
29. Hauser, A., Bahzad, D., Stanislaus, A. and Behbahani, M., Thermogravimetric Analysis Studies on the Thermal Stability of Asphaltenes: Pyrolysis Behavior of Heavy Oil Asphaltenes. *Energy & Fuels* **2008**, *22* (1), 449-454.
30. Hinkle, A., Shin, E.-J., Liberatore, M. W., Herring, A. M. and Batzle, M., Correlating the Chemical and Physical Properties of a Set of Heavy Oils from around the World. *Fuel* **2008**, *87* (13), 3065-3070.
31. Höhne, G. W. H., Hemminger, W. and Flammersheim, H.-J., *Differential Scanning Calorimetry: An Introduction for Practitioners*. Springer Berlin Heidelberg: 1996.
32. Jiménez Riobóo, R. J., Philipp, M., Ramos, M. A. and Krüger, J. K., Concentration and Temperature Dependence of the Refractive Index of Ethanol-Water Mixtures: Influence of Intermolecular Interactions. *The European Physical Journal E* **2009**, *30* (1), 19.
33. Khulbe, K. C., Chan, B. W., Manoogian, A. and Patmore, D. J., E.s.r of Alberta Tar Sand Bitumen and Thermally Hydrocracked Products. *Fuel* **1986**, *65* (11), 1594-1599.

34. Khulbe, K. C., Mann, R. S., Lu, B. C. Y., Lamarche, G. and Lamarche, A. M., Effects of Solvents on Free Radicals of Bitumen and Asphaltenes. *Fuel Processing Technology* **1992**, 32 (3), 133-141.
35. Kopsch, H., On the Thermal Behavior of Petroleum Asphaltenes. *Thermochimica Acta* **1994**, 235 (2), 271-275.
36. Lee, J. M., Shin, S., Ahn, S., Chun, J. H., Lee, K. B., Mun, S., Jeon, S. G., Na, J. G. and Nho, N. S., Separation of Solvent and Deasphalted Oil for Solvent Deasphalting Process. *Fuel Processing Technology* **2014**, 119, 204-210.
37. Lee, J. M., Shin, S., Ahn, S., Chun, J. H., Lee, K. B., Mun, S., Jeon, S. G., Na, J. G. and Nho, N. S., Separation of Solvent and Deasphalted Oil for Solvent Deasphalting Process. *Fuel Processing Technology* **2014**, 119, 204-210.
38. León, O., Rogel, E., Espidel, J. and Torres, G., Asphaltenes: Structural Characterization, Self-Association, and Stability Behavior. *Energy & Fuels* **2000**, 14 (1), 6-10.
39. Liu, P., Zhu, M., Zhang, Z., Wan, W., Yani, S. and Zhang, D., Thermogravimetric Studies of Characteristics and Kinetics of Pyrolysis of Buton Oil Sand. *Energy Procedia* **2014**, 61, 2741-2744.
40. Luo, P., Wang, X. and Gu, Y., Characterization of Asphaltenes Precipitated with Three Light Alkanes under Different Experimental Conditions. *Fluid Phase Equilibria* **2010**, 291 (2), 103-110.
41. Maqbool, T., Balgoa, A. T. and Fogler, H. S., Revisiting Asphaltene Precipitation from Crude Oils: A Case of Neglected Kinetic Effects. *Energy & Fuels* **2009**, 23 (7), 3681-3686.

42. Merola, M. C., Carotenuto, C., Gargiulo, V., Stanzione, F., Ciajolo, A. and Minale, M., Chemical–Physical Analysis of Rheologically Different Samples of a Heavy Crude Oil. *Fuel Processing Technology* **2016**, *148*, 236-247.
43. Mitchell, D. L. and Speight, J. G., The Solubility of Asphaltenes in Hydrocarbon Solvents. *Fuel* **1973**, *52* (2), 149-152.
44. Mozaffari, S., Tchoukov, P., Atias, J., Czarnecki, J. and Nazemifard, N., Effect of Asphaltene Aggregation on Rheological Properties of Diluted Athabasca Bitumen. *Energy & Fuels* **2015**, *29* (9), 5595-5599.
45. Niizuma, S., Steele, C. T., Gunning, H. E. and Strausz, O. P., Electron Spin Resonance Study of Free Radicals in Athabasca Asphaltene. *Fuel* **1977**, *56* (3), 249-256.
46. Nikooyeh, K. and Shaw, J. M., On the Applicability of the Regular Solution Theory to Asphaltene + Diluent Mixtures. *Energy & Fuels* **2012**, *26* (1), 576-585.
47. Ortega, L. C., Rogel, E., Vien, J., Ovalles, C., Guzman, H., Lopez-Linares, F. and Pereira-Almao, P., Effect of Precipitating Conditions on Asphaltene Properties and Aggregation. *Energy & Fuels* **2015**, *29* (6), 3664-3674.
48. Painter, P., Veytsman, B. and Youtcheff, J., Phase Behavior of Bituminous Materials. *Energy & Fuels* **2015**, *29* (11), 7048-7057.
49. Peraza, A., Sánchez, M. and Ruelle, F., Modeling Free-Radical Reactions, Produced by Hydrocarbon Cracking, with Asphaltenes. *Energy & Fuels* **2010**, *24* (7), 3990-3997.
50. Prado, G. H. C. and de Klerk, A., Metals Removal from Metal-Bridged Molecules by Acid Treatment of Oilsands Bitumen and Subfractions. *Energy & Fuels* **2016**, *30* (1), 20-30.
51. Rahimi, P., Gentzis, T., Dawson, W. H., Fairbridge, C., Khulbe, C., Chung, K., Nowlan, V. and DelBianco, A., Investigation of Coking Propensity of Narrow Cut Fractions from

- Athabasca Bitumen Using Hot-Stage Microscopy. *Energy & Fuels* **1998**, *12* (5), 1020-1030.
52. Rahmani, S., McCaffrey, W., Elliott, J. A. W. and Gray, M. R., Liquid-Phase Behavior During the Cracking of Asphaltenes. *Industrial & Engineering Chemistry Research* **2003**, *42* (17), 4101-4108.
53. Rahmani, S., McCaffrey, W. C., Dettman, H. D. and Gray, M. R., Coking Kinetics of Asphaltenes as a Function of Chemical Structure. *Energy & Fuels* **2003**, *17* (4), 1048-1056.
54. Redelius, P. and Soenen, H., Relation between Bitumen Chemistry and Performance. *Fuel* **2015**, *140*, 34-43.
55. Reynolds, J. G., Chapter 10 Effects of Asphaltene Precipitation on the Size of Vanadium-, Nickel-, and Sulfur-Containing Compounds in Heavy Crude Oils and Residua. *Developments in Petroleum Science* **1994**, *40*, 233-248.
56. Shafiee Neistanak, M. Kinetics of Asphaltene Precipitation and Flocculation from Diluted Bitumen. University of Calgary, 2014.
57. Shin, S., Im, S. I., Kwon, E. H., Na, J.-G., Nho, N. S. and Lee, K. B., Kinetic Study on the Nonisothermal Pyrolysis of Oil Sand Bitumen and Its Maltene and Asphaltene Fractions. *Journal of Analytical and Applied Pyrolysis* **2017**, *124*, 658-665.
58. Shin, S., Lee, J. M., Hwang, J. W., Jung, H. W., Nho, N. S. and Lee, K. B., Physical and Rheological Properties of Deasphalted Oil Produced from Solvent Deasphalting. *Chemical Engineering Journal* **2014**, *257*, 242-247.
59. Siddiquee, M. N. Autoxidation of Oilsands Bitumen: Applied, Model Compounds and Microfluidic Study. University of Alberta, Edmonton, Canada, 2016.
60. Speight, J. G., *Petroleum Refining Processes*. Marcel Dekker: New York, 2001.

61. Speight, J. G., *Handbook of Petroleum Analysis*. Wiley-Interscience: New York, 2001.
62. Speight, J. G., *The Chemistry and Technology of Petroleum, Fifth Edition*. CRC Press: Hoboken, 2014.
63. Speight, J. G., *Fouling in Refineries*. Elsevier: Amsterdam, 2015.
64. Speight, J. G., Chapter 9 - Fouling During Deasphalting and Dewaxing. In *Fouling in Refineries*, Gulf Professional Publishing: Boston, 2015; pp 209-235.
65. Speight, J. G., Long, R. B. and Trowbridge, T. D., Factors Influencing the Separation of Asphaltenes from Heavy Petroleum Feedstocks. *Fuel* **1984**, 63 (5), 616-620.
66. Spiecker, P. M., Gawrys, K. L. and Kilpatrick, P. K., Aggregation and Solubility Behavior of Asphaltenes and Their Subfractions. *Journal of Colloid and Interface Science* **2003**, 267 (1), 178-193.
67. Strausz, O. P. and Lown, E. M., *The Chemistry of Alberta Oil Sands, Bitumens and Heavy Oils*. Alberta Energy Research Institute: Calgary, 2003.
68. Stuart, B., *Infrared Spectroscopy Fundamentals and Applications*. J. Wiley: Chichester, West Sussex, England, 2004.
69. Trejo, F., Rana, M. S. and Ancheyta, J., Thermogravimetric Determination of Coke from Asphaltenes, Resins and Sediments and Coking Kinetics of Heavy Crude Asphaltenes. *Catalysis Today* **2010**, 150 (3), 272-278.
70. Wang, J. and Anthony, E. J., A Study of Thermal-Cracking Behavior of Asphaltenes. *Chemical Engineering Science* **2003**, 58 (1), 157-162.
71. Wang, J. X. and Buckley, J. S., A Two-Component Solubility Model of the Onset of Asphaltene Flocculation in Crude Oils. *Energy & Fuels* **2001**, 15 (5), 1004-1012.

72. Wauquier, J.-P., *Petroleum Refining, Volume 1 - Crude Oil, Petroleum Products, Process Flowsheets*. Editions Technip: 1995.
73. Wiehe, I. A., *Process Chemistry of Petroleum Macromolecules*. CRC Press: Boca Raton, 2008.
74. Wiehe, I. A., Yarranton, H. W., Akbarzadeh, K., Rahimi, P. M. and Teclemariam, A., The Paradox of Asphaltene Precipitation with Normal Paraffins. *Energy & Fuels* **2005**, *19* (4), 1261-1267.
75. Yanez Jaramillo, L. M. Visbreaking of Oilsands Bitumen between 150° and 300°C. MSc Thesis, University of Alberta, Edmonton, AB, Canada, 2016.
76. Zhang, Y., Takanohashi, T., Sato, S., Saito, I. and Tanaka, R., Observation of Glass Transition in Asphaltenes. *Energy & Fuels* **2004**, *18* (1), 283-284.
77. Zhao, Y., Gray, M. R. and Chung, K. H., Molar Kinetics and Selectivity in Cracking of Athabasca Asphaltenes. *Energy & Fuels* **2001**, *15* (3), 751-755.